

NANOSTRUCTURE FORMATION IN THIN POLYMER FILMS

Dissertation

zur Erlangung des Grades eines
Doktors der Naturwissenschaften
an der Fakultät für Biologie, Chemie und Geowissenschaften
der Universität Bayreuth

vorgelegt am 26. Januar 2004

von

Nicolaus Rehse

geboren am 27. Januar 1972 in Kiel

Die vorliegende Arbeit wurde in der Zeit von Juni 1999 bis Januar 2004 in Bayreuth am Lehrstuhl für Physikalische Chemie II unter der Betreuung von Prof. Dr. Georg Krausch angefertigt.

Erstgutachter: Prof. Dr. Georg Krausch

Zweitgutachter: Prof. Dr. Axel H. E. Müller

1	Overview	9
1.1	<i>General Introduction</i>	9
1.2	<i>Patterned Substrates via Hierarchical Self Assembly</i>	9
1.3	<i>Pattern Formation via Surface Reconstruction in Thin ABC Triblock Copolymer Films</i>	15
1.4	<i>Individual Contributions of Authors</i>	20
1.5	<i>References</i>	21
2	Automated preparation of chemically nano-patterned substrates	
	27	
2.1	<i>Introduction</i>	27
2.2	<i>Apparatus</i>	29
2.3	<i>Procedure</i>	31
2.4	<i>References</i>	38
3	Stability of Thin Polymer Films on a Corrugated Substrate	41
3.1	<i>Introduction</i>	41
3.2	<i>Experimental</i>	43
3.3	<i>Results</i>	45
3.4	<i>Discussion</i>	49
3.5	<i>Conclusions</i>	53
3.6	<i>References</i>	53
4	Surface Reconstruction of an Ordered Fluid: An Analogy with	
	Crystal Surfaces	57
4.1	<i>References</i>	64

5	Surface Reconstructions of Lamellar ABC Triblock Copolymer Mesostructures	67
5.1	<i>Introduction</i>	67
5.2	<i>Experimental.....</i>	68
5.3	<i>Results</i>	70
5.3.1	Surface reconstructions: SBM.....	70
5.3.2	Effect of block copolymer molecular weight: SBM ⁵⁴	78
5.3.3	Role of molecular topology: BSM.....	79
5.3.4	Strength of the surface field: SBT	81
5.4	<i>Discussion.....</i>	82
5.4.1	Similarity to surface reconstructions of inorganic crystals	82
5.4.2	Nomenclature	85
5.4.3	Experimental conditions for block copolymer surface studies	87
5.4.4	Comparison to earlier experimental results	90
5.5	<i>Conclusion.....</i>	91
5.6	<i>References.....</i>	91
6	Summary / Zusammenfassung	94
6.1	<i>Summary.....</i>	94
6.2	<i>Zusammenfassung.....</i>	95
7	Acknowledgement / Danksagung	98

‘Did you ever discover or hear tell of the Atomic Theory?’ he inquired.

‘No,’ I answered.

(...)

‘Now take a sheep,’ the Sergeant said. ‘What is a sheep only millions of little bits of sheepness whirling around and doing intricate convolutions inside the sheep? What else is it but that?’

Flann O’Brien, ‘The Third Policeman’

1 Overview

1.1 General Introduction

In February 1960, Richard Feynman [1] published his now-legendary article entitled "There's Plenty of Room at the Bottom: An Invitation to Enter a New Field of Physics". It took quite a while for this new field – nanotechnology – to grow to the size it has now. One reason for the slow development in the beginning is the strong interdisciplinarity of this field. Feynman already realized how important this field would be for biologists, chemists and engineers. Hence scientists had to overcome many barriers between the ‘classic’ fields. In the field of nanostructured materials, polymers together with biological materials, semiconductors and colloids found their place in the overlap of the different scientific fields [2-5]. In this particular area, self organization is an important concept for fabricating structures on the nanometer length scale [6]. In contrast to the direct manipulation of atoms or molecules, patterns are formed by well defined interplay between inter- and/or intramolecular forces as well as external fields. This route is much more efficient compared to the direct manipulation of individual molecules but it is limited to more or less periodic structures. An exception is the assembly based on specific DNA interactions where well defined binding sites lead to a recognition process between building blocks [7, 8]. In case of the polymers the number of interesting patterns is growing day by day [9-15]. The challenge is to control the structures by controlling internal and external forces [5, 16-20]. In this thesis, two areas of this broad field are addressed [21-24]. First I will discuss the preparation of patterned substrates via hierarchical self assembly and their use as substrates to study the stability of polymer films. Pattern formation via surface reconstruction in thin ABC triblock copolymer films will be discussed in the second part of this thesis.

1.2 Patterned Substrates via Hierarchical Self Assembly

Most techniques to create nanometer sized structures are based on either lithography [25-36] or self assembly [31-34] or a combination of both (Fig. 1) [5, 35-38]. A common limitation of all lithographical methods is the decreasing size of the patterned area with decreasing size of the pattern features. On the other hand most self assembly methods to create lateral structures are limited to simple shapes (e.g. stripes or hexagonal dot arrays). A second limitation is the size of domains with a certain orientation, which rarely exceeds some μm^2 [29].

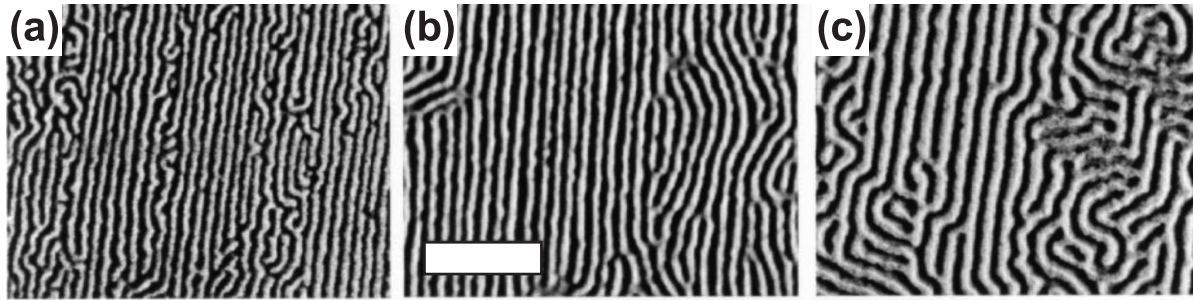


Figure 1: AFM tapping mode phase images of poly(styrene)-*block*-poly(methylmethacrylate) block copolymer films on a nanopatterned substrate. The images show samples with different degrees of commensurability: (a) 0.78, (b) 0.99, (c) 1.4 (Scale bar = 500 nm). Adopted from Ref. [36].

Photolithographic methods based on the use of masks [29] will not be discussed here since they are limited to the wavelength of the light used. Furthermore, they are most efficient when a very large number of patterned substrates is needed [29]. In the following, I shall first present some common methods to produce such patterns and then introduce a route based on self organization of single crystal surfaces [31, 39, 40], which was improved by automation.

In electron beam lithography a focused electron beam is used to destroy or modify either a self assembled monolayer (SAM) [30] or a photoresist polymer (e.g. polyacrylates) [29]. In case of the SAMs the induced topographic pattern is usually negligible compared to the effect of the chemical pattern. These patterns are usually used without further modification. To create a topographic structure the pattern is written into a thin film of a photoresist and is then transferred into the underlying substrate via etching. The typical feature size of such patterns lies between 10 and 100 nm with an overall size which rarely exceeds some 100 μm . Another method based on electron beam lithography is micro contact printing [41-43]. It has become very popular because it is easy to use and only a single master has to be prepared via a lithographic method. From this master a soft polymer stamp (i.e. polydimethylsiloxane) is fabricated. This stamp can be soaked with a solution of SAM molecules and the pattern can then easily be transferred onto a flat substrate many times. Finally, scanning probe techniques can also be used to manipulate self assembled monolayers [44] or to alter the substrate via electrochemical etching [45].

Patterns based on self-organization often use block copolymer structures as a template [46-48]. Since the formation of these structures is discussed later, I will only give a brief overview how to transfer block copolymer structures into a chemical or a topographical pattern. The components of a block copolymer have often different etching rates, which can

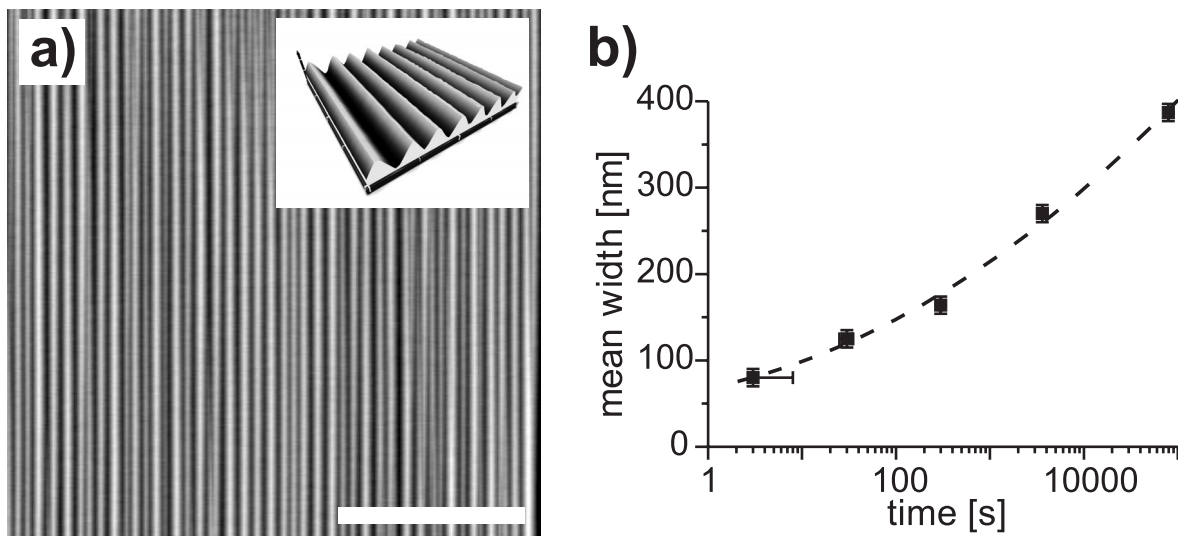


Figure 2: (a) SFM Tapping Mode™ topography image of corrugated silicon. The scale bar is 4 μm . In the inset we show a three-dimensional image of a $2\ \mu\text{m} \times 2\ \mu\text{m}$ area of the scan. (b) The mean groove width of the corrugated substrates as a function of the annealing time at 800°C under ultra-high vacuum. The dashed line is a guide to the eye. From Ref. [23].

enhanced via selective staining. The block copolymer structures can be directly etched into an underlying substrate to create topographic patterns. Loading one of the microdomains with metal salts or nanoparticles gives a different chemical contrast if the polymer is removed [49-50]. Block copolymers can also be used as a mask for evaporation or as an etching mask for a layered substrate. In both cases one gets pure inorganic structures with a topographical and chemical pattern.

In this thesis, single crystals were used to create topographic patterns [31, 39, 40]. Anisotropic etching of certain crystal facets leads to a patterned surface which can be used as is or can be used as a master for microcontact printing [43]. If a single crystal is miscut between two low indexed surface planes and the mobility of the surface atoms is high enough, the surface forms facets to reduce the surface energy [51]. These facets usually form at relatively high temperatures (i.e. close to melting temperature) and under ultrahigh vacuum conditions. In case of a miscut silicon (113) surface the resulting structures are quite large hence the topographic pattern is still present after oxidation [31, 39, 40] (Fig. 2a). Practically a piece of a miscut silicon wafer is transferred into an ultra high vacuum chamber. Then the native oxide layer is removed via subsequent resistive heating of the sample. After this cleaning process the sample is heated to $900\ ^\circ\text{C}$ and kept at this temperature for a certain time which controls the size of the facets formed (Fig 2b). Quenching the sample to room temperature stops the

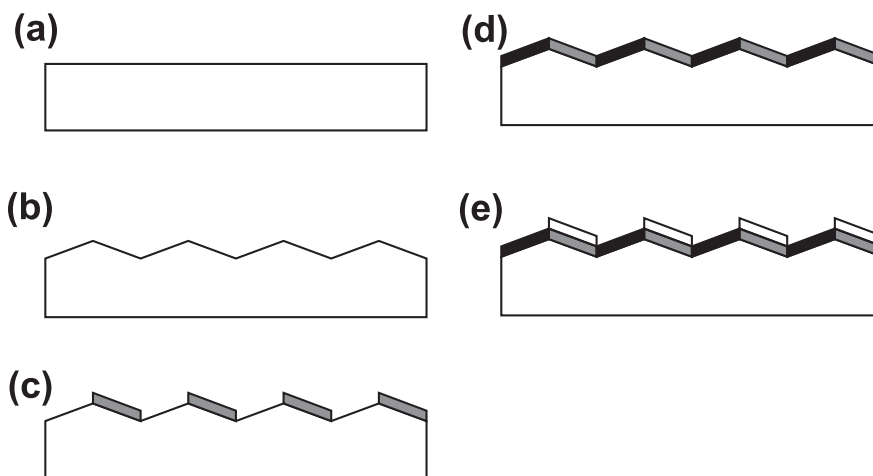


Figure 3: Schematic drawing of various substrate structures based on the method described in Ref. [21]. (a) bare silicon, (b) topographic structure, (c) topographic structure after metal evaporation, (d) and (e) further modifications with SAMs.

reorganization of the surface. The sample is now removed from the vacuum chamber and thereby oxidized. Scanning probe microscopy reveals a triangular pattern which extends over the whole sample surface.

We established an automated process for the cleaning and control the temperature during heating. As the cleaning is very sensitive to traces of oxygen, which can lead to a very rough surface [52], pressure is a crucial parameter. In addition the heating current might be too high in the beginning so the sample gets too hot and melts. Therefore a computer program controls temperature, pressure, and heating current of the sample and stops the cleaning process if the pressure gets too high. The heating current is subsequently raised during several cleaning steps until the desired temperature is reached. With the help of this program the sample loss is reduced to a minimum. As the size of the structures (i.e. the width of the facets) is controlled by the preparation time and temperature, it is again straightforward to control the parameters by a computer program. This is even more important because there is no simple way to check the size of the structures during the experiment.

As an optional modification gold can be evaporated on one side of the facets under a glancing angle [36]. This leads to an additional chemical pattern. To adjust the shallow angle under which the gold is evaporated a light pointing setup is used. The gold decorated substrates can be modified further by the use of SAMs of thiols or silanes (Fig. 3). Because of the large variety of these molecules this leads to a broad range of possible surface modifications. This thesis investigates the wetting properties of such substrates.

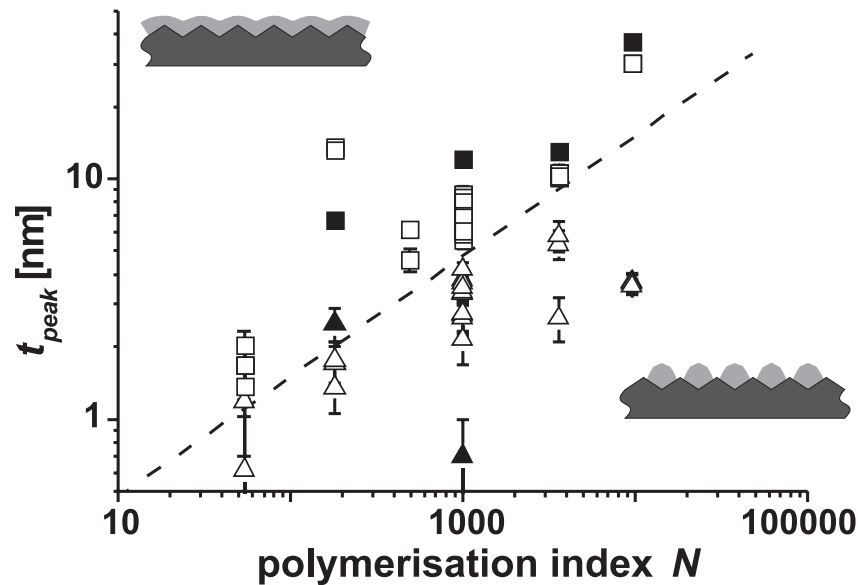


Figure 4: Stability of thin polystyrene films on corrugated substrates. Squares indicate stable PS films, while triangles refer to films, where the formation of nano-channels was observed. The dashed line indicates $t_{\text{peak}} = 0.55 R_g$. The solid symbols indicate data taken from substrates with no corrugation. From Ref. [22]

The wetting of structured substrates is an area of current interest [53-55]. The fundamental equation which describes the relation between the contact angle of the liquid and the surface energies of the components was already found in 1805 by Young [56]. In many experiments that study the wetting behavior polymers are used as model liquids. Their high viscosity and their negligible vapor pressure make them ideal to investigate several phenomena which are related to wetting. In addition, most polymers have a glass transition which makes it possible to interrupt the experiment at any given point. The stability of films that consist of low molecular liquids (e.g. water, organic solvents or metal melts) is influenced by van der Waals forces and the Hamaker constant [57]. With these parameters it is possible to give a quite complete description of wetting scenarios. However, if polymers are used additional effects are found. Most of these effects can be related to the intrinsic size of the polymer, given by the length of the chains which are confined between two interfaces (e.g. the glass transition temperature is not a constant in very thin films [58]).

Almost any real surface shows inhomogeneities in the surface chemistry or topography. Therefore substrates with a defined pattern are useful tools to control certain effects. First very thin films of polystyrene on substrates with a topographic pattern are studied. After preparation via spincoating, the film surface is relatively flat since the surface tension tries to

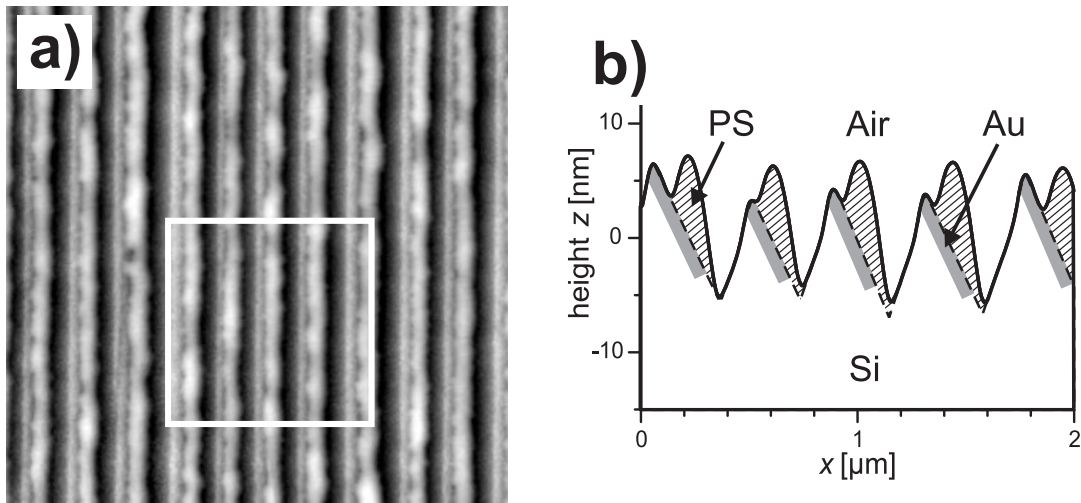


Figure 5: (a) SFM TappingMode™ topography image of a thin PS film on a chemically patterned, corrugated silicon substrate after annealing. The film has broken into linear anisotropic channels, with the PS dewetting preferentially to the side of the facet covered with gold. (b) Average line scan along the horizontal taken from the area inside the box indicated in image (a). The solid line is the experimental result. The dashed line depicts the position of the substrate surface. The approximate location of the gold is sketched on the figure. From Ref. [22]

reduce the surface area. This effect leads to a variation in the film thickness. After heating the film above the glass transition the film stays either stable with even a decreased surface roughness or breaks up forming polymer channels, if the film thickness drops below a critical value, which scales as $0.55 R_g$ (Fig. 4). The channels which are formed fill the grooves of the corrugation. To examine the influence of the corrugation, the results were also checked with films on a flat substrate (filled symbols in Fig. 4). Again the same behavior is found. In all cases the dewetting is nucleated at the thinnest regions, either at the ridge of the corrugation or at a particle on the flat surface. This shows that the intrinsic length scale of the polymer plays an important role on the stability of the film and should not be neglected when polymers are used as model liquids in wetting experiments.

On topographically and chemically structured substrates there is an additional driving force for dewetting. Polystyrene is known to preferentially wet gold [59] so polymer covered gold stripes are expected. This is true with exception of the highest parts of the corrugation (Fig. 5). Here the polystyrene is also dewetting the gold, which indicates an influence of the substrate topography. The position of the resulting polymer channels is now shifted towards the gold covered stripes. The variation of the surface energy gives the opportunity to study the dewetting of more realistic surfaces.

1.3 Pattern Formation via Surface Reconstruction in Thin ABC Triblock Copolymer Films

Other materials that form patterns on the nanometer scale are block copolymers. Microphase separation together with the connectivity of chemically different parts (blocks) of the molecule are the reason for the formation of ordered nanostructures [2]. Block copolymers can be synthesized via living anionic polymerization [60] or living radical polymerization [61]. With these techniques it is possible to create many possible combinations of polymers. Since most polymers are immiscible the blocks demix into different domains, which form periodic patterns with crystal-like order.

In contrast to classic crystals block copolymers show euclidian symmetry so their morphologies follow the more general principle of space groups. The most common morphologies are lamellae and, with decreasing block length of one component, cylinders and spheres as predicted in theoretical phase diagrams [2, 3]. Additionally there are narrow regions with other morphologies like the gyroid phase or the perforated lamella. The gyroid phase is of special interest since it is bicontinuous.

If block copolymers are brought into contact with an interface like a wall or a free surface, the interfacial tension between the individual blocks and the interface is an additional parameter which controls the morphology of the polymer. To minimize the interfacial tension the component with the lowest surface tension is found at the free surface [62, 63]. This effect leads to an alignment of the domains at the interface. Lamellae and cylinders are aligned parallel to the interface and the effect can extend deep into the bulk of the polymer film. In thin films, the influences of two surfaces overlap while the film thickness decreases [64]. If one component of a block copolymer is found at both interfaces we speak of symmetric

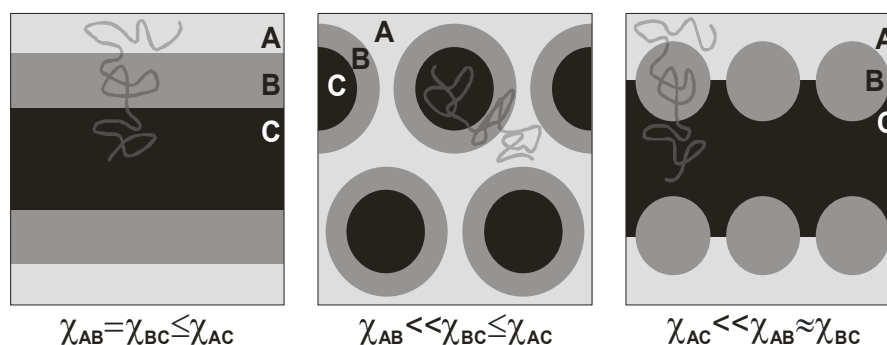


Figure 6: Morphologies of a symmetric ABC triblock copolymer with different interaction parameters of the three components. Adopted from Ref. [3]

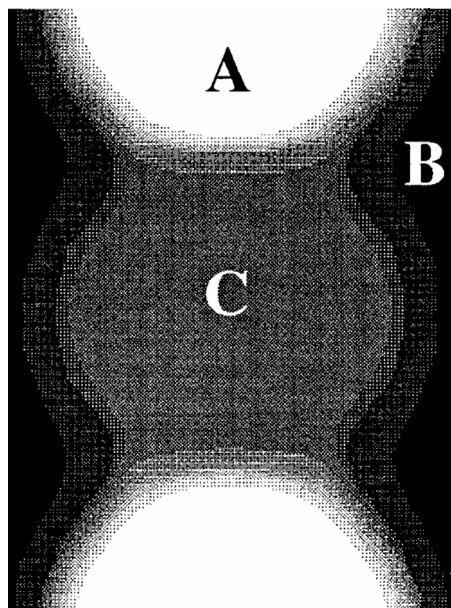


Figure 7: Computer simulation of the morphology of an ABC triblock copolymer confined between two wall which prefer the middle block. From Ref. [67]

wetting, otherwise it is called asymmetric wetting. If the film thickness does not match the intrinsic length scales, the system forms islands or holes with a higher or lower film thickness to circumvent an unfavorable situation [62].

The use of ABC triblock copolymers leads to a multitude of morphologies in the bulk (Fig. 6) [3, 65, 66]. For thin films simulations have already predicted new morphologies which differ remarkably from the bulk (Fig. 7) [67]. Experimental results also show a large variety of patterns in thin films (Fig. 8) [14, 68, 69]. With blends of ABC triblock and AC diblock copolymers it is possible to create non-centrosymmetric structures which open the field to new applications [13]. In the bulk, these morphologies typically form small domains of different orientation; therefore it is necessary to find ways to control the structures and their macroscopic alignment. The fact that the influence of interfaces on AB systems is well studied and interfaces appear in almost any system, it seems straightforward to investigate their influence on ABC systems in more detail. As a starting point we choose poly(styrene)-*block*-poly(butadiene)-*block*-poly(methylmethacrylate) (SBM) [70] with a lamellar morphology in the bulk phase. After preparing a film of several hundred nanometers thickness, the films were exposed to a chloroform vapor to equilibrate the system. Similar to the behavior of AB or ABA block copolymers the formation of islands and holes is observed. More detailed investigation of the film surface with atomic force microscopy (AFM) reveals two dot like patterns which appear alternating on different thicknesses of the film (Fig. 9). To identify the three different polymers we used selective etching in combination with AFM

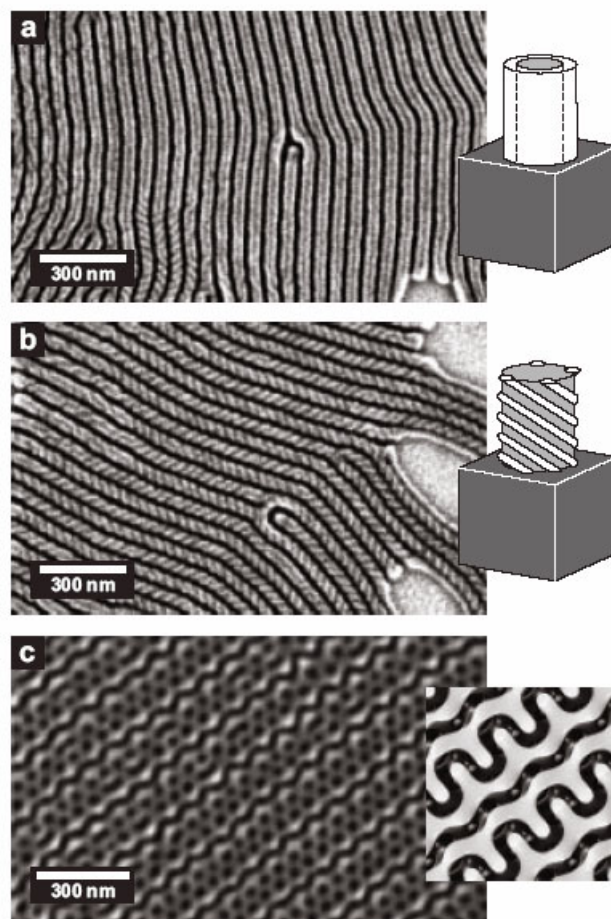


Figure 8: Thin film morphologies of different ABC triblock copolymers. (a) core-shell cylinders, (b) helices wound around a cylinder, (c) [112] plane of a double gyroid structure. From Ref. [34].

[71, 72], selective staining [70] combined with scanning electron microscopy, and quantitative TappingMode AFM [73] so that polystyrene, polymethylmethacrylate, and polybutadiene domains could be identified. With this information we proposed a model of the surface structure (Fig. 10) [24]. The two different layers can be described as a perforated lamella of polystyrene in a matrix of polymethylmethacrylate and vice versa. In both cases we find a thin layer of polybutadiene which covers the free surface. This is consistent with the results for AB block copolymer films. The rearrangement of the polymer domains is driven by the reduction of the surface energy. Furthermore, the gain in energy by placing the polybutadiene at the free surface is large enough to compensate the loss by the formation of an additional interface between polystyrene and polymethylmethacrylate. To test the influence of the molecular weight we used a smaller SBM which shows the same behavior. If the block sequence is changed to BSM, no lateral surface pattern is found because there is no rearrangement needed to expose polybutadiene, the block with the lowest surface energy, to

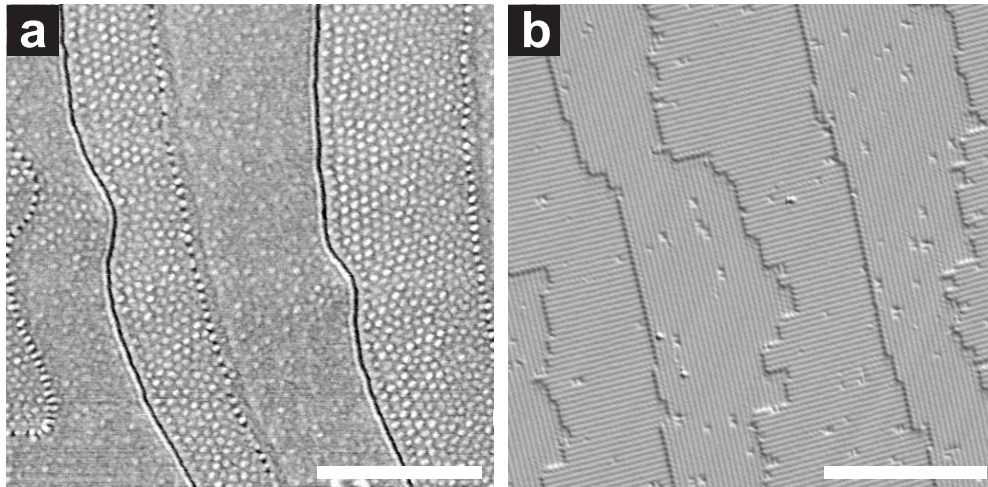


Figure 9: (a) TappingMode™ SFM phase image of a SBM¹⁶² film showing the two different kinds of terraces at the free surface. Scale bar: 1 μm . (b) Scanning tunneling microscopy image of a stepped Si(100) surface forming a (2 \times 1) surface reconstruction (Courtesy of M.G. Lagally, University of Wisconsin, Madison). The different orientations of neighboring terraces are clearly visible. Scale bar: 5 nm. From Ref. [24].

the free surface. By using polybutylmethacrylate instead of polymethylmethacrylate the chemistry of the third block is changed and the interaction between the three components is altered. So the end block and the middle block have now comparable surface tensions [70]. Again we do not find a lateral surface pattern, but a featureless surface and film thicknesses which are typical for a block copolymer film under symmetric wetting conditions.

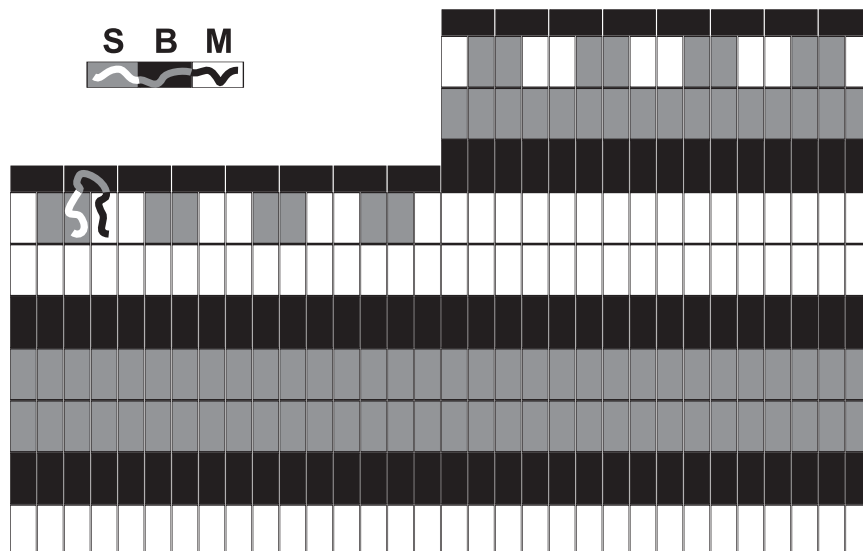


Figure 10: Schematic model of the near surface morphology of SBM¹⁶². From Ref. [24].

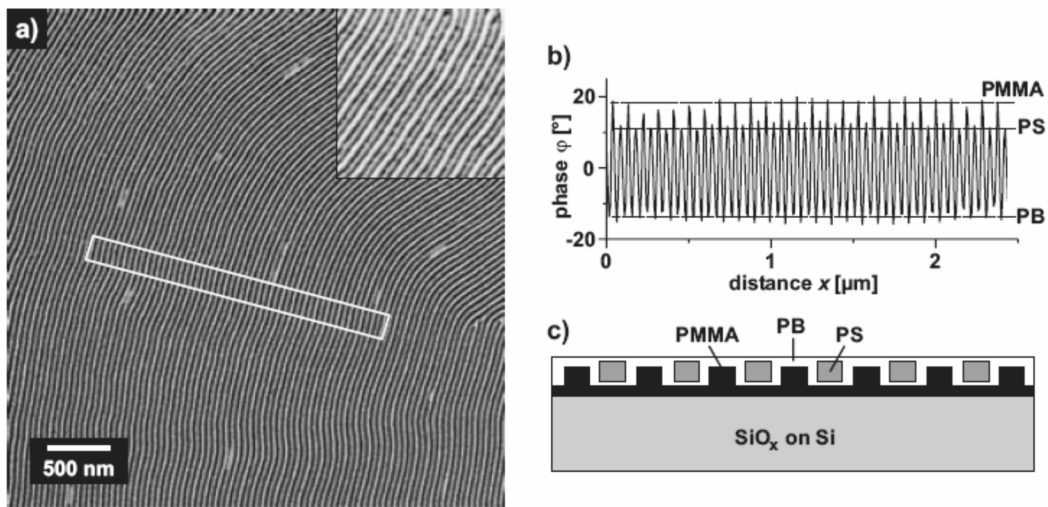


Figure 11: (a) TappingMode phase image of an SBM triblock copolymer. (b) Phase signal averaged along the short side of the box in (a). (c) Schematic model of the thin film morphology. From Ref. [34].

If the films of SBM are thinner than one long period of the lamellar spacing all three polymers are present at the surface and form a stripe-like pattern (Fig. 11) [24]. Here the effects of interfacial energies at the substrate and the free surface overlap with confinement effects.

The reconstruction of a block copolymer surface was first described by Stocker *et. al.* [74]. There are remarkable similarities to surface reconstructions in single crystals. Instead of highly ordered electron densities, block copolymers consist of ordered polymer components.

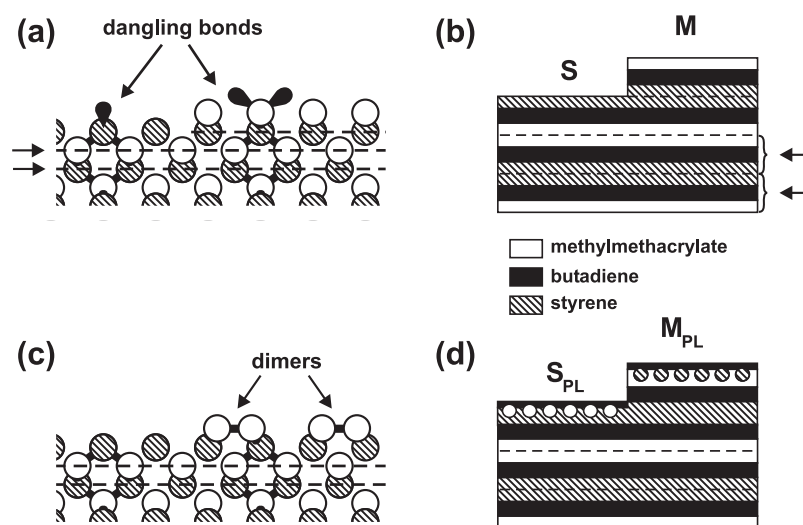


Figure 12: Schematic model of ideal (left) and reconstructed surfaces (right) of Si(100) (a, c) and SBM (b, d). The arrows in (a) and (b) indicate the non-equivalent layers. From Ref. [24]

In both cases a rearrangement of the ideal surface structure is found to reduce the total free energy of the system [51]. The comparison of the lamellar ABC triblock copolymer with the Si(100) surface [75, 76] shows another striking similarity. Both systems have two non-equivalent layers of matter parallel to the surface which leads to two different terminations of the surface (Fig. 12). Along with the two different surface patterns, the shape of the steps alternates as well.

This work shows the significance of surface energies and confinement on the formation of laterally patterned structures. Triblock copolymers form patterned surfaces with very periodic and, compared to diblock copolymers, rather complex structures. However, over large areas these structures have no common orientation. The structured substrates, on the other hand, have a defined orientation over very large areas but their patterns lack the high periodicity of the block copolymers. A combination of both advantages might lead to very defined structures with interesting properties.

1.4 Individual Contributions of the Authors

I have improved a method to prepare substrates with a chemical and topographical structure on the nanometer scale (Chapter 2). Markus Hund has assisted me writing the control program for this automated procedure. Also part of the experiments was planned and discussed with Markus Hund. I have analyzed the data and successively improved the method by applying several new steps to the procedures. I have profited from scientific discussions with Georg Krausch.

I have studied the stability of thin polymer films on such nanostructured substrates (Chapter 3). I have performed all relevant experiments and have analyzed all data. Some of the experiments have been done by Chun Wang in close collaboration with me. Markus Hund has prepared some of the substrates and has done the programming for the substrate preparation. Mark Geoghegan has contributed to the interpretation of the results in the context of existing theories. I have also profited from discussions with Georg Krausch and Robert Magerle.

I have planned and performed all experiments to analyze and to interpret the surface reconstruction of triblock copolymers (Chapter 4 and 5) except the quantitative scanning probe measurement which was done together with Armin Knoll. The experiment to obtain the etching rates which was done by Matthias Konrad. During the interpretation of the data I profited from discussions with Georg Krausch and Robert Magerle. I set up the model for the

structure of the reconstructed surface and did further experiments to verify this model. I have also studied the influence of the molecular weight. Together with Georg Krausch and Robert Magerle I have elaborated the analogies to single crystal surface reconstructions. The proposed nomenclature was introduced mainly by Robert Magerle in discussion with Georg Krausch and me.

1.5 References

- [1] R. P. Feynman, *Eng. Sci.* **1960**, *23*, 22.
- [2] I.W. Hamley, *The Physics of Block Copolymers*; Oxford University Press: Oxford, **1998**.
- [3] F. S. Bates and G. H. Fredrickson, *Phys. Today* **1999** *52*, 32.
- [4] I.W. Hamley, *Angew. Chem. Int. Ed.* **2003**, *42*, 1692.
- [5] C. Park, J. Yoon, E.L. Thomas, *Polymer* **2003**, *44*, 6725
- [6] G.M. Whitesides, B. Grzybowski, *Science* **2002**, *295*, 2418.
- [7] N.C. Seeman, *Trends Biotechnol.* **1999**, *17*, 437.
- [8] C.M. Niemeyer, *Curr. Opin. Chem. Biol.* **2000**, *4*, 609
- [9] U. Breiner, U. Krappe, and R. Stadler *Macromol. Rapid Commun.* **1996**, *17*, 567.
- [10] T. Goldacker, V. Abetz, *Macromolecules* **1999**, *32*, 5165-5167.
- [11] T.A. Shefelbine, M.E. Vigild, M.W. Matsen, D.A. Hajduk, M.A. Hillmyer, E.L. Cussler, F. S. Bates, *J. Am. Chem. Soc.* **1999**, *121*, 8457
- [12] T. Hashimoto, N. Mitsumura, D. Yamaguchi, M. Takenaka, H. Morita, T. Kawakatsu, and M. Doi, *Polymer* **2000**, *42*, 8477.
- [13] V. Abetz, T. Goldacker, *Macromol. Rapid Commun.* **2000**, *21*, 16.
- [14] S. Ludwigs, A. Böker, A. Voronov, N. Rehse, R. Magerle, and G. Krausch, *Nature Mat.* **2003**, *2*, 744.
- [15] A.C. Finnefrock, R. Ulrich, G.E.S. Toombes, S.M. Gruner, and U. Wiesner, *J. Am. Chem. Soc.* **2003**, *125*, 13084.
- [16] K. Amundson, E. Helfand, D.D. Davis, X. Quan, S.S. Patel, and S.D. Smith, *Macromolecules* **1991**, *24*, 6546

- [17] P. Mansky, Y. Liu, E. Huang, T.P. Russell, C. Hawker, *Science* **1997**, 275, 1458
- [18] T.L. Morkved, M. Lu, A.M. Urbas, E.E. Ehrichs, H.M. Jaeger, P. Mansky, T.P. Russell, *Science* **1996**, 273, 931.
- [19] Y. Bohbot-Raviv and Z.-G. Wang, *Phys. Rev. Lett.* **2000**, 85, 3428
- [20] F. Ebert and T. Thurn-Albrecht, *Macromolecules* **2003**, 36, 8685
- [21] M. Hund, N. Rehse, and G. Krausch, *to be published*.
- [22] N. Rehse, C. Wang, M. Hund, M. Geoghegan, R. Magerle, and G. Krausch, *Eur. Phys. J. E* **2001**, 4, 69.
- [23] N. Rehse, A. Knoll, M. Konrad, R. Magerle, and G. Krausch, *Phys. Rev. Lett.* **2001**, 87, 035505.
- [24] N. Rehse, A. Knoll, R. Magerle, and G. Krausch, *Macromolecules* **2003**, 36, 3261.
- [25] R.D. Piner, J. Zhu, F. Xu, S. Hong, and C. Mirkin, *Science* **1999**, 283, 661.
- [26] A. Ivanisevic and C. A. Mirkin, *J. Am. Chem. Soc.* **2001**, 123, 7887.
- [27] S. Krämer, R.R. Fuierer, C.B. Gorman, *Chem. Rev.* **2003**, 103, 4367.
- [28] P. B. Fischer and S. Y. Chou, *Appl. Phys. Lett.* **1993**, 62, 2989.
- [29] D.M. Tennant in G. Timp (Ed.) *Nanotechnology*; Springer-Verlag: Heidelberg, **1999**.
- [30] X. Wang, W. Hu, R. Ramasubramaniam, G. H. Bernstein, G. Snider, and M. Lieberman, *Langmuir* **2003**, 19, 9748.
- [31] S. Song and S.G.J. Mochrie, *Phys. Rev. Lett.* **1994**, 73, 995.
- [32] K. Fukunaga, H. Elbs, and G. Krausch, *Langmuir* **2000**, 16, 3474.
- [33] L. Chi, S. Jacobi, B. Anczykowski, M. Overs, H.-J. Schäfer, and H. Fuchs, *Adv. Mater.* **2000**, 12, 25.
- [34] G. Krausch and R. Magerle, *Adv. Mat.* **2002**, 14, 1579.
- [35] M.J. Fasolka, D.J. Harris, A.M. Mayes, M. Yoon, and S.G.J. Mochrie, *Phys. Rev. Lett.* **1997**, 79, 3018.
- [36] L. Rockford, Y. Liu, P. Mansky, T.P. Russell, M. Yoon, and S.G.J. Mochrie, *Phys. Rev. Lett.* **1999**, 82, 2602.
- [37] C. Park, J.Y. Cheng, C. De Rosa, M.J. Fasolka, A.M. Mayes, C.A. Ross, and E.L. Thomas, *Appl. Phys. Lett.* **2001**, 79, 848.

- [38] K. Naito, H. Hieda, M. Sakurai, Y. Kamata, and K. Asakawa *IEEE Trans. Magn.* **2002**, 38, 1949.
- [39] S. Song and S.G.J. Mochrie, *Phys. Rev. B* **1995**, 51, 10068.
- [40] S. Song, S.G.J. Mochrie, and G.P. Stephenson, *Phys. Rev. Lett.* **1995**, 74, 5240.
- [41] A. Kumar and G.M. Whitesides, *Appl. Phys. Lett.* **1993**, 63, 2002.
- [42] N.L. Abbott, J.P. Folkers, and G.M. Whitesides, *Science* **1992**, 257, 1380.
- [43] Y. Xia and G.M. Whitesides, *Angew. Chem. Int. Ed.* **1998**, 37, 550.
- [44] G. Reiter, G. Castelein, P. Hoerner, G. Riess, A. Blumen, and J.-U. Sommer, *Phys. Rev. Lett.* **1999**, 83, 3844.
- [45] J. A. Dagata, J. Schneir, H. H. Harary, C. J. Evans, M. T. Postek, and J. Bennett, *Appl. Phys. Lett.* **1990**, 56, 2001
- [46] P. Mansky, P. Chaikin, and E.L. Thomas, *J. Mater. Sci* **1995**, 30, 1987.
- [47] M. Park, C. Harrison, P.M. Chaikin, R.A. Register, and D.H. Adamson, *Science* **1997**, 276, 1401.
- [48] R.G.H. Lammertink, M.A. Hempenius, J.E. Van Den Enk, V.Z.H. Chan, E.L. Thomas, and G.J. Vansco, *Adv. Mater.* **2000**, 12, 98.
- [49] J.P. Spatz, S. Mössmer, C. Hartmann, M. Möller, T. Herzog, M. Krieger, H.-G. Boyen, P. Ziemann, and B. Kabius, *Langmuir* **2000**, 16, 407.
- [50] M. Haupt, S. Miller, A. Ladenburger, R. Sauer, K. Thonke, J.P. Spatz, S. Riethmüller, M. Möller, and F. Banhart, *J. Appl. Phys.* **2002**, 91, 6057.
- [51] A. Zangwill, *Physics at Surfaces*; Cambridge University Press: Cambridge, **1988**.
- [52] B.S. Swartzentruber, Y.-W. Mo, M.B. Webb, and M.G. Lagally, *J. Vac. Sci. Technol. A* **1989**, 7, 2901.
- [53] P.G. de Gennes, *Rev. Mod. Phys.* **1985**, 57, 827.
- [54] G.H. Findenegg and S. Herminghaus, *Curr. Opin. Colloid. Interf. Sci.* **1997**, 2, 301.
- [55] M. Geoghegan and G. Krausch, *Prog. Polym. Sci.* **2003**, 28, 261.
- [56] T. Young, *Phil. Trans. Roy. Soc.* **1805**, 95, 65.
- [57] J. Israelachvili, *Intermolecular and Surface Forces*; Academic Press: New York, **1992**.
- [58] S. Herminghaus, K. Jacobs, and R. Seemann, *Eur. Phys. J. E* **2003**, 12, 101.

- [59] T.P. Russell, G. Coulon, V.R. Deline, and D.C. Miller, *Macromolecules* **1989**, *22*, 4600.
- [60] M. Szwarc, *Nature* 1956, *178*, 1168.
- [61] C.J. Hawker, *J. Am. Chem. Soc.* **1994**, *116*, 11185.
- [62] S. H. Anastasiadis, T. P. Russell, S. K. Satija, and C. F. Majkrzak, *Phys. Rev. Lett.* **1989**, *62*, 1852.
- [63] H. Hasegawa and T. Hashimoto, *Macromolecules*, **1985**, *18*, 589.
- [64] A. Knoll, A. Horvat, K.S. Lyakhova, G. Krausch, G.J.A. Sevink, A.V. Zvelindovsky, R. Magerle, *Phys. Rev. Lett.* **2002**, *89*, 035501.
- [65] C. Auschra and R. Stadler, *Macromolecules* **1993**, *26*, 2171.
- [66] Y. Mogi, M. Nomura, H. Kotsuji, K. Ohnishi, Y. Matsushita, and I. Noda, *Macromolecules* **1994**, *27*, 6755.
- [67] G.T. Pickett, A.C. Balazs, *Macromol. Theory Simul.* **1998**, *7*, 249.
- [68] H. Elbs, C. Drummer, V. Abetz, G. Hadziioannou, and G. Krausch, *Macromolecules* **2001**, *34*, 7917.
- [69] H. Elbs, C. Drummer, V. Abetz, and G. Krausch, *Macromolecules* **2002**, *35*, 5570.
- [70] T. Goldacker, Ph.D. Thesis, Universität Bayreuth, Bayreuth, **1999**.
- [71] M. Konrad, Diploma Thesis, Universität Bayreuth, Bayreuth, **1999**
- [72] M. Konrad, A. Knoll, G. Krausch, and R. Magerle, *Macromolecules* **2000**, *33*, 5518.
- [73] A. Knoll, R. Magerle, G. Krausch, *Macromolecules* **2001**, *34*, 4159.
- [74] W. Stocker, J. Beckmann, R. Stadler, and J.P. Rabe, *Macromolecules* **1996**, *29*, 7502.
- [75] R.M. Tromp, R.J. Hamers, and J.E. Demuth, *Phys. Rev. Lett.* **1985**, *55*, 1303.
- [76] D. Dijkamp, A.J. Hoeven; E.J. v. Loenen, J.M. Lenssinck, and J. Dieleman, *Appl. Phys. Lett.* **1990**, *56*, 39.

Preface to Chapter 2

This chapter is not yet published.

2 Automated preparation of chemically nanopatterned substrates

Nicolaus Rehse*, Markus Hund, and Georg Krausch

Lehrstuhl für Physikalische Chemie II, Universität Bayreuth, D-95440 Bayreuth, Germany

*corresponding author

2.1 Introduction

Great efforts have been made to produce nanometer scaled structures for many applications. Most of the methods are based on lithography which brings certain limitations [1]. As an alternative, self organization of matter offers the opportunity to create very regular structures [2]. Here we present an automated procedure to prepare chemically and topographically patterned structures with nanometer sized features on a cm^2 sized silicon wafer. The method is

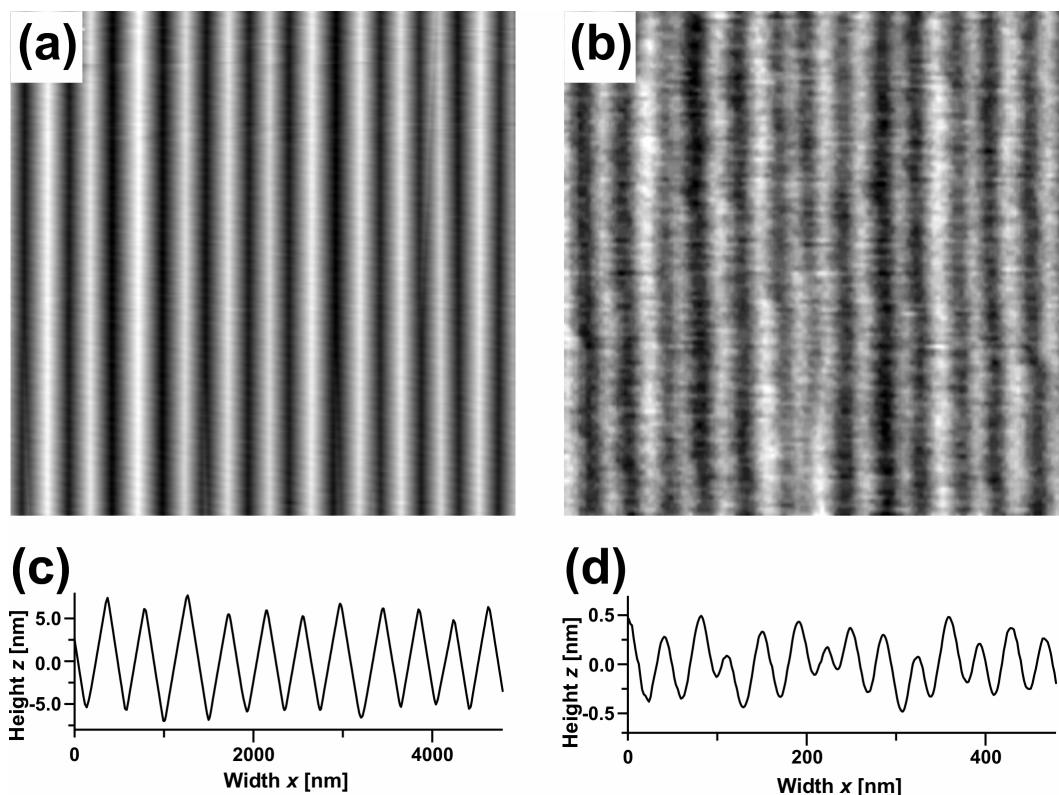


Figure 1: Topography images of stepped silicon surfaces with 400 nm (a; $4.5 \times 4.5 \mu\text{m}^2$) and 40 nm (b, $0.45 \times 0.45 \mu\text{m}^2$) mean step width obtained by TappingMode AFM. (c) and (d) show the height profiles averaged along the direction of the steps of (a) and (b), respectively.

based on the faceting of semiconductor surfaces [3]. We use a silicon wafer with a Si(113) surface which was miscut by a few degrees towards the $\langle 114 \rangle$ direction. The phase behavior of this surface was studied in detail by Mochrie and coworkers [4-6]. The distance between the resulting facets is in a range of 40 – 400 nm and the corrugation depth ranges between 1 and 10 nm (Fig. 1). These lengths and the fact that the facets, which form on the clean silicon surface, are preserved during oxidation make this surface an ideal starting point for further

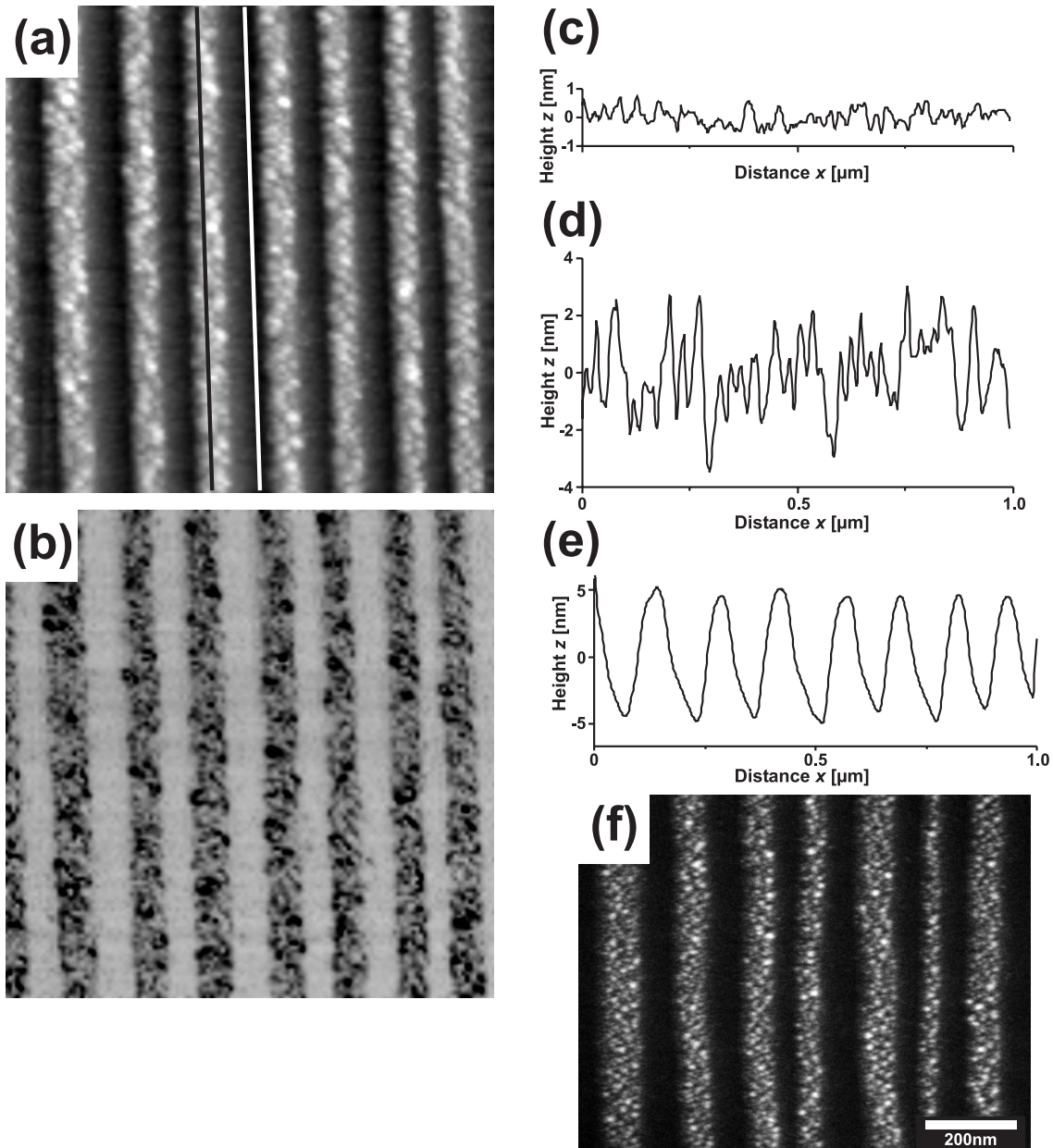


Figure 2: Topography (a) and TappingMode phase (b) image ($1.0 \times 1.0 \mu\text{m}^2$) of a stepped silicon surface with metal stripes. (c) and (d) show the height profiles along the black and the white line in (a), respectively. (e) shows a height profiles averaged along the direction of the steps. (f) SEM image of this sample.

manipulation. Metal evaporation under a glancing incidence leads to a deposition of metal on every other facet, resulting in a chemically patterned surface (Fig. 2) [7].

Structures of this kind have been used to study the influence of the corrugation and the chemical heterogeneity on the ordering of block copolymer films [7-9] and the dewetting behavior of ultra thin homopolymer films [7, 10].

Since the preparation of such structures involves numerous processing steps between the starting material and the final patterned substrate, automation is a straightforward idea to produce samples with a higher throughput, high quality, and less loss through waste. In this way preparing nano-patterned substrates gets a routine method which can be carried out by a technically skilled person after a relatively short training.

2.2 Apparatus

First we shall give a description of the setup we use for our experiments. A schematic of the UHV chamber and the additional components to produce stepped silicon samples is shown in Fig. 3. The chamber is based on a spherical 6-way cross with a diameter of 300 mm and 6

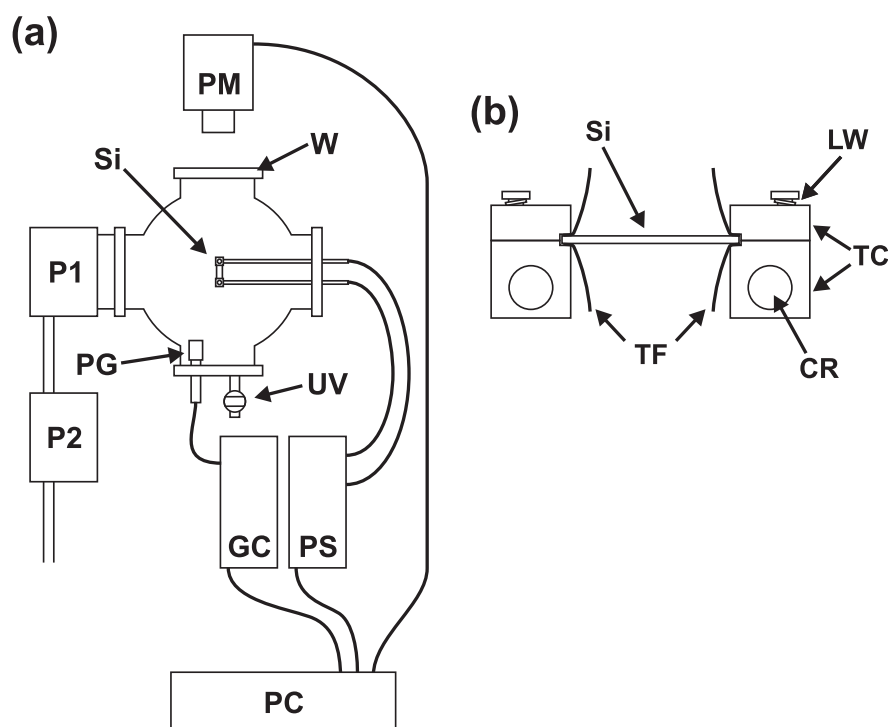


Figure 3: Schematic drawing of the UHV setup (a) and the sample holder (b). Note that the pyrometer is not focusing on the sample surface for drawing reason. The labeling is as follows: Si: silicon sample, PM: pyrometer, W: window, PS: power supply, P1: turbo pump, P2: forevacuum pump, PG: pressure gauge, UV: UHV valve, GC: gauge controller, LW: lock washer, TC: tantalum clamp, TF: tantalum foil, CR: copper rod.

ISO 100 ultrahigh vacuum (UHV) flanges (CX6LS-100, Caburn-MDC, Glynde, UK). It is equipped with a UHV-valve for venting the UHV chamber with various gases and a nude Bayard-Alpert type ionization gauge (Varian Type 580 with senTorr gauge controller BA2C with RS232 interface, Varian Vacuum Products Turin, Italy) to measure pressures in the range of 2×10^{-1} to 5×10^{-10} mbar. An RS232 interface is used to monitor the pressure during all steps of the preparation. The pumping system consists of a turbo molecular pump (Turbo-V 150HT, Varian, 130 l/s) directly attached to the UHV chamber and a rotary roughing pump. The sample temperature is measured with a pyrometer (Infratherm IS 10, IMPAC Electronic, Frankfurt/Main, Germany) with a response time of 1ms and an accuracy of ± 1 K. The output of the pyrometer is monitored via an RS232 interface. The sample holder is based on an electrical feed-through (Caburn-MDC) with two copper rods. A detailed sketch is shown in Fig. 3 (b). All parts of the clamps are made from tantalum to withstand the high temperatures with minimum degassing. We use small pieces of annealed tantalum foil to assure good electrical contact between the silicon and the clamps. To avoid fracture of the brittle silicon the screws are equipped with a lock washer. The copper rods are connected to a computer controlled power supply (EA-PS 5032-30A with IEEE 488.1 interface EA-PSP 5612, Elektro-Automatik, Viersen, Germany) with an output current ranging from 0 to 30 A and an output voltage range of 0...32 V. The current resolution is given by 7.5 mA. It was our intention to build a compact setup which fits into a standard laboratory. All electronic devices including the computer are mounted in a 19"-rack. The UHV chamber and the pumping system fit on an area of 1 m².

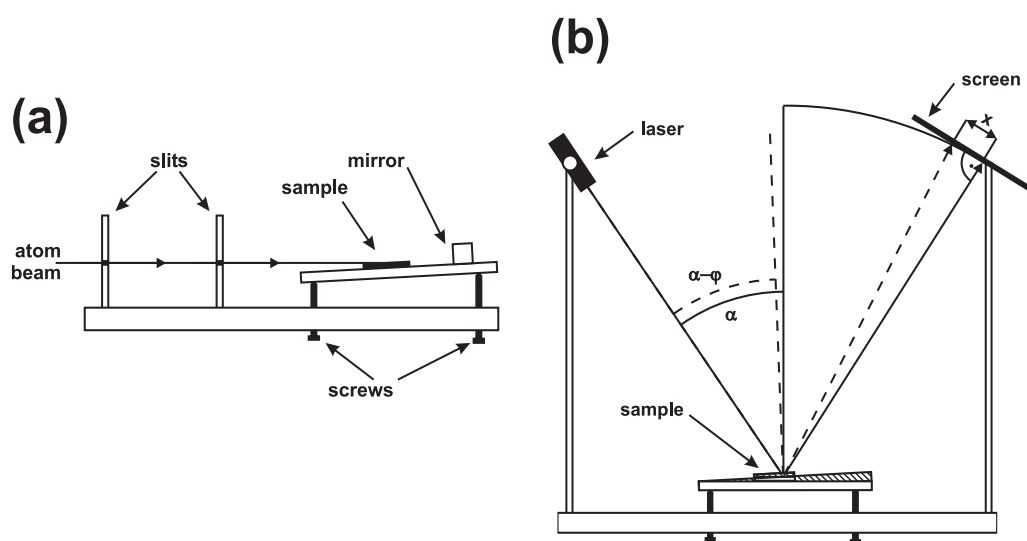


Figure 4: Schematic drawing of the evaporation stage (a) and adjustment setup (b). Note that we left out the slits and the mirror in (b) for clearness.

The preparation of the chemical pattern is done in a vacuum evaporation chamber (BA 360, Balzers AG, Balzers, Liechtenstein) with diameter and height of the bell jar of 350 mm and 450 mm, respectively. The thickness of evaporated metals is monitored by a quartz microbalance (QSG 301, Balzers). The resulting frequency shifts are passed to a frequency monitor (6½-digit multimeter, Keithley 2000, Keithley Instruments, Cleveland, OH) connected to a personal computer. The evaporation stage and adjustment setup for the samples are sketched in Figure 4. The stage is based on an aluminum plate with a pair of slits (1 mm width) mounted vertically in a row with a distance of 30 mm. Behind the slits, a smaller plate with a spring is mounted on the base. Three screws allow us to tilt the table in two directions. The smaller plate has two small sheets of copper attached, which fix the sample to the plate. Perpendicular to the small plate a piece of silicon is mounted as a mirror for the alignment procedure and for film thickness calibration.

To adjust of the tilt angle, two aluminum rods with a length of 300 mm are attached to the base plate (Fig 4b). One is carrying a small laser diode, the other one carries a screen made from scale paper.

2.3 Procedure

To produce corrugated silicon substrates we use commercially available silicon wafers (Crystec, Berlin, Germany) with a size of $5 \times 12 \times 0.5 \text{ mm}^3$ and a resistance of

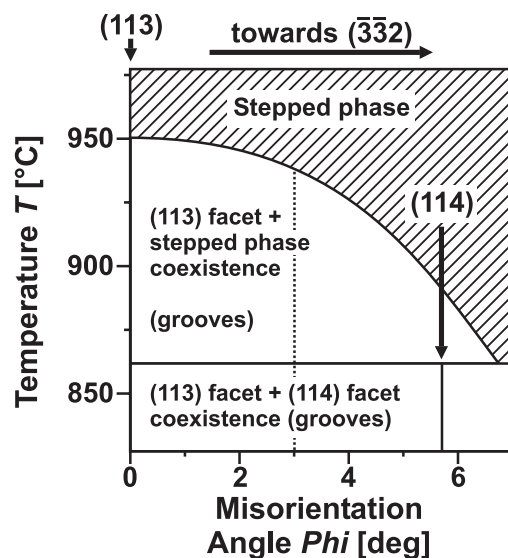


Figure 5: Orientational phase diagram of the silicon (113) surface miscut towards $(\bar{3}\bar{3}2)$
Adopted from Ref. [6]. The dashed line indicates a miscut angle of 3° . The arrows indicate the (113) and the (114) surfaces, respectively.

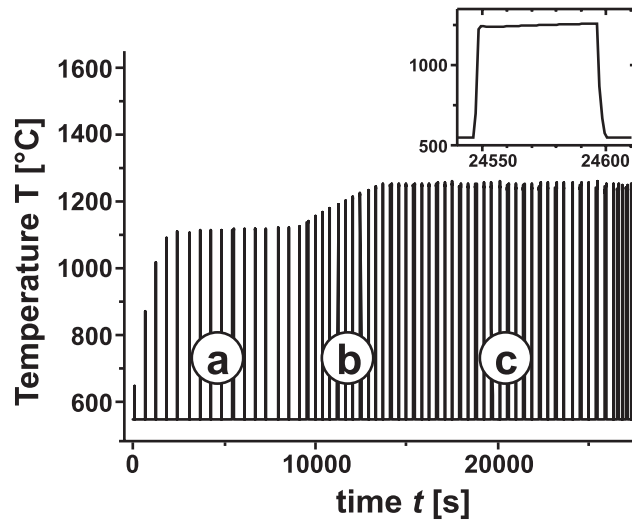


Figure 6: Temperature vs. time diagram of a typical cleaning procedure. (a) marks the first cleaning sequence with a threshold pressure $p_{thres.} = 5 \times 10^{-9}$ mbar. (b) marks the second sequence in which the temperature is adjusted between 1230° and 1250°C by altering the current in steps of $\Delta I = 0.3$ A. (c) marks the following cleaning steps. The inset shows a single cleaning step.

$\rho \leq 20 \text{ m}\Omega \text{ cm}^{-1}$ (arsenic doped) to enable resistive heating. The wafers were polished on one side with an rms roughness $< 1 \text{ nm}$ as measured by atomic force microscopy (AFM). The surface normal of the samples is pointing $3 \pm 0.5^\circ$ off the $\langle 113 \rangle$ crystal axis towards the $\langle 001 \rangle$ axis. This orientation results in equal surface areas covered with (113) and (114) facets, respectively [6]. By changing the surface orientation it is possible to adjust the ratio of the area covered by the two facets according to the surface phase diagram shown in Figure 5.

The wafers were rinsed three times with a 50 vol.-% mixture of *n*-hexane in acetone (both *p.a.*, Merck, Germany). Subsequently they were cleaned with a stream of gaseous and solid CO_2 (Snow-Jet) to remove possible organic residues from the polishing process. This procedure is necessary to avoid contamination of the UHV chamber and the sample surface itself. The samples were then installed into the sample holder which clamps the wafer on both short sides. It is important to mount the sample with the $\langle 001 \rangle$ direction pointing parallel to the electrical current to avoid the growth of very large terraces [6]. After installing the sample holder and closing the UHV chamber, we evacuate the UHV chamber and bake it out for 10 hours at 200°C . After this procedure pressure should fall below $p < 3 \times 10^{-9}$ mbar.

The native oxide layer of the silicon sample is then removed by cyclic heating. Care has to be taken not to exceed a certain pressure value during this procedure. Therefore the heating of the silicon wafer is switched off as soon as the pressure in the vacuum chamber exceeds a

threshold value of $p_{thres.} = 5 \times 10^{-9}$ mbar (Fig. 6). Especially in the beginning of the cleaning this is very delicate as the sample becomes hazy quite fast [11]. This hazy appearance is a result of micrometer large roughness on the surface which cannot be removed by further cleaning. Since the pressure increases within milliseconds during the initial heating steps the whole cleaning process is computer controlled enabling fast reaction to the rising pressure. When the threshold pressure is reached, the heating is interrupted for 10 minutes to reduce the pressure again. In a first sequence this procedure is repeated 15 times. In the following sequence of heating cycles the current is subsequently increased until the temperature of the sample has reached 1250°C . Two additional sequences follow in which the threshold pressure $p_{thres.}$ is raised incrementally to 1×10^{-8} mbar. The temperature is monitored using the pyrometer. The sample is considered clean if the pressure stays below $p_{crit.} = 1 \times 10^{-8}$ mbar for $t = 2$ min at a substrate surface temperature of $T \approx 1250^\circ\text{C}$. A typical cleaning procedure takes about 10 h and needs no attention during the process.

After the cleaning process the sample is heated up to 1250°C again for 30 seconds and then cooled down to 980°C regulated by the computer. The sample is kept at this temperature for 100 seconds to equilibrate in the disordered phase (i.e. above 960°C , see Fig. 5). During these steps of the preparation the pressure is monitored and the preparation is stopped if the pressure exceeds $p_{thres.} = 3 \times 10^{-8}$ mbar to avoid damage of the sample. Subsequently, the sample is cooled at a cooling rate of $r = -2$ K/min to $T_{prep.} = 800^\circ\text{C}$. The cooling rate is controlled by the computer decreasing the temperature in steps of 1K (see inset in Fig. 7a). At

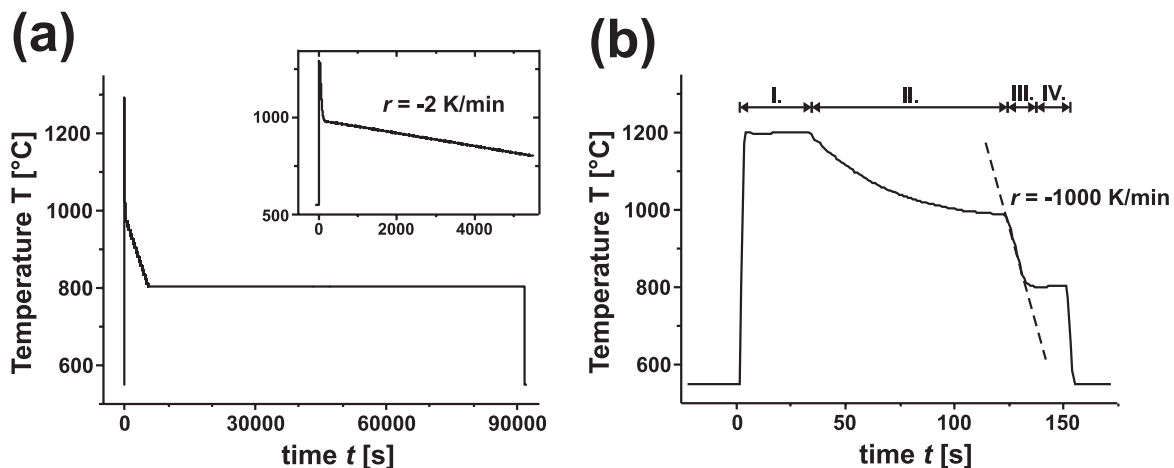


Figure 7: Temperature vs. time diagrams of the preparation of large (a) and small (b) steps. The inset in (a) shows a magnification of the cooling ramp from 980°C to 800°C with a rate of $r = -2$ K/min. I. labels the initial jump to 1200°C , II. is the cooling to 980°C , III. marks the fast cooling ramp from 980°C to 820°C with a rate of $r = -1000$ K/min indicated by the dashed line. IV. marks the preparation time $t_{prep.}$.

this temperature the sample is kept for a certain time $t_{prep.}$. To keep the temperature constant, a PID algorithm is used to adjust the heating current. Otherwise slight changes in the transition resistance and effects of increasing temperature of the setup would alter $T_{prep.}$. By switching off the current we stop the procedure. The sample is then allowed to cool down to room temperature. Since the working range of the pyrometer ends at 549°C we are not able to monitor the whole cooling process. A temperature curve for preparation of 400 nm steps is given in Figure 7a.

To create step widths below 100 nm the last part of the procedure is slightly different (Fig. 7b). In order to improve the time resolution, the sampling rate of the pyrometer is increased to 1 ms⁻¹ (Large steps are made with a sampling rate of 1 s⁻¹). The ramp beginning at 980°C has a very fast cooling rate of $r \approx -1000$ K/min. This ramp is not regulated and we use empirical values for ΔI and Δt in order to keep the cooling rate fast. At $T = 840^\circ\text{C}$, the current is not further decreased but the temperature continues to drop down to $T_{prep.} \approx 800^\circ\text{C}$. We do not use regulation this time because of the very short time used for preparation of samples with small terraces ($t_{prep.} < 20$ s). Again the temperature quench at the end of the treatment is realized by simply switching off the current.

The preparation time $t_{prep.}$ can be correlated to the width of the grooves in both cases since a power law for the dynamics of step formation is found theoretically and in in-situ experiments with $\phi = 1/6$ [6]. The exponent of the power law based on our results $\phi = 0.17$ deviates little from the published results at a given temperature which may be due to the undefined cooling of the samples. We also did not include the temperature ramp (III. in Fig. 7) in our calculations of the annealing time since we have no constant temperature at this time of preparation. Nevertheless our experiments agree reasonably well.

After preparation of the stepped surface the UHV chamber is filled with air filtered through a particle filter. The silicon will instantaneously form an amorphous oxide layer but the stepped structure of the surface will remain. We then investigate the surface with TappingMode AFM to measure the mean width between the grooves (Fig. 1). Typically we get deviation of $\pm 10\%$ of the mean width throughout the whole sample. This is based on small differences of the surface temperature during preparation. To avoid larger deviations a good electrical contact between the clamps and the sample is important.

The surface exhibits triangularly shaped grooves with mean widths ranging from 40 nm - 4000 nm depending on the choice of the annealing time $t_{prep.}$. The angle between successive facets is determined by the angle between the (113) and (114) crystallographic planes

($\alpha = 5.8^\circ$). As a result, the grooves are 2 - 10 nm deep. We note that the height scale and the lateral scales of the height profiles in Figure 1 are significantly different, strongly exaggerating the aspect ratio of the grooves. The pattern extends over the entire wafer and the orientation of the grooves is the same over the entire area since it is determined by the orientation of the crystallographic planes.

To create a chemical pattern the sample is placed on the evaporation setup shown in Figure 4a. First we adjust the sample's surface to the same height as the two aperture slits with help of a laser beam which illuminates the front of the sample and the mirror behind the sample. If the light is reflected back through the two slits, the sample is parallel to the axis defined by the two slits. If then the front of the sample is also illuminated the height is adjusted. Afterwards we can easily adjust a very small tilt angle of the table by using a simple geometric light pointer setup (Fig. 4b). The light of the laser pointer which is now mounted to one of the aluminum rods points at the sample surface and is reflected onto the screen. By measuring the shift of the reflected laser spot, we are able to position the sample in a well defined angle.

By adjusting the tilt angle between 0° and 4° we can deposit material only on top of the gratings or on every other facet, respectively. Depositing some nanometers of material from the direction of the initial surface normal would lead to a completely covered surface preserving the stepped structure of the substrate so one can study for example a stepped surface with different metals.

The whole plate is transferred into the bell jar after removing the aluminum rods. The distance between the evaporation dish and the sample is 400 mm. We evacuate the evaporation chamber to $p = 10^{-5}$ mbar. To provide an adhesive layer for the gold a thin chromium layer is evaporated at first. Then the gold is evaporated in the same way. The thickness ratio between the chromium and the gold layer should be 1:3 according to Rockford *et al.* [7]. To improve the evaporation results we calibrate the evaporation setup with a piece of silicon which is mounted vertically on the evaporation setup (i.e. the position of the mirror in Figure 4a) so the vapor beam hits the surface under an angle of 90° . The process is monitored by a quartz microbalance. After the evaporation of the metal layer its thickness is measured by AFM and correlated to the change in frequency of the quartz microbalance. Using the values for both metals we are able to calculate a frequency ratio for the quartz microbalance. Since all samples are measured before and after evaporation we can improve the process iteratively using the thickness and frequency values from the last experiment.

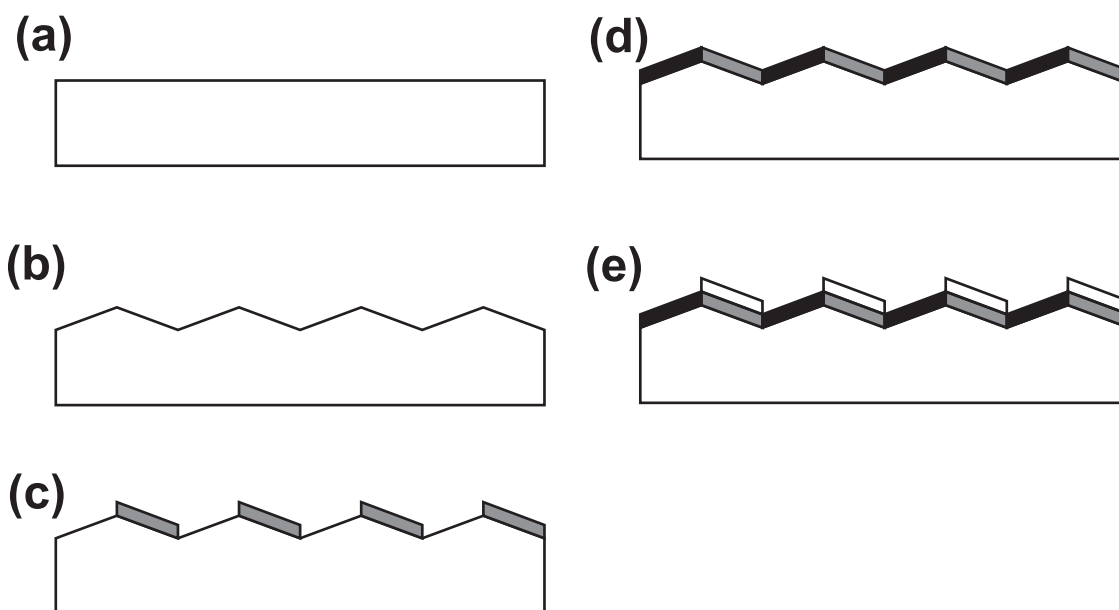


Figure 8: Schematic drawing of various substrate structures based on the method described in this text. (a) bare silicon, (b) topographic structure, (c) topographic structure after metal evaporation, (d) and (e) further modifications with SAMs.

Figure 2 shows an AFM image of a substrate partially covered with gold. We find an increased roughness on the gold covered parts of the sample. Several methods are known to overcome the problem [14], unfortunately many of them are restricted to relatively small areas. Cooling the sample during evaporation should reduce the mobility of the gold on the surface and therefore suppress growth of gold islands. Following this idea, we cooled the sample stage down to -196°C . Another approach was to heat the sample under reductive conditions *after* evaporation. This procedure leads to a smoother surface of the gold on the atomic scale and should even work for larger areas [15]. Both methods did not lead to a significant decrease of roughness. Even worse, we observed a remarkable amount of contaminations on the surface after these procedures. Using sputtering technique instead of thermal evaporation might give the best improvement. Nevertheless, the roughness of the gold covered areas is still much smaller than the size of the pattern (Fig. 2 c, d). Varying the amount of material evaporated on the sample we are able to vary the roughness. To control the evaporation results we did scanning electron microscopy (Fig. 2 f), which clearly shows no gold on the silicon stripes. This image also indicates that the stripes are not covered homogeneously by the gold.

The resulting structures are chemically patterned substrates with a difference in surface energy given by the silicon oxide and the evaporated metal layer. This difference can be amplified via self assembled monolayers (SAM) with different chemical end groups on the

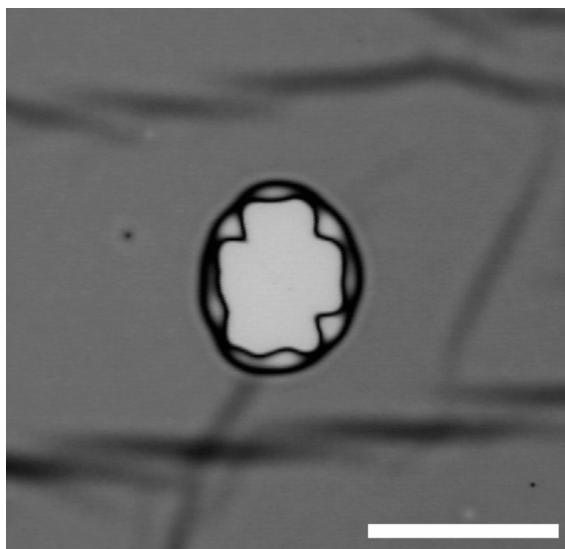


Figure 9: Anisotropic dewetting of a 60 nm thick polystyrene film after annealing. The silanized substrate had a mean width of 150 nm and was partially covered with gold. [16] The scale bar corresponds to 20 μm .

two stripes (Fig. 8). We have used octadecyl trichlorosilane (OTS) in order to modify the silicon oxide stripes with alkyl groups following established preparation methods [15]. Figure 9 shows polystyrene film that began to dewet the surface upon annealing above the glass transition. The hole has a very unusual shape, which is a result of the underlying substrate with a pattern on a much smaller length scale. A variety of molecules form SAMs on either gold or oxide surfaces so many chemical patterns can be realized.

We summarize the preparation process following the sketch in Figure 8. Starting with a single crystal silicon wafer which is miscut between two relatively low indexed surfaces (a), we get a grooved surface (b). The mean width of the grooves ranges from 40 to 400 nm given by the preparation time. The whole process is done in UHV and is mostly automated. To achieve a chemical pattern metals are evaporated under a grazing angle (c). Additional modification with self assembling monolayers leads to a large variety of possible surfaces (d, e). Most of the preparation steps are automated so the actual time required for attendance is only a fraction of the total time needed for the preparation. Considering a UHV experiment involved this is an enormous advantage to the conventional methods used before.

The authors would like to acknowledge Clarissa Abetz for SEM measurements and Ulrike Mock and Hubert Elbs for helpful discussions. This work was financially supported by the German Science Foundation (SPP 1052).

2.4 References

- [1] D.M. Tennant in G. Timp (Ed.) *Nanotechnology*; Springer-Verlag: Heidelberg, **1999**.
- [2] C. Park, J. Yoon, E.L. Thomas, *Polymer* **2003**, *44*, 6725
- [3] A. Zangwill, *Physics at Surfaces*; Cambridge University Press: Cambridge, **1988**.
- [4] S. Song and S.G.J. Mochrie, *Phys. Rev. Lett.* **1994**, *73*, 995.
- [5] S. Song and S.G.J. Mochrie, *Phys. Rev. B* **1995**, *51*, 10068.
- [6] S. Song, M. Yoon, S.G.J. Mochrie, and G.P. Stephenson, and S.T. Milner, *Surf. Sci.* **1997**, *372*, 37.
- [7] L. Rockford, Y. Liu, P. Mansky, T.P. Russell, M. Yoon, and S.G.J. Mochrie, *Phys. Rev. Lett.* **1999**, *82*, 2602.
- [8] L. Rockford, T.P. Russell, and S.G.J. Mochrie, *Macromolecules* **2001**, *34*, 1487
- [9] M.J. Fasolka, D.J. Harris, A.M. Mayes, M. Yoon, and S.G.J. Mochrie, *Phys. Rev. Lett.* **1997**, *79*, 3018.
- [10] N. Rehse, C. Wang, M. Hund, M. Geoghegan, R. Magerle, and G. Krausch, *Eur. Phys. J. E* **2001**, *4*, 69.
- [11] B.S. Swartzentruber, Y.-W. Mo, M.B. Webb, and M.G. Lagally, *J. Vac. Sci. Technol. A* **1989**, *7*, 2901.
- [12] A.A.R. Elshabini-Riad and F.D. Barlow, *Thin Film Technology Handbook*: McGraw-Hill: New York, **1998**.
- [13] R.F. Knarr, R.A. Quon, and T.K. Vanderlick, *Langmuir* **1998**, *14*, 6414 and U. Höpfner, H. Hehl, and L. Brehmer, *Appl. Surf. Sci.* **1999**, *152*, 259, and references therein.
- [14] K. Jacobs, *personal communication*.
- [15] J. Sagiv, *J. Am. Chem. Soc.* **1980**, *102*, 92.
- [16] C. Wang, N. Rehse, M. Hund, M. Geoghegan, R. Magerle, and G. Krausch, unpublished.

Preface to Chapter 3

This chapter has been published under the title ‘Stability of Thin Polymer Films on a Corrugated Substrate’ by N.R., Chun Wang, Markus Hund, Mark Geoghegan, Robert Magerle, and Georg Krausch in *The European Physical Journal E* **2001**, 4, 69.

3 Stability of Thin Polymer Films on a Corrugated Substrate

*Nicolaus Rehse, Chun Wang, Markus Hund, Mark Geoghegan, Robert Magerle, and Georg Krausch**

Lehrstuhl für Physikalische Chemie II and Bayreuther Zentrum für Kolloide und Grenzflächen (BZKG), Universität Bayreuth, D-95440 Bayreuth, Germany

**corresponding author*

3.1 Introduction

The stability of thin liquid films on solid substrates is an area of great current interest [1-11]. Aside from its technological importance (coatings, lubricants, etc.) there remain various basic issues related to the underlying mechanisms and the relevant forces involved. Since any real surface tends to exhibit both heterogeneities in chemical composition and a certain degree of roughness, recent studies have focused on the wetting behavior of heterogeneous model surfaces [5, 12-14]. Such surfaces are typically characterized by a well-defined lateral variation of the surface energy and/or a regular corrugation of well-defined shape, depth, and lateral width. In addition to their importance for a sound understanding of the wetting behavior of real surfaces, such model experiments have demonstrated routes to create liquid microstructures [4,12], which may be of interest for the manipulation of the smallest amounts of liquids in chemical or biochemical applications. In many of the studies referred to above, high molecular weight polymers have played an important role as model liquids. Both the negligible vapor pressure and the high viscosity of polymers facilitate experimental studies of wetting and dewetting because the relevant time scales give easy access to real time observation of kinetic processes. Furthermore, both the viscosity and the molecular size can be easily controlled by changing the degree of polymerization, without significantly influencing the surface and interfacial energies involved.

Patterned model substrates have been prepared following different routes. In order to produce micron scale surface energy patterns, different types of lithography have been applied [4,15,16]. As a rule, the overall lateral dimensions of the patterned area created using such techniques decreases with decreasing pattern size. Alternatively, self-assembly processes can be utilized with the potential to create patterns of nanoscopic characteristic lengths over

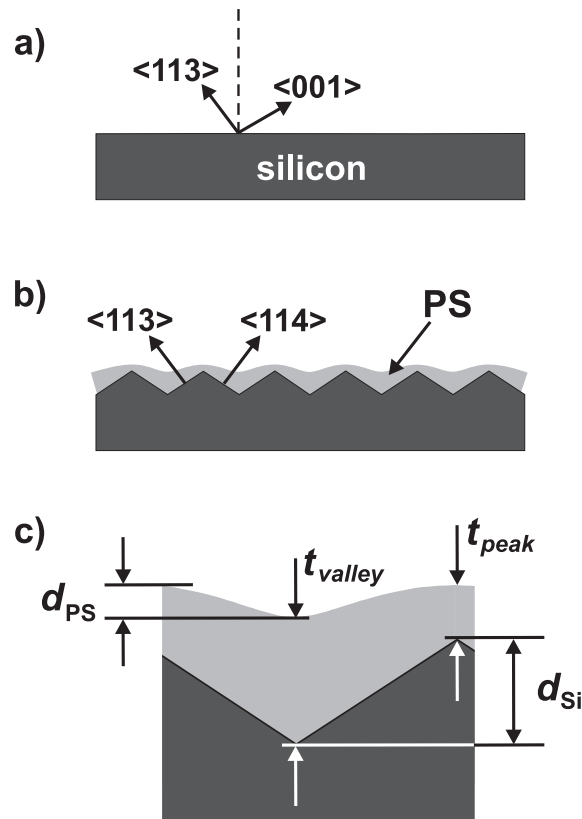


Figure 1: Sketch of the substrates used in the earlier [17, 18] and in the present work. Following the established annealing procedures [19-21], the initially flat surface of the miscut silicon single crystal (a) can be transformed into a regularly grooved surface (b). A layer of polystyrene is shown in both (b) and (c). In (c) we introduce the respective lengths referred to in the text.

macroscopically large areas. As an example, Mayes and co-workers [17] have used mis-oriented silicon single crystals to produce large areas of saw-tooth like surface morphologies (Figure 1). Here, a characteristic lateral spacing of order 100 nm can easily be achieved over cm^2 -sized surface areas. The authors studied the micro-domain morphology of symmetric diblock copolymer thin films of laterally varying film thickness induced by the surface morphology of the substrate. Russell and co-workers [18] introduced the idea of glancing angle metal evaporation on such silicon surfaces, leading to a regular chemical heterogeneity by shadowing effects. On such surfaces they studied the wetting behavior of thin films of homopolymers, polymer blends, and block copolymers.

In the present paper, we have investigated in detail the stability of thin polystyrene (PS) films of varying molecular weight on regularly grooved silicon surfaces *without* chemical heterogeneity. We find that the films become unstable below a certain critical thickness t_{crit} ,

which increases with increasing molecular weight. The data are discussed in view of recent related experiments and theoretical concepts.

3.2 Experimental

For the preparation of the substrates we used polished silicon wafers ($5 \times 12 \times 0.5 \text{ mm}^3$) with the surface normal pointing $3 \pm 0.5^\circ$ off the $\langle 113 \rangle$ crystal axis towards the $\langle 001 \rangle$ axis (Crystec, Berlin). n-type (arsenic doped) material ($\rho \leq 20 \text{ m}\Omega \text{ cm}$) was used to enable resistive heating. The wafers were repeatedly heated at increasing temperatures up to a maximum of 1250°C under ultra-high vacuum conditions. Heating was interrupted whenever the pressure in the vacuum system increased to above 10^{-8} mbar. 25-50 steps were typically needed to remove the native oxide layer under sufficiently high vacuum conditions. After the last heating step the sample was slowly cooled to temperatures around 800°C and kept there for various times to produce the grooved surface morphology [19-21]. Finally the wafers were quenched to room temperature and exposed to ambient conditions. The entire heating procedure was computer controlled. The resulting surface structure was investigated by

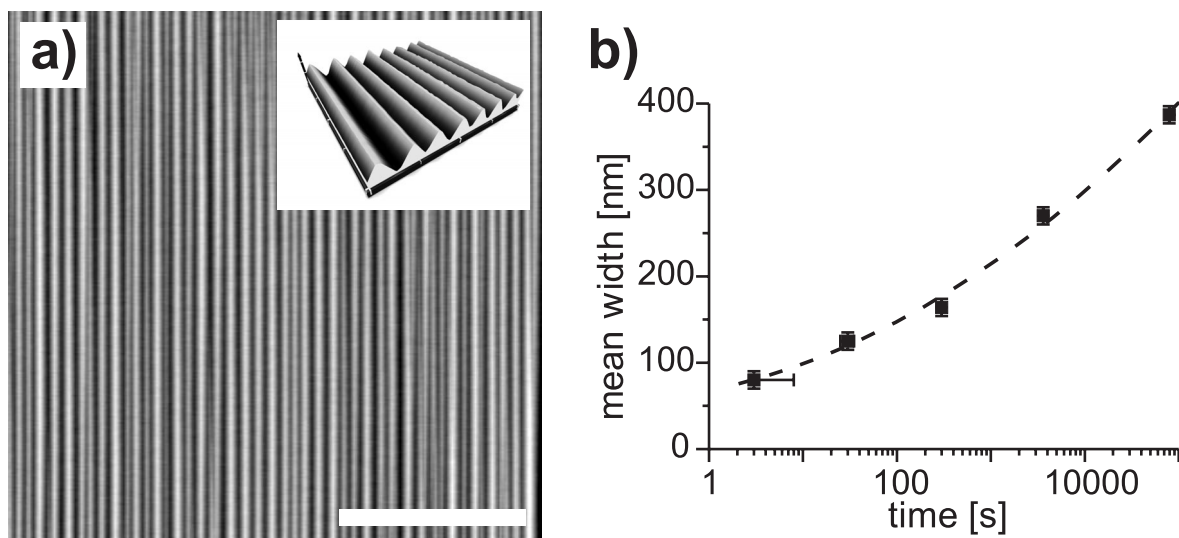


Figure 2: (a) SFM Tapping Mode™ topography image of a corrugated silicon surface used for the wetting experiments. The scale bar is $4 \mu\text{m}$. In the inset we show a three-dimensional image of a $2 \mu\text{m} \times 2 \mu\text{m}$ area of the scan. Note that the height scale and the lateral scales are different, strongly exaggerating the aspect ratio of the surface structure. (b) The mean groove width of the corrugated substrates as a function of the annealing time at 800°C under ultra-high vacuum. The errors in time correspond to sample cooling and are approximately 5 s. The uncertainty in the mean groove width is of the same size as the symbols. The dashed line is a guide to the eye.

scanning force microscopy (SFM) operated in TappingMode™. In Figure 2a we show a typical SFM image taken after a heat treatment at 835°C for 7 h. The surface exhibits triangularly shaped grooves with a mean width of some 250 nm and a mean peak-to-valley depth d_{Si} of 5 nm. The angle between successive facets is determined by the angle between the (113) and (114) crystallographic planes respectively (5.8°), resulting in a very shallow grating (Figures 1b and 2a). We note that the height scale and the lateral scales of the SFM image in the inset to Figure 2a are significantly different, strongly exaggerating the aspect ratio of the grating. The absolute values of the mean groove width and the peak-to-valley depth can be varied over a wide range by suitable choice of annealing time (Figure 2b) [19-21]. The pattern extends over the entire wafer and the orientation of the grooves is the same over the entire area since it is determined by the macroscopic miscut of the silicon single crystal.

Monodisperse batches of polystyrene of different molecular weights were purchased from Polymer Standards Service, Mainz. The relevant molecular parameters are listed in Table 1. Thin films of PS were prepared by spin casting from toluene solution. Different film thicknesses were realized by variation of both PS concentration and spinning speed. Each film was prepared under identical conditions on both a grooved silicon surface and on a flat silicon surface. The latter was used to determine the film thickness. To this end, scratches were applied to the polymer films on the flat silicon wafers and the thickness of the film was determined by SFM relative to the underlying substrate.

M_w [Da]	M_w/M_n	N
5610	1.06	54
18800	1.02	181
51500	1.03	495
100000	1.03	962
376000	1.04	3615
1000000	1.04	9615

Table 1: Molecular weights, polydispersities and polymerization indices of the polystyrenes used in the present work.

The films prepared on the grooved substrates were investigated by SFM after spin casting to check that the film completely wetted the substrate. Furthermore, the average peak-to-valley depth d_{PS} of the PS film was determined and compared to the respective silicon surface in order to check for systematic variations of the PS film thickness on the grating. The same region (to within $\pm 10 \mu\text{m}$) of the substrate was imaged before and after PS deposition in order to avoid possible errors due to small lateral differences in PS film thickness. To check the stability of the films against dewetting, the samples were heated to 150°C at ambient conditions for various annealing times. (A small number of samples were annealed at 180°C and these gave the same results as those annealed at 150°C .) After each annealing step, the samples were investigated by SFM. Care was taken to image the same spot on the sample ($\pm 10 \mu\text{m}$) in order to minimize potential errors due to small lateral variations in the surface structure of the substrates.

3.3 Results

After spin casting, the PS surfaces (Figure 3b) exhibit qualitatively the same corrugation pattern as the bare Si surfaces (Figure 3a). This finding shows that homogeneous PS films

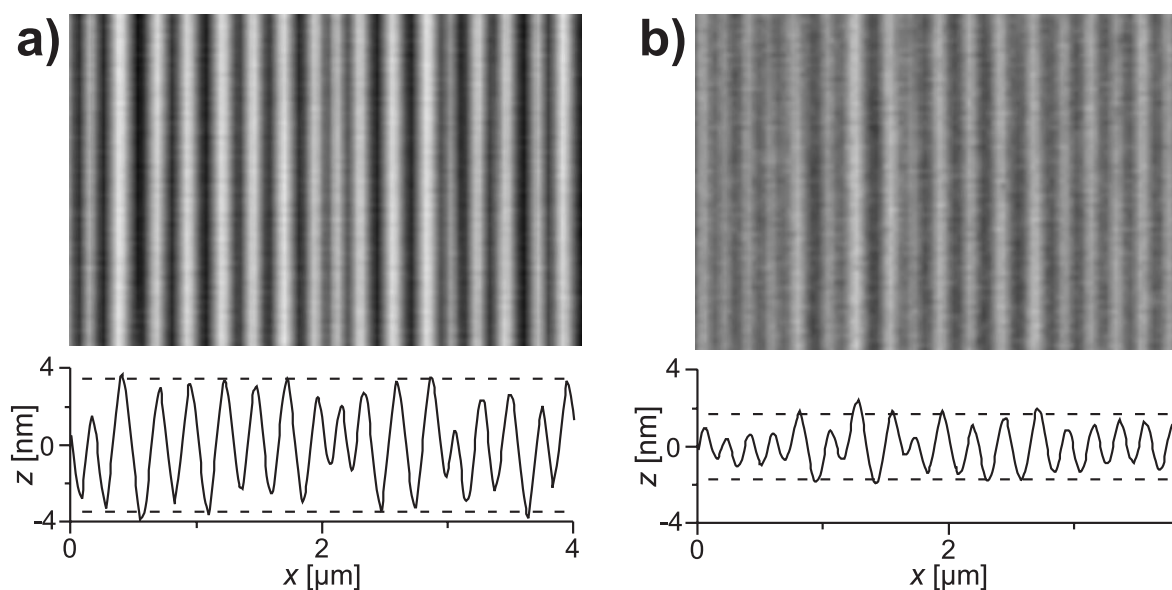


Figure: SFM TappingMode™ topography image of a corrugated silicon substrate before (a) and after (b) casting a thin PS film ($M_w = 100 \text{ kDa}$, $t_{\text{av}} = 4.5 \text{ nm}$) from toluene solution. The images have been taken at about the same lateral position of the sample ($\pm 10 \mu\text{m}$). Under each image we show a line scan, averaged along the horizontal direction. The mean square roughness σ_{Si} and σ_{PS} were calculated from the averaged line scans. The dashed lines indicate the respective roughness values.

are formed which follow the underlying grating. For a quantitative analysis of the peak-to-valley depths d_{Si} and d_{PS} , we have averaged the horizontal SFM line scans along the direction parallel to the grooves. The result of this procedure is shown in Figure 3 for a grooved Si surface prior to and after deposition of a 4.5 nm thick layer of PS ($M_w = 100$ kDa). From Figure 3b it is obvious that the peak-to-valley depth of the polymer surface is somewhat smaller than the respective value of the underlying substrate, i.e. $d_{\text{PS}} < d_{\text{Si}}$. This effect is due to the interplay between surface tension and van der Waals interactions, which typically flattens the surface of a polymer film on a rough substrate surface [5,22,23]. Consequently, the film thickness above the peaks, t_{peak} will be somewhat smaller than the thickness in the valleys, t_{valley} . For a quantitative analysis, we determine the root-mean-square roughness σ_i ($i = \text{Si}, \text{PS}$) of the respective surfaces, which, for a perfect triangular grating, is related to the peak-to-valley depths as $d_i = 2\sqrt{3}\sigma_i$. Based on this assumption, we calculate d_{Si} and d_{PS} from the respective roughness data. If the average film thickness is denoted by t_{av} , we can determine $t_{\text{peak}} = t_{\text{av}} - \frac{1}{2}(d_{\text{Si}} - d_{\text{PS}})$ and $t_{\text{valley}} = t_{\text{av}} + \frac{1}{2}(d_{\text{Si}} - d_{\text{PS}})$, respectively. For the particular sample shown in Figure 3, we find $t_{\text{av}} = 4.5 \pm 0.4$ nm (as determined on a flat substrate), $d_{\text{Si}} = 6.9 \pm 0.4$ nm and $d_{\text{PS}} = 3.4 \pm 0.4$ nm. From these numbers we calculate $t_{\text{peak}} = 2.8 \pm 0.5$ nm and $t_{\text{valley}} = 6.3 \pm 0.5$ nm, respectively.

After annealing, the morphology of the PS film changes markedly. Figure 4 shows the surface morphology of the PS sample discussed above after heat treatment at 150°C for 3 h. The originally homogenous film has broken up into thin channels filling the grooves in

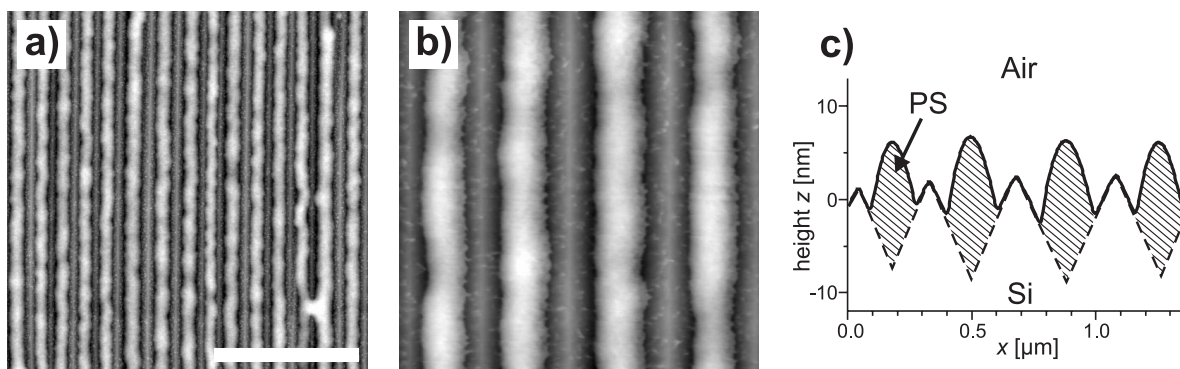


Figure 4. (a) SFM TappingMode™ topography images (the scale bar is 2 μm) of a thin PS film ($M_w = 100$ kDa, $t_{\text{av}} = 5$ nm) on a corrugated silicon substrate after annealing at 150°C for 3 h. The film has broken into linear channels following the grooves of the substrate. The area shown in (b) is a $1.5 \times 1.5 \mu\text{m}^2$ scan. (c) Average line scan along the horizontal taken from image (b). The solid line is the experimental result. The dashed line depicts the position of the substrate surface.

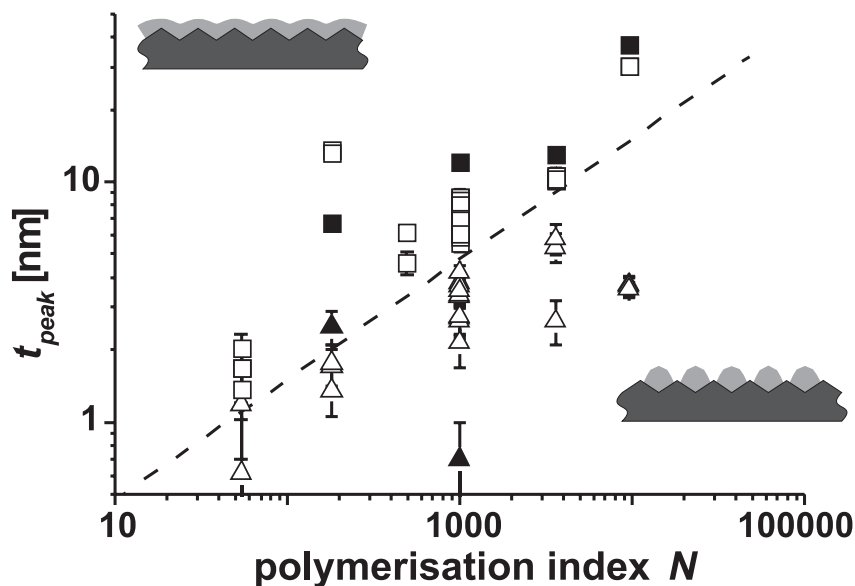


Figure 5: Summary of the experimental results. Squares indicate stable PS films, while triangles refer to films, where the formation of nano-channels was observed. The dashed line indicates $t_{peak} = 0.55 R_g$. The solid symbols indicate data taken from substrates with no corrugation.

the underlying Si grating. The channels extend over rather large distances. Further annealing does not alter the film morphology. Figure 4c shows an average line scan similar to the ones displayed in Figure 3. One can clearly see the sharp peaks of the Si grating in between neighboring PS channels. While the solid line is the experimental result, the dotted line has been added by extrapolation to indicate the position of the PS/Si interface for clarity.

Aiming towards a deeper understanding of the mechanisms responsible for the observed effect, we repeated the above experiment for different film thicknesses t_{av} and different PS polymerization index N . We find that the PS films break up into a regular array of channels only if the average film thickness is smaller than a critical value, t_{crit} . Films thicker than t_{crit} remain stable even after several days of annealing. The critical film thickness below which the instability is observed increases systematically with increasing chain length. This leads us to infer that the confinement of the chains into films thinner than their radius of gyration ($R_g = 0.67\sqrt{N/6}$ nm) may be responsible for the observed phenomenon. As the films are thinnest above the peaks of the silicon grating, we present the quantitative results of our study in a double logarithmic plot of t_{peak} against N (Figure 5). Squares indicate stable PS films while triangles refer to films which after annealing broke up into channels filling the grooves. The most systematic experiment was performed with $N = 962$ ($M_w = 100$ kDa), where a clear transition between stable films and PS channels appears at around $t_{peak} = 0.55 R_g$. The data for

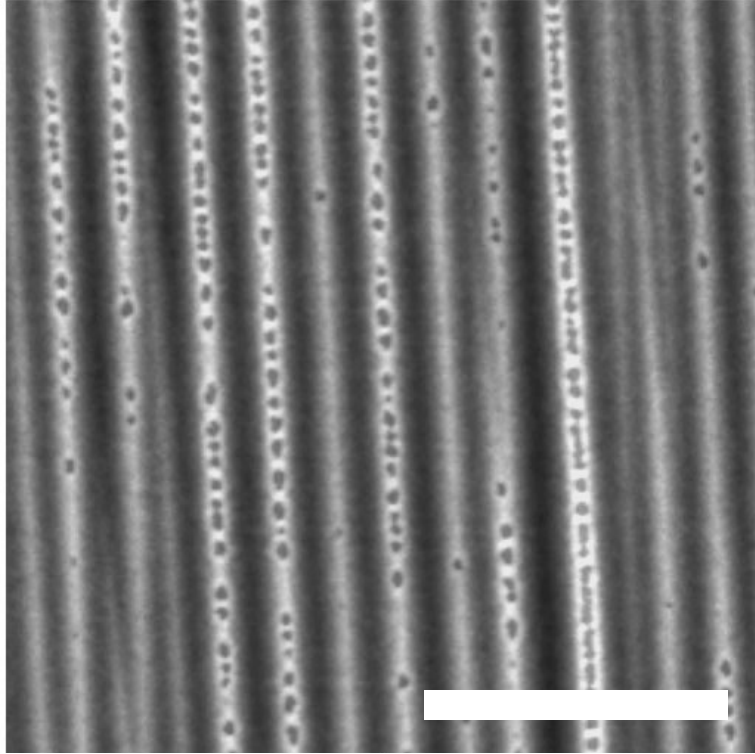


Figure 6: SFM TappingMode™ topography image of a thin PS film ($M_w = 100$ kDa, $d_{av} = 4.5$ nm) after annealing for 3 min at 120°C . The scale bar is $2\ \mu\text{m}$.

$N = 3615$ ($M_w = 376$ kDa) also agree with this relation. For $N = 54$ ($M_w = 5610$ Da) and $N = 495$ ($M_w = 51.5$ kDa) stable films were observed for t_{peak} larger but close to $0.55 R_g$ while for $N = 181$ ($M_w = 18.8$ kDa), PS channels appeared at t_{peak} smaller but close to $0.55 R_g$. All data presented in Figure 5 therefore agree with the notion that films with $t_{peak} > 0.55 R_g$ remain stable while those with $t_{peak} < 0.55 R_g$ break up into channels filling the grooves. We have included the boundary $t_{peak} = 1.50 \pm 0.15 N^{0.5 \pm 0.05}$ ($= 0.55 R_g$) into Figure 5 as a dashed line dividing the diagram into a stable and an unstable regime. The errors of both the prefactor and the exponent present a range of possible boundaries, which are also compatible with the experimental results.

In order to shed some light on the early stages of the dewetting process finally leading to the observed PS channels, we have performed some preliminary short time annealing experiments. As an example, Figure 6 shows an SFM image of a 4.5 nm thick PS ($M_w = 100$ kDa) film after 3 min annealing at 120°C . The film breaks up by formation of holes lining up above the peaks of the grating. While a systematic study of the time dependence of the dewetting process is beyond the scope of the present paper, the data corroborate the importance of the film thickness t_{peak} for the dewetting behavior of the films.

The experimental results can be summarized as follows: On chemically homogeneous, grooved silicon substrates, thin PS films break up into channels filling the grooves of the pattern as soon as the film thickness in the thinnest regions above the peaks of the corrugation is smaller than roughly $0.55 R_g$. Break-up of the films begins with the formation of holes along the peaks of the corrugation. The resulting PS channels appear stable on further annealing. Thicker films appear to be stable against break-up into channels.

3.4 Discussion

In general, the free energy of thin polymer films on heterogeneous substrates will exhibit lateral variations. On chemically homogeneous substrates only corrugations need to be considered and the local film thickness is the relevant parameter. As we observe dewetting whenever the thinnest parts of the films are thinner than a critical value $t_{crit} \approx 0.55 R_g$, one is led to the issue of chain confinement (the R_g dependence precludes an explanation due to long-range forces). In the following discussion, we therefore consider the potential influence of polymer chain conformation and confinement on the free energy of the films.

To understand the role of chain conformation and confinement in ultra-thin polymer films, we need to know whether the chains retain a statistical random walk (Gaussian) distribution near a hard boundary. Silberberg argued that chain conformations remain Gaussian near the surface by assuming that the part of the chain that statistically would want to cross a hard wall is reflected by that wall [24]. This suggests that chains retain their statistical distribution, which in turn means that there is no driving force for a film thickness instability and dewetting. A further development of this theme demonstrated that chain ends induce a long-range repulsion from walls acting over a distance of order R_g , leading to a possible (small) driving force for dewetting [25]. The Silberberg argument has been further criticized in a discussion of computer simulations of thin films confined between neutral walls [26].

We therefore propose that, in confined films, chains will try to reduce distortions induced by the surfaces by moving into thicker regions of the film, triggering dewetting. In thicker films, an increasing number of chains will *not* be distorted by the boundary surfaces. Since an exchange of undistorted chains between regions of different film thickness does not change the total free energy of the system, films thicker than some critical thickness are expected to remain stable against dewetting. This critical thickness should have a length scale of order R_g . Further support for such a mechanism comes from simulations on the shape of polymer chains in the melt [27]. The chain ends are not located next to each other, and so the polymer chain is

actually longer on an axis connecting the chain ends, leading to a cigar conformation for the polymer chain. There is very little change in the polymer size perpendicular to the line joining the chain ends. Therefore, polymers close to hard walls will align themselves such that their long axis is parallel to the wall, avoiding confinement. However, for very thin films of the order of the polymer radius of gyration or thinner, there will be distortions in the chain conformation and dewetting will proceed as described above.

The above argument is also expected to hold on flat substrates. We have therefore performed some test experiments on the stability of ultra-thin PS films of different chain length and thickness on *flat* silicon substrates (Figure 5). The same substrates were used, with the same preparation procedure. The only difference being that, after annealing at 1250°C, the substrates were not heated at ~800°C to induce the corrugations. Although a systematic study is beyond the scope of this work, both stable and unstable films were observed. The results support our conclusions for the corrugated substrate experiments.

We note that earlier experiments on the wetting behavior of ultra-thin polymer films [3] on flat substrates showed that otherwise stable films become unstable for thicknesses smaller than some critical value, which again was found to scale as R_g . If films below a certain thickness are indeed inherently unstable, local variations in film thickness (e.g. due to capillary waves) will be amplified, leading to the observed behavior on flat substrates as well. In the earlier experiments [3] the films were stable at higher temperatures in agreement with the notion of confinement (i.e. entropy-related) effects. It has been demonstrated using self-consistent field theory that this dewetting could proceed according to a spinodal mechanism [28]. A systematic study of the role of the annealing temperature in our films could shed light on the importance of such a mechanism.

Recent experiments have addressed the question as to whether the in-plane characteristic dimension of polymer chains changes in films of thickness comparable or smaller than R_g . While it was generally assumed that within the plane of the films the chains retain their unperturbed Gaussian conformation even in the thin film limit [24,29], recent experiments lead to contradictory conclusions. Jones *et al.* supported the above assumption by neutron scattering experiments on ultra-thin PS films [30]. Other experiments on similar systems indicated a systematic increase of the in-plane dimensions of the chains [31] in ultra-thin films in qualitative agreement with simulation results [27]. Experiments on polydimethylsiloxane films coated on PS brushes [32] indicated that chain ordering near a surface occurs. It is probably fair to say that this issue is not yet satisfactorily settled.

In the above discussion we have assumed that the equilibrium conformation of polymer chains in the ultra-thin films leads to chain distortion. We cannot, however, exclude the possibility that the preparation of the film leads to the dewetting structure that we observe. For example, during the spin coating, the film can vitrify before all of the solvent has evaporated, possibly leading to some internal tension in the film [33]. In this case one could suppose that the holes formed at the start of the dewetting process (Figure 6) were nucleated by polymer chain distortions frozen in during spin coating and not due to confinement. Such an explanation is also consistent with the observed effect; the dewetting would be expected to start at the thinnest points on the film (the peaks of the corrugations), and also the radius of gyration scaling of the critical thickness cannot be ruled out under this nucleated mechanism. We therefore only note that significant deformations of the PS chains within the thinnest regions of the films may influence the dependence of the free energy per unit area on film thickness and may be of importance for the effects observed here and in the related experiments [3,18].

The observation of a channel structure initiated by polymer dewetting has been observed in other experiments. Higgins and Jones [34] have shown that an interfacial roughness (of the order of Ångstroms) but with a dominant direction (a kind of nematic roughness) was shown to initiate a corrugated dewetting pattern at a polymer-polymer interface. Such an anisotropic spinodal dewetting at a polymer-polymer interface is probably initiated by small changes in dispersion forces due to the very small differences in film thickness (spinodal dewetting is a very sensitive function of film thickness [2]). The lateral length scale of the dewetting is selected by the polymer system itself, rather than by the (undefined) size of the roughness. Shorter wavelengths are suppressed due to the energy cost in having a large interface, whilst long wavelengths grow too slowly in comparison with the observed dominant wavelength. This is in contrast to our results, whereby the dewetting has a length scale imposed by the size of the corrugations. The existence of a dominant wavelength is usually associated with a spinodal mechanism, and is manifest by a wavelength term in the free energy. In order to assess such a possibility in our system, future work should include a detailed analysis of the dewetting of ultra-thin polystyrene films on flat substrates.

We end our discussion by noting that the resulting structures observed on the chemically homogeneous, grooved substrates are quite similar to the ones reported by Rockford *et al.* [18], who studied the stability of thin PS films on grooved *and* chemically patterned substrates. (In these experiments, the mean groove width was 170 nm, which corresponds to $d_{Si} \approx 4$ nm. Since a 9 nm thick metal layer was evaporated on every other facet, the effective

peak-to-valley depth amounted to some 13 nm.) The authors reported a single experiment ($M_w = 100$ kDa, $t_{av} = 5$ nm) and showed that the PS film broke up into channels aligned along the grating. They explained their observation by different wetting properties of the SiO_x and Au surfaces, respectively [35]. While the interfacial energy between PS and SiO_x may indeed be larger than for the respective interface with Au [36], our experiments clearly show that no such chemical heterogeneity is needed to induce an instability which finally leads to the formation of PS channels.

To relate our experimental work closer to the situation described by Rockford *et al.* [18], we have in addition prepared grooved silicon surfaces with Au evaporated on every other facet. As an example, Figure 7a shows the morphology of a 5 nm thick PS film ($M_w = 100$ kDa) formed on such a chemically heterogeneous substrate after annealing. PS channels are formed, and these are similar to those on the chemically homogeneous, grooved substrates (Figure 4), although the centre of gravity of the channels is no longer located symmetrically within the grooves. As is clearly visible in the average line scan (Figure 7b), the PS channels try to cover the facets covered by Au, in agreement with the earlier work [18]. However,

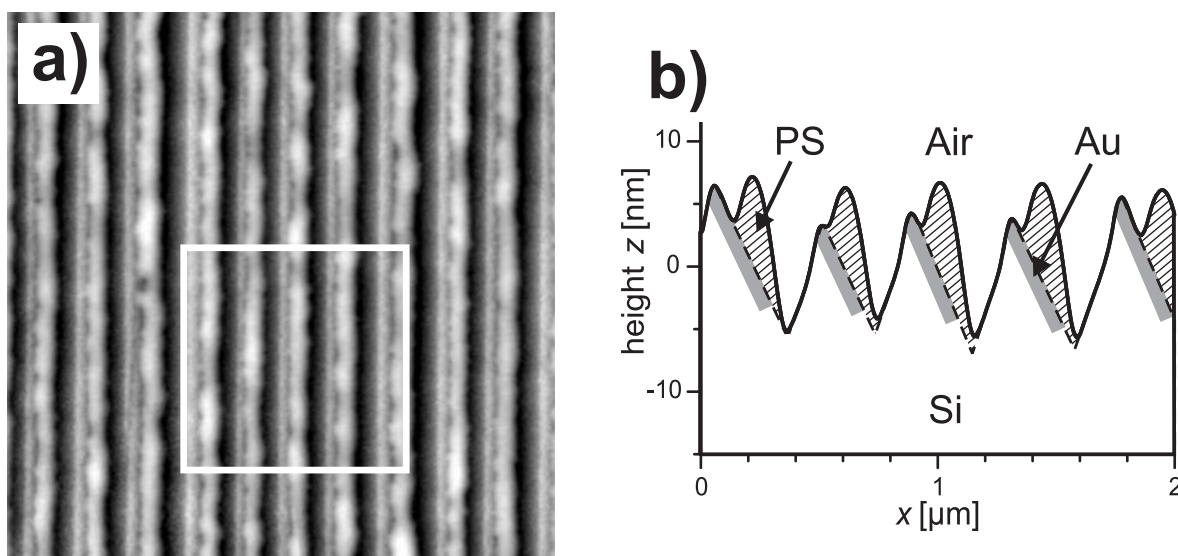


Figure 7: (a) SFM TappingMode™ topography image of a thin PS film ($M_w = 100$ kDa, $d_{av} = 5$ nm) on a chemically patterned, corrugated silicon substrate after annealing at 150°C for 3 h. The film has broken into linear anisotropic channels, with the PS dewetting preferentially to the side of the facet covered with gold. (b) Average line scan along the horizontal taken from the area inside the box indicated in image (a). The solid line is the experimental result. The dashed line depicts the position of the substrate surface. The approximate location of the gold is sketched on the figure (these SFM measurements do not identify the exact position of the gold).

we also note that polystyrene has dewetted the very top of the facets. Since gold has also been evaporated onto this part of the substrate, this is clear evidence that the substrate topography must also play a role in such dewetting behavior.

3.5 Conclusions

In conclusion, we have demonstrated that a rather small surface corrugation has significant influence on the wetting properties of thin polymer films. In particular, in thin enough films, the spontaneous formation of an ordered array of polymeric nano-channels is observed. The characteristic width of the channels is determined by the corrugation period of the substrate, which can be varied over a rather wide range. The PS films become unstable only if the thickness in the thinnest regions of the films falls beyond a critical value of about $0.55 R_g$. It was further suggested that the films dewet by the formation of holes nucleating along the peaks of the corrugation. Given that the substrate corrugation extends over macroscopic areas, this dewetting process leads to a large-scale, highly anisotropic ordered structure.

Films thicker than the critical value of $0.55 R_g$ are seen to be stable, probably due to an increasing number of undistorted chains. Such chains do not seek to minimize their free energy by diffusing to thicker areas of the film. In comparison to earlier work on similar, but chemically patterned substrates [18], our results indicate that the roughness itself plays a crucial role in the stability of ultra-thin polymer films. Consequently, the potential role of surface roughness should be considered whenever rough surfaces are used to create chemically heterogeneous model surfaces.

The dramatic creation of a macroscopically large ordered array of sub-micron sized polymer channels induced by a small corrugation in the substrate may inspire further work on the controlled creation of new liquid micro- and nano-structures. We also hope that these results will lead to further experiments aiming to a deeper understanding of the processes involved in the coating of rough surfaces. Furthermore, the results point to the importance of in-depth studies on the chain conformation in ultra-thin polymer films and its effect of thin film stability.

3.6 References

- [1] P.G. de Gennes, *Rev. Mod. Phys.* **1985**, *57*, 827.
- [2] F. Brochard-Wyart and J. Daillant, *Can. J. Phys.* **1990**, *68*, 1084.

- [3] W. Zhao, M.H. Rafailovich, J. Sokolov, L.J. Fetters, R. Plano, M.K. Sanyal, S.K. Sinha, and B.B. Sauer, *Phys. Rev. Lett.* **1993**, *70*, 1453.
- [4] N.L. Abbott, J.P. Folkers, and G.M. Whitesides, *Science* **1992**, *257*, 1380.
- [5] D. Andelman, J.-F. Joanny, and M.O. Robbins, *Europhys. Lett.* **1988**, *7*, 731.
- [6] Y. Liu, M.H. Rafailovich, J. Sokolov, S.A. Schwarz, X. Zhong, A. Eisenberg, E.J. Kramer, B.B. Sauer, and S. Satija, *Phys. Rev. Lett.* **1994**, *73*, 440.
- [7] G. Reiter, *Phys. Rev. Lett.* **1992**, *68*, 75.
- [8] R. Yerushalmi-Rozen, J. Klein, and L.J. Fetters, *Science* **1994**, *263*, 793.
- [9] G. Reiter, *Science* **1998**, *282*, 888.
- [10] K. Jacobs, S. Herminghaus, and K.R. Mecke, *Langmuir* **1998**, *14*, 965.
- [11] S. Herminghaus, K. Jacobs, K. Mecke, J. Bischof, A. Fery, M. Ibn-Elhaj, and S. Schlagowski, *Science* **1998**, *282*, 916.
- [12] H. Gau, S. Herminghaus, P. Lenz, and R. Lipowsky, *Science* **1999**, *283*, 46.
- [13] C. Bauer and S. Dietrich, *Phys. Rev. E* **1999**, *60*, 6919.
- [14] C. Bauer, S. Dietrich, and A.O. Parry, *Europhys. Lett.* **1999**, *47*, 474.
- [15] Y. Xia, X.-M. Zhao, and G.M. Whitesides, *Microelectr. Eng.* **1996**, *32*, 255.
- [16] M. Böltau, S. Walheim, J. Mlynek, G. Krausch, and U. Steiner, *Nature* **1998**, *391*, 877.
- [17] M.J. Fasolka, D.J. Harris, A.M. Mayes, M. Yoon, and S.G.J. Mochrie, *Phys. Rev. Lett.* **1997**, *79*, 3018.
- [18] L. Rockford, Y. Liu, P. Mansky, T.P. Russell, M. Yoon, and S.G.J. Mochrie, *Phys. Rev. Lett.* **1999**, *82*, 2602.
- [19] S. Song and S.G.J. Mochrie, *Phys. Rev. Lett.* **1994**, *73*, 995.
- [20] S. Song and S.G.J. Mochrie, *Phys. Rev. B* **1995**, *51*, 10068.
- [21] S. Song, S.G.J. Mochrie, and G.P. Stephenson, *Phys. Rev. Lett.* **1995**, *74*, 5240.
- [22] M.O. Robbins, D. Andelman, and J.-F. Joanny, *Phys. Rev. A* **1991**, *43*, 4344.
- [23] Z. Li, M. Tolan, T. Höhr, D. Kharas, S. Qu, J. Sokolov, M.H. Rafailovich, H. Lorenz, J.P. Kotthaus, J. Wang, S.K. Sinha, and A. Gibaud, *Macromolecules* **1998**, *31*, 1915.

- [24] Silberberg, *J. Colloid Interface Sci.* **1982**, *90*, 86.
- [25] A.N. Semenov, *J. Phys. II France* **1996**, *6*, 1759.
- [26] J.-U. Sommer, A. Hoffmann, and A. Blumen, *J. Chem. Phys.* **1999**, *111*, 3728.
- [27] T. Pakula, *J. Chem. Phys.* **1991**, *95*, 4685.
- [28] M. Müller and K. Binder, *Macromolecules* **1998**, *31*, 8323.
- [29] G.J. Fleer, M.A. Cohen-Stuart, J.M.H.M. Scheutjens, T. Cosgrove, and B. Vincent, in *Polymers at Interfaces*, Chapman & Hall, London, **1993**).
- [30] R.L. Jones, K.S. Kumar, D.L. Ho, R.M. Briber, and T.P. Russell, *Nature* **1999**, *400*, 146.
- [31] Brûlet, F. Boué, A. Menelle, and J.P. Cotton, *Macromolecules* **2000**, *33*, 997.
- [32] S. Rivillon, P. Auroy, and B. Deloche, *Phys. Rev. Lett.* **2000**, *84*, 499.
- [33] S. Herminghaus private communication.
- [34] A.M. Higgins and R.A.L. Jones, *Nature* **2000**, *404*, 476.
- [35] R. Konnur, K. Kargupta, and A. Sharma, *Phys. Rev. Lett.* **2000**, *84*, 931.
- [36] T.P. Russell, G. Coulon, V.R. Deline, and D.C. Miller, *Macromolecules* **1989**, *22*, 4600.

Preface to Chapter 4

This chapter has been published under the title ‘Surface Reconstruction of an Ordered Fluid: An Analogy with Crystal Surfaces’ by N.R., Armin Knoll, Matthias Konrad, Robert Magerle, and Georg Krausch in *Physical Review Letters* **2001**, 87, 035505.

4 Surface Reconstruction of an Ordered Fluid: An Analogy with Crystal Surfaces

Nicolaus Rehse, Armin Knoll, Matthias Konrad, Robert Magerle, and Georg Krausch*

Physikalische Chemie II, Universität Bayreuth, D-95440 Bayreuth, Germany

**corresponding author*

The identification of analogous behavior of rather different types of matter is an important aspect of science since it can reveal the generality of the underlying concepts of physics. In the present Letter we follow this line and discuss the analogy between the surface structure of a mesoscopically ordered complex fluid and the well-known surface reconstructions of inorganic single crystals. In general, the presence of a surface can alter the equilibrium structure of any (ordered) system by a local rearrangement of matter leading to a state of lower (surface) free energy. As an example, the surface structures of many inorganic crystals differ both in the characteristic spacings as well as in their symmetry from the respective bulk crystal structure. Typical examples are the Si(111)-(7×7) [1] and the Si(100)-(2×1) “buckling row” reconstructions [2-4].

Block copolymers are long chain molecules composed of two or more blocks of different chemical composition. A frequent incompatibility between the constituent blocks together with their molecular connectivity gives rise to the formation of ordered microdomain structures, which exhibit crystal like order on mesoscopic length scales [5]. Together with surfactant solutions and liquid crystals, block copolymers belong to the class of ordered complex fluids, which often form regular structures with lamellar and cylindrical microdomains. In recent years, the influence of boundary surfaces on the microdomain structure of block copolymers has received increasing attention, both experimentally [6-11] and theoretically [11-15]. However, a thorough comparison between the phenomena observed at the free surface of a complex fluid and the well-studied behavior of single crystal surfaces is still lacking. While crystals have point-group symmetry, ordered complex fluids often belong to more general space groups and therefore display higher degrees of symmetry. In this Letter, we show that despite the very different types of matter and order a complex fluid can form a surface reconstruction. This finding extends the analogy between ordered fluids and crystals and reveals common underlying fundamentals.

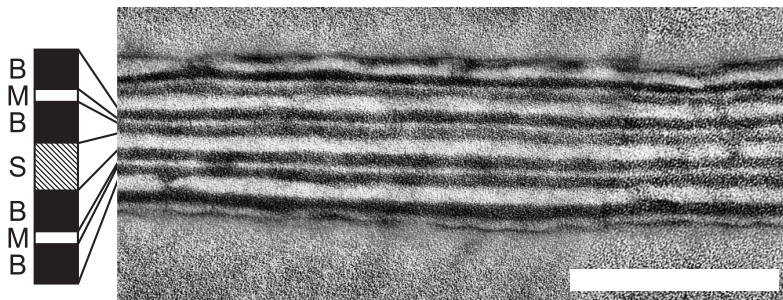


Figure 1: TEM image of a cross section (stained with OsO_4) of an chloroform-vapor-annealed SBM film floated-off from a Si substrate. The scale bar corresponds to 250 nm.

As a model system, we investigate the *free* surface structure of thin films of a nearly symmetric polystyrene-*block*-polybutadiene-*block*-polymethylmethacrylate (SBM) triblock copolymer, which exhibits a lamellar microdomain structure in the bulk [16]. When thin films of this material are prepared on a polar substrate like SiO_x , the poly(methylmethacrylate) (M) end block is expected to accumulate preferentially on the substrate thereby aligning the lamellae parallel to the plane of the film [6,17]. In the absence of specific surface interactions, one would expect the film to be terminated by one of the two lamellar sub-layers SBM or MBS, respectively, both leading to a laterally homogenous, “ideal” surface exhibiting two-dimensional continuous translational symmetry. However, the near-surface region of SBM films exhibits a complex reconstruction, which breaks the symmetry of the ideal surface and exhibits striking similarities with the $\text{Si}(200)-(2\times 1)$ surface reconstruction. In the following, we shall present the experimental data on the block copolymer surfaces, briefly recall the results known for $\text{Si}(100)-(2\times 1)$, and finally discuss similarities between both phenomena on the basis of symmetry considerations.

SBM triblock copolymer films with thicknesses in the range 100-1000 nm were prepared on polished Si wafers by dip coating from a 5 wt% polymer solution in chloroform (SBM molecular weight $M_w = 162$ kDa, volume fractions $\Phi_{PS} = 0.34$, $\Phi_{PB} = 0.43$, $\Phi_{PMMA} = 0.23$, where PS is polystyrene, PB is polybutadiene, and PMMA is polymethylmethacrylate [16]). In order to drive the system towards thermodynamic equilibrium, the films were exposed to chloroform vapor at 95% saturation for 1 day and dried subsequently, by reducing the vapor pressure continuously over a period of 10h. This procedure resembles the preparation used for bulk samples of the same material [16]. The resulting thin film samples were investigated by optical microscopy, Tapping Mode™ scanning force microscopy (SFM), transmission electron microscopy (TEM), and scanning electron microscopy (SEM).

We start our discussion with the “bulk structure” of the films as revealed from cross sectional TEM experiments. The films were floated off the SiO_x covered Si substrates onto aqueous KOH solution, picked up onto a TEM grid, embedded into epoxy, and subsequently cut into ~ 50 nm thick slices. TEM images taken after an OsO_4 stain (Fig. 1) clearly show a lamellar micro domain structure, which is aligned parallel to the boundary surfaces. The lamellar spacing is comparable to that of the bulk structure. An assignment of the different blocks is straightforward, as the B-micro domains appear dark due to selective staining, while the M-micro domains typically appear thinner than the S-micro domains due to electron beam damage of the acrylate side groups [19]. In regions of laterally varying film thickness,

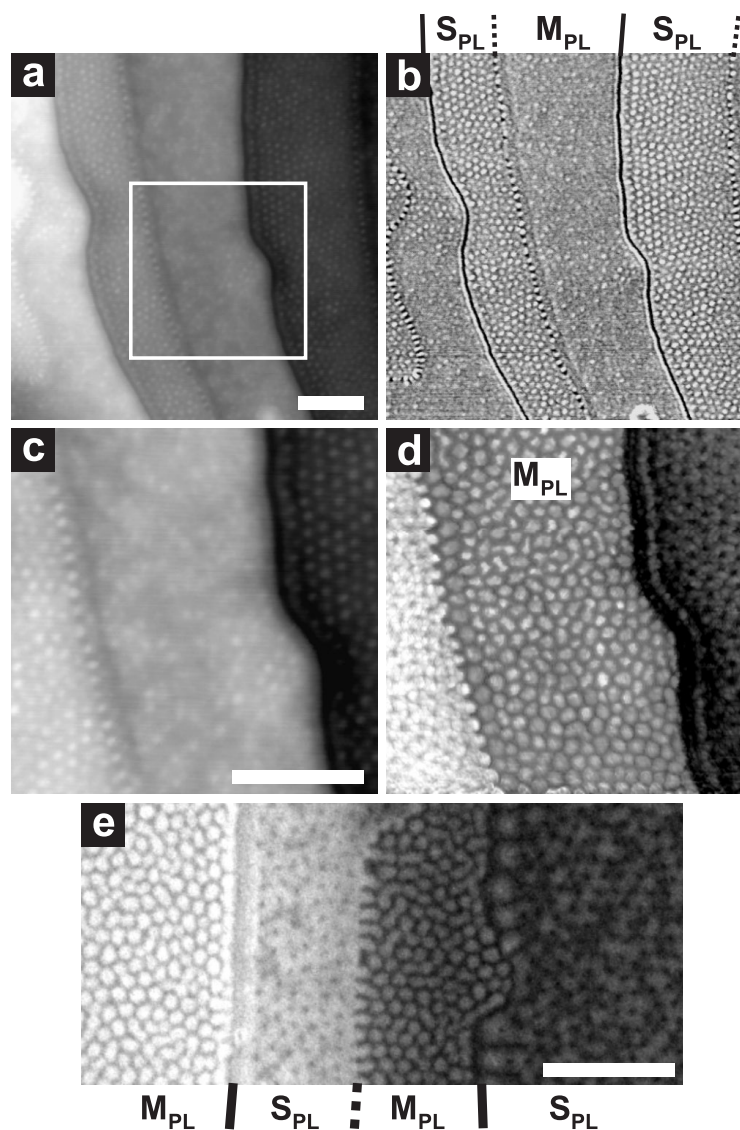


Figure 2: TM-SFM height (a) and phase (b) image of a SBM-groß film (~ 160 nm thick) on a Si substrate after annealing in chloroform vapor. Height image before (c) and after (d) plasma etching. (d) SEM image of SBM surface (stained with RuO_4) (operated at 1 eV, resulting in ~ 15 nm sampling depth). Scale bars correspond to 500 nm in all cases.

the SBM film surface exhibits terraces separated by steps of well defined height (Fig. 2a), reflecting the layered morphology of the underlying film. So far, the results resemble the well known alignment of lamellae found, e.g. in thin films of SM diblock copolymers [6,17,18,20,21].

Closer inspection of the surface, however, reveals a well-defined lateral structure within each terrace. This can be seen in Fig. 2a and 2b. While the height image (Fig. 2a) clearly shows the stepped nature of the film surface, the phase image (Fig. 2b) reveals the existence of two distinctly different types of terrace structures, referred to as S_{PL} and M_{PL} in the following. Terrace S_{PL} is characterized by a dotted structure in the SFM phase image with a typical lateral repeat distance of some 60 ± 3 nm between neighboring dots. Terrace M_{PL} exhibits some lateral structure as well; however, no further details can be extracted from Fig. 2b. The surface structure alternates between the two types as one moves along the surface, i.e. every other terrace exhibits qualitatively the same surface morphology. It is interesting to note that along with the changing terrace structures, the shape of the steps varies systematically, too, and changes between a "dotted" and a "continuous" appearance. The height difference between like terraces (80 ± 10 nm on average) is somewhat smaller than the bulk lamellar spacing (110 nm) possibly due to shrinkage during the drying process [22]. We conclude at this point that the block copolymer forms a layered structure aligned parallel to the substrate and two different terminations of the layers are observed at the free surface of the films.

To get further insight into the near-surface morphologies responsible for the observed surface structures, we have exposed our samples to an oxygen plasma (1 mbar, 60 W, 45 sec). This procedure removes about the topmost 14 nm of the polymeric material. In Fig. 2c and d height images of the same area of the sample (white box in Fig. 2a) are shown prior to and after plasma etching, respectively. The isolated protrusions visible on terrace S_{PL} (Fig. 2c) are turned in isolated depressions after the plasma treatment. Accordingly, the rather featureless surface of terrace M_{PL} exhibits isolated protrusions after the etch. Given the different etching rates of the three polymers (~ 10 nm/min for PS and ~ 20 nm/min for both PB and PMMA, respectively), we conclude that terrace S_{PL} consists of a PS matrix whereas in terrace M_{PL} isolated PS micro domains are found. To further corroborate this assignment, we have imaged the samples with a field emission source scanning electron microscope (Fig. 2e). The sample was stained with RuO_4 prior to imaging. Again, two distinct types of terraces are observed ending by two distinctly different types of steps. Terrace S_{PL} is characterized by isolated dark spots in the SEM image, while terrace M_{PL} exhibits an array of isolated bright micro domains. Since RuO_4 is known to preferentially stain both the PS and the PB blocks, they are expected

to appear bright in the SEM image. Therefore, we find isolated PMMA domains on terrace S_{PL} while a continuous PMMA matrix can be attributed to terrace M_{PL} . The SEM images therefore confirm and complement the SFM results discussed above. Quantitative measurements of the tip indentation during SFM experiments [23] reveal that the surface is covered by a continuous (rubbery) PB layer.

We note that surfaces of thicker films (1 μm , not shown here) show the same type of surface reconstruction thereby excluding significant substrate or confinement effects on the observed microdomain structures. Moreover, experiments with a lower molecular weight SBM copolymer reveal the same type of terraces, surface structures, and steps, however with smaller length scales corresponding to the smaller length of blocks.

If we combine the results presented so far, the following picture evolves: Terrace S_{PL} is characterized by isolated PMMA micro domains in a continuous PS matrix, while isolated PS micro domains in a continuous PMMA matrix are observed on terrace M_{PL} . As a working hypothesis, we may explain the experimental observations by a model as depicted in Fig. 3. The lamellar structure of the block copolymer is preserved in the bulk of the thin film and aligned with respect to the substrate surface. As a result, quantized thicknesses are observed in agreement with earlier work on symmetric diblock copolymers [6]. However, the near-surface structure deviates from the lamella morphology. This *surface reconstruction* is driven by the fact that an ideal surface termination does not expose the lowest surface energy butadiene block to the surface and therefore is energetically unfavorable. An exposure of the B middle block may be accomplished by some backfolding of either PS or PMMA chains

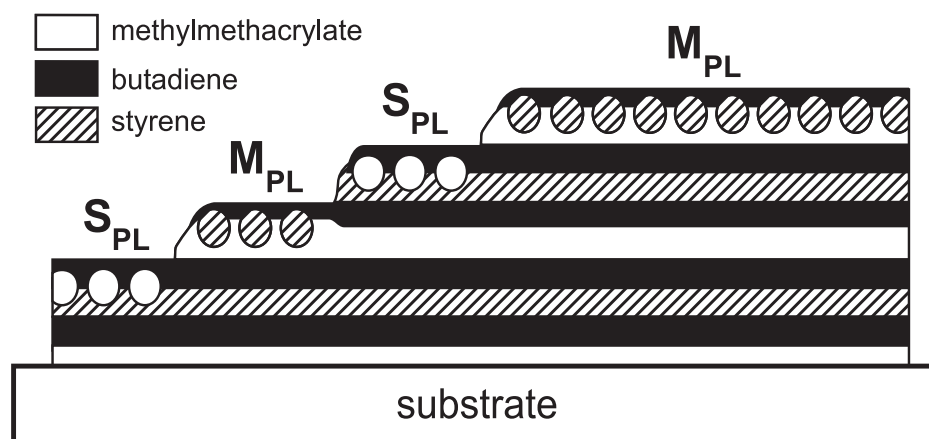


Figure 3: Schematic model of the surface reconstruction of SBM block copolymers with lamellar microdomain structure in the bulk

allowing the free surface to be covered by PB. This picture is in qualitative agreement with earlier 2D computer simulations on the structure of triblock copolymer thin films with symmetric boundary conditions [12]. In contrast, in case of SBM the topmost polymer layer is facing asymmetric boundary conditions: The middle block is attracted by the free surface and one of the end blocks is attracted to the termination of the underlying (bulk) lamellar structure. As the underlying lamellae can be terminated by either S or M , two different surface structures are formed. These structures may best be described as isolated microdomains of the backfolding species embedded in a perforated lamella of the respective other end block, which lead us to the nomenclature S_{PL} and M_{PL} , respectively.

To critically test the role of the surface energy differences between the respective blocks, we have studied another block copolymer of similar molecular weight and volume fractions, however with a different succession of the blocks, i.e., BSM instead of SBM. Here, the lowest surface energy component (B) is an end block and an ideal surface terminating with the B end block should be energetically favorable. Indeed, BSM films prepared in the same way form terraces with well defined film thicknesses, too. In contrast, however, no lateral structure whatsoever is observed on the terrace surfaces. Details of these experiments are beyond the scope of this Letter, however, we note that our findings on BSM thin films closely resemble the situation of *di*-block copolymer thin films with asymmetric wetting conditions [17].

Despite totally different types of matter and order, the experimental observations on SBM surfaces display remarkable similarities with the surface reconstructions of single crystal surfaces, in particular with the (2×1) buckling row reconstruction of Si(100) [3,4]. Indeed, the latter also exhibits two different terrace terminations, characterized by a characteristic 90° rotation of the buckled rows between successive terraces on stepped surfaces. In addition, two different types of steps are observed, depending on the relative orientation of the buckled dimer rows and the steps (see, e.g., Fig 2 in Ref. [4]).

For a thorough discussion of the similarities between ordered complex fluids and "classical" crystals, we first consider the symmetry of the respective structures. The structure of a classical crystal is described by the periodic spatial arrangement of electron density and *point-like* nuclei. Therefore its symmetry belongs to the class of *point groups*. The microdomain structure of a block copolymer on the other hand is described by the density of its components (S , B , and M in case of SBM) and a region with an increased density of one component is called a microdomain. Microdomains can form spheres, cylinders, lamellae or more complex shapes which self-assemble into regular periodic structures resembling crystal like order.

However, since cylinders and lamellae exhibit (partial) continuous translational symmetry, the corresponding bulk microdomain structures belong to the more general class of *space groups*. (Smectic and columnar phases of liquid crystals exhibit a similar symmetry.) The bulk structures of silicon and SBM can both be described as an alternating stack of two non-equivalent layers. In case of Si, successive (100) planes of the diamond lattice differ in terms of the bond directions to the neighboring atomic layer. The two lamellar sub-units SBM and MBS of a lamellar structure, on the other hand, differ in the orientation of blocks. In both cases, the introduction of a surface causes a local rearrangement of matter which leads to a state of lower free energy. In case of the Si(100)-(2×1) “buckling row” reconstruction atomic nuclei and electron density are rearranged in order to decrease the number of dangling bonds and thereby lower the surface free energy of the system. The same is achieved in case of SBM by rearranging the microdomain structure in the topmost layer such that the low surface energy *B* block is exposed to the surface (Fig. 3). Since the bulk structure can be terminated by either one of the non-equivalent layers, two non-equivalent surface structures are observed both on Si(100) and on SBM.

The lateral order within the layers of the bulk structure is different for the two materials: Si is a classical crystal with 2D lattice symmetry within its (100) plane, while the SBM bulk structure is lamellar with continuous 2-dimensional translational symmetry (Euclidian symmetry) within the lamellae. In both cases the symmetry of the reconstructed surface is lowered with respect to the ideal surface, however in very different ways. In case of the Si(100) surface the size of the unit cell of the 2D surface lattice doubles. In case of SBM, the Euclidian symmetry is broken. We emphasize the fact that in both cases a boundary condition imposed in the direction *perpendicular* to the layer breaks the *in-plane* symmetry of the ideal surfaces. This indicates that all three spatial coordinates are coupled on an underlying microscopic scale. This coupling is due to the 3-dimensional nature of the underlying elements (atoms in one case and polymer molecules in the other). The same phenomenon is found in other fields of physics (e.g. high energy physics), where the type of symmetry breaking can reveal properties of underlying (invisible) microscopic particles and processes. An important consequence for block copolymer physics is that the assumption that bulk symmetry is preserved in thin films and at surfaces, which is often made for reasons of simplicity in computer simulations of thin block copolymer films [11,12,15], is not necessarily justified. Therefore, truly 3-dimensional calculations without any symmetry constraints [13,14] are required for an unbiased prediction of thin film and surface structures of block copolymers.

In conclusion, we have shown that the surface structure of a mesoscopically ordered block copolymer exhibits a remarkable analogy to the well-studied surface reconstructions of classical crystals. Both systems differ significantly in the type of matter and order. Common to both is only the presence of a surface, a bulk structure with two non-equivalent alternating layers along the surface normal, and a 3-dimensional structure of the underlying elements. Nevertheless, in both cases the presence of a surface leads to a surface reconstruction with (1) a spontaneous breaking of lateral symmetry of the ideal surface, (2) two types of alternating terraces, and (3) two types of alternating steps. Given the wealth and complexity of ordered bulk structures of block copolymers and surfactant based complex fluids, the study of their surface behavior is expected to become a rewarding field of science.

The authors acknowledge the help of T. Goldacker (polymer synthesis and characterization), C. Drummer (SEM), C. Kunert (TEM), and financial support through the Deutsche Forschungsgemeinschaft (SFB 481).

4.1 References

- [1] Binnig, G.; Rohrer, H.; Gerber, C.; Weibel, E. *Phys. Rev. Lett.* **1983**, *50*, 120.
- [2] Tromp, R. M.; Hamers, R. J.; Demuth, J. E. *Phys. Rev. Lett.* **1985**, *55*, 1303.
- [3] Dijkamp, D.; Hoeven, A. J.; Loenen, E. J. v.; Lenssinck, J. M.; Dieleman, J. *Appl. Phys. Lett.* **1990**, *56*, 39.
- [4] Swartzentruber, B. S.; Kitamura, N.; Lagally, M. G.; Webb, M. B. *Phys. Rev. B* **1993**, *47*, 13432.
- [5] For recent reviews, see Bates, F. S.; Fredrickson, G. H. Bates *Annu. Rev. Phys. Chem.* **1990**, *41*, 525; F. S.; Fredrickson, G. H. Bates *Physics Today* **1999**, *52*, 32; J. W. Hamley, *The Physics of Block Copolymers*, Oxford University Press, Oxford, 1998.
- [6] Anastasiadis, S. H.; Russell, T. P.; Satija, S. K.; Majkrzak, C. F. *Phys. Rev. Lett.* **1989**, *62*, 1852.
- [7] Lambooy, P.; Russell, T. P.; Kellogg, G. J.; Mayes, A. M.; Gallagher, P. D.; Satija, S. K. *Phys. Rev. Lett.* **1994**, *72*, 2899.
- [8] Radzilowski, L. H.; Carvalho, B. L.; Thomas, E. L. *J. Poly. Sci. B Poly. Phys.* **1996**, *34*, 3081.
- [9] Morkved, T. L.; Jäger, H. M. *Europhys. Lett.* **1997**, *40*, 643

- [10] Stocker, W.; Beckmann, J.; Stadler, R.; Rabe, J. P. *Macromolecules* **1996**, *29*, 7502.
- [11] Fasolka, M. J.; Banerjee, P.; Mayes, A. M.; Pickett, G.; Balasz, A. *Macromolecules* **2000**, *33*, 5702.
- [12] Pickett, G. T.; Balazs, A. C. *Macromol. Theory Simul.* **1998**, *7*, 249.
- [13] Sevink, G. J. A.; Zvelindovsky, A. V.; van Vlimmeren, B. A. C.; Maurits, N. M.; Fraaije, J. G. E. M. *J. Chem. Phys.* **1999**, *110*, 2250
- [14] Huinink, H. P.; Brokken-Zijp, J. C. M.; van Dijk, M. A.; Sevink, G. J. A. *J. Chem. Phys.* **2000**, *112*, 2452.
- [15] Matsen, M. W., *J. Chem. Phys.* **1997**, *106*, 7781
- [16] Goldacker, T., Ph.D. Thesis, Universität Bayreuth, Bayreuth, 1999.
- [17] Russell, T.P.; Coulon, G.; Deline, V. R.; Miller D. C. *Macromolecules* **1989**, *22*, 4600
- [18] Anastasiadis, S. H.; Russell, T. P.; Satija, S. K.; Majkrzak, C. F. *J. Chem. Phys.* **1990**, *92*, 5677.
- [19] Brinkmann, S.; Stadler, R.; Thomas, E. L. *Macromolecules* **1998**, *31*, 6566.
- [20] Coulon, G.; Collin, B.; Ausserre, D.; Chatenay, D.; Russell, T. P. *J. Phys. II (France)* **1990**, *51*, 2801
- [21] Limary, R.; Green, P. F. *Macromolecules* **1999**, *32*, 8167
- [22] Kim, G.; Libera, M. *Macromolecules* **1998**, *31*, 2670
- [23] Knoll, A.; Magerle, R.; Krausch, G. *Macromolecules* **2001**, *34*, 4159.

Preface to Chapter 5

This chapter has been published under the title ‘Surface Reconstructions of Lamellar ABC Triblock Copolymer Mesostructures’ by N.R., Armin Knoll, Robert Magerle, and Georg Krausch in *Macromolecules* **2003**, 36, 3261.

5 Surface Reconstructions of Lamellar ABC Triblock Copolymer Mesostructures

Nicolaus Rehse, Armin Knoll, Robert Magerle, and Georg Krausch*

*Physikalische Chemie II and Bayreuther Zentrum für Kolloide und Grenzflächen (BZKG),
Universität Bayreuth, D-95440 Bayreuth, Germany*

**corresponding author*

5.1 Introduction

Microphase separated block copolymers present a class of ordered materials [1], which in many respects resemble crystalline matter. While the latter may be viewed as a three dimensional periodic arrangement of atomic nuclei and electron density, an ordered block copolymer structure is a periodic array of polymer density. Despite the fact that the characteristic length scales differ by some four orders of magnitude, the search for similarities between the rather different types of ordered matter has repeatedly attracted scientific interest [2-4]. Examples are the determination and classification of the symmetry of the ordered mesophases, the characterization of defect structures and their thermal behavior, and certain routes of “single crystal” preparation, such as the moving thermal gradient technique recently devised by Hashimoto and coworkers [5], which closely resembles the zone melting procedure established for metal and semiconductor single crystal preparation. An interesting similarity, which has not yet widely been investigated, concerns the *surface behavior* of ordered block copolymer samples. It is well established in classical surface science that the absence of nearest neighbors can lead to significant deviations of the structure of the topmost atomic layer(s) of a crystal [6]. If only the lattice spacing perpendicular to the surface is changed, the effect of the surface is referred to as a “*surface relaxation*”. If, in addition, the lateral arrangement of the atoms is affected by the surface, the effect is referred to as “*surface reconstruction*”. Both relaxation and reconstruction can affect more than just the topmost atomic layer. The prominent example of the Si(111)7×7 reconstruction [7], for example, is brought about by structural rearrangements (both laterally and perpendicular to the surface) of as much as the topmost five atomic layers.

The study of block copolymer surfaces dates back to the early eighties when it was realized that irrespective of the underlying microdomain structure, the surface of diblock copolymer

specimens is usually covered by the lower surface energy block [8]. Initiated by the thin film work of Anastasiadis *et al.*[9], surface effects became an area of increasing interest at the beginning of the last decade, as they tend to dominate the morphology of block copolymer films in a thickness range of several bulk lamellar spacings [10,11]. Much of the work concentrated on lamella forming diblock copolymers, where the major effect lies in an alignment of the lamellae parallel to the confining surfaces. The more complex situation of ternary block copolymers has only recently been addressed both theoretically [12,13] and experimentally [14-16]. The first explicit comparison between structural effects on block copolymer surfaces and classical surface science was put forward by Stocker *et al.* [14], who investigated the surface structure of an ABC triblock copolymer and interpreted the experimental findings as a surface reconstruction. Despite a constantly growing number of publications dealing with block copolymer thin films, an in-depth discussion of the observed effects in the light (and language) of classical surface science is still lacking. In a recent letter, we have started such a discussion based on experimental results on the near-surface structure of a lamellar ABC triblock copolymer forming a non-lamellar, reconstructed surface structure [17]. In the present publication, we present further experimental data on the surface behavior of the same and similar block copolymer systems. Furthermore we work out in more detail the comparison between the effects found on the surfaces of block copolymer and the surface behavior of classical crystals. Our work is motivated by the conviction that similarities in the behavior of rather different classes of matter can reveal information on the underlying (general) concepts of nature.

The remainder of the paper is organized as follows. We first describe experimental results on the thin film and near-surface structure of four different ABC triblock copolymers, all of which exhibit a lamellar morphology in the bulk of the films (Fig. 1). We then discuss the experimental results in view of the concepts established in classical surface science and try to identify similarities and differences of the surface behavior of these rather different classes of material.

5.2 Experimental

Monodisperse batches of different linear triblock copolymers of the type polystyrene-*block*-polybutadiene-*block*-poly(methylmethacrylate) (SBM), polybutadiene-*block*-polystyrene-*block*-poly(methylmethacrylate) (BSM), and polystyrene-*block*-polybutadiene-*block*-poly(*tert*-butylmethacrylate) (SBT) were investigated in this study. All polymers were synthesized anionically following standard procedures [18]. Details concerning the synthesis

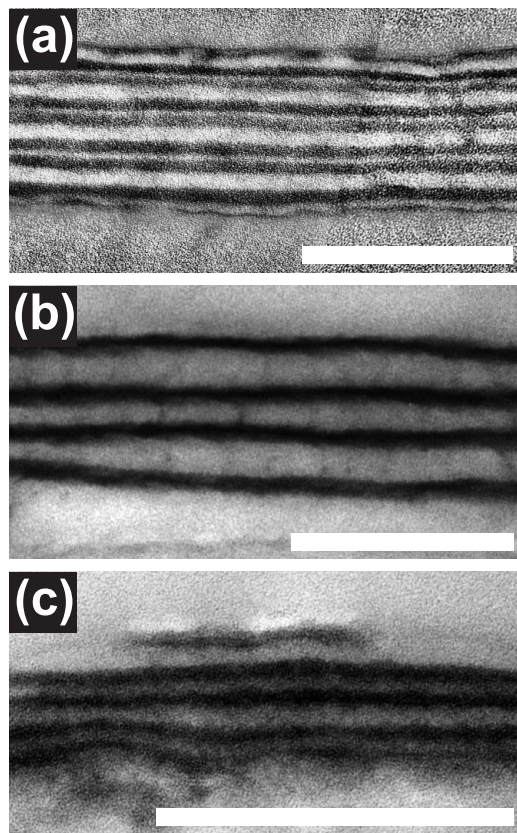


Figure 1: Cross sectional TEM images of thin films of SBM¹⁶² (a), BSM¹⁹⁶ (b) and SBT¹⁶⁰ (c). All samples were stained with OsO₄, therefore the dark regions can be assigned to PB. The scale bars represent 200 nm.

and the bulk properties of the materials can be found in Ref. [19]. The molecular parameters of the polymers are listed in Table 1. All four polymers exhibit a lamellar microstructure in the bulk. The characteristic lamellar spacing L_0 is included in Table 1.

Copolymer films of thickness 100 - 1000 nm were prepared on polished Si wafers by dip coating from 5 wt-% polymer solutions in chloroform. In order to drive the samples towards thermodynamic equilibrium, the films were exposed to a well-controlled pressure of chloroform vapor (near but below saturation) for 1 day and dried slowly, by reducing the vapor pressure continuously over a period of 10 hours. The samples were kept at a temperature $T_{sample} = 20.0 \pm 0.1$ °C in a closed vessel together with a chloroform reservoir kept at a slightly lower temperature $T_{solvent} = 19.5 \pm 0.1$ °C. The solvent vapor pressure was varied by variation of $T_{solvent}$. Care was taken to keep $T_{solvent} < T_{sample}$ to avoid infinite swelling of the polymer film and to assure reproducible sample preparation. The preparation procedure resembles the solvent casting (slow drying) process typically used for bulk samples of these [19] and similar materials.

Polymer	M_w [kg/mol]	ϕ_{PS}	ϕ_{PB}	$\phi_{PMMA/PtBMA}$	M_w/M_n	L_0 [nm]
SBM ¹⁶²	162	0.33	0.47	0.20	1.02	$\sim 80^a$
SBM ⁵⁴	54	0.34	0.37	0.29	1.04	47 ^b
BSM ¹⁹⁶	196	0.35	0.35	0.30	1.12	105 ^b
SBT ¹⁶⁰	160	0.32	0.35	0.33	1.04	85 ^b

Table 1: Molecular parameters of the polymers used in this paper. M_w and M_w/M_n are determined by size exclusion chromatography (SEC) using a PS standard. (^a For SBM¹⁶², the characteristic bulk spacing L_0 was estimated based on the data provided in Ref. [38]; ^b For the three remaining copolymers, the characteristic bulk spacing L_0 is taken from small angle X-ray scattering (SAXS) experiments [19]).

The resulting thin film samples were investigated by optical microscopy (OM), TappingMode™ scanning force microscopy (SFM), cross sectional transmission electron microscopy (TEM), and low energy scanning electron microscopy (SEM). For the TEM experiments the films were floated off the SiO_x covered Si substrates onto aqueous KOH solution, picked up onto a TEM grid, embedded into epoxy, and subsequently cut into ~ 50 nm thick slices. In order to avoid swelling in unreacted epoxy, the films were coated with a thin carbon layer prior to embedding. To enhance contrast the films were stained with OsO₄. For the SEM investigations RuO₄ was used as a selective stain. A field emission source with low energy electron beam (~ 1 kV) was used. No further coating with a conductive material was needed.

5.3 Results

5.3.1 Surface reconstructions: SBM

We start our discussion with the two SBM triblock copolymers. Prior to investigating the near-surface structure of the block copolymer, we have to unambiguously determine the “bulk structure” of our thin film samples. Based on the work on thin films of symmetric polystyrene-*block*-poly(methyl methacrylate) (SM) *diblock* copolymers [9,20], one expects an attraction of the polar M end block to the polar SiO_x substrate surface. In the diblock copolymer case, this attraction is known to lead to an alignment of the lamellae parallel to the

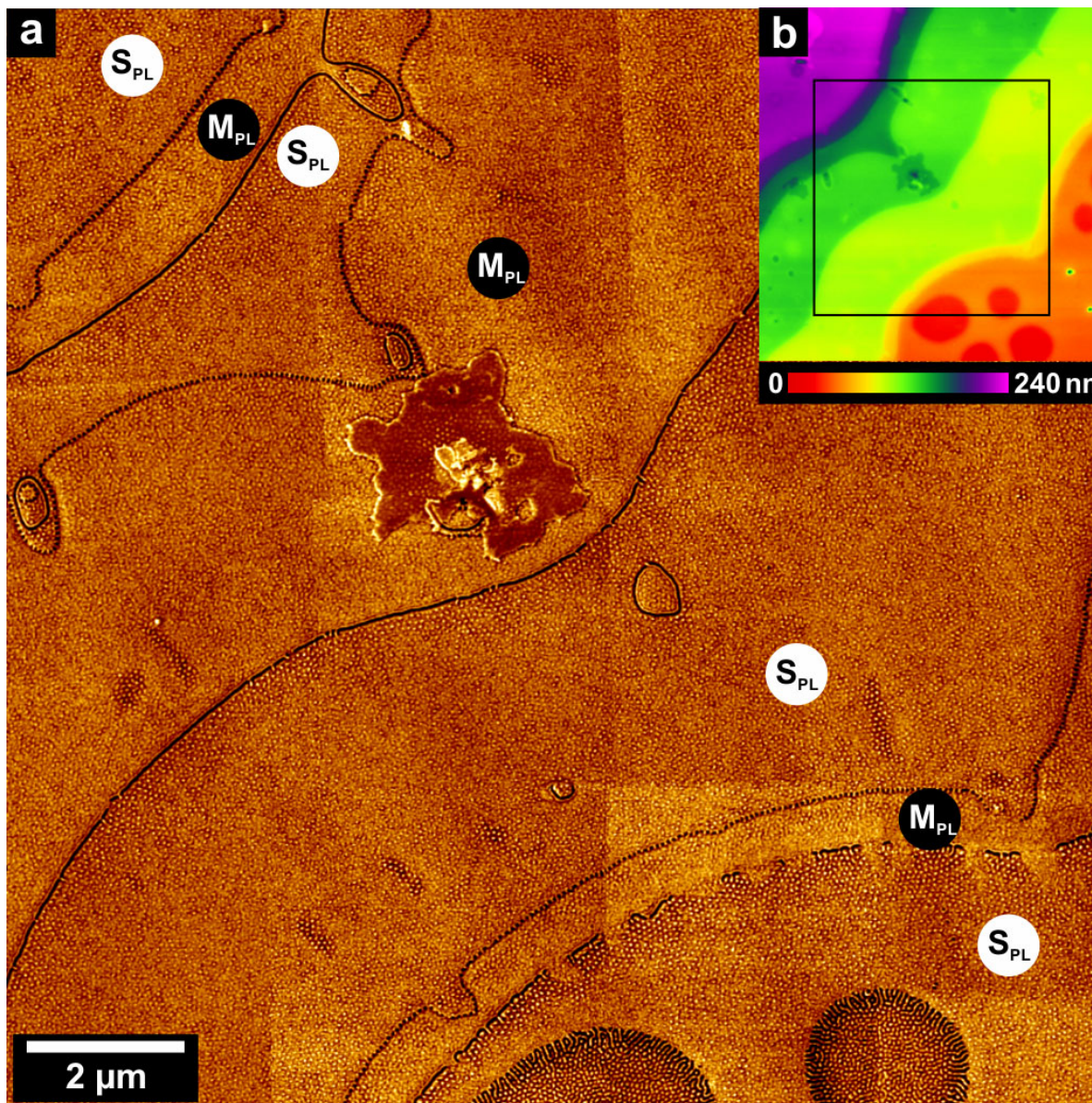


Figure 2: TappingMode SFM images of the phase contrast (a) and the topography (b) of the surface of a thin SBM¹⁶² film. The phase contrast image corresponds to the black square in (b) and is a composite of 16 individual SFM images.

plane of the film. To establish the “bulk structure” of the SBM triblock copolymer films, cross-sectional TEM images were taken. Figure 1a shows such an image for SBM¹⁶². One can clearly see the lamellar microdomain structure of the block copolymer aligned parallel to the plane of the film. The black regions can be assigned to PB, which is stained preferentially on exposure to OsO₄ vapor. According to the PMMA volume fraction, the thinner bright regions are assigned to PMMA. The wider bright regions are considered to be PS. The lamellar spacing $L_{0, film}$ amounts to 47 ± 5 nm and therefore is somewhat smaller than the bulk lamellar period $L_0 = 80$ nm (see Table 1). This deviation may be due both to beam damage on the

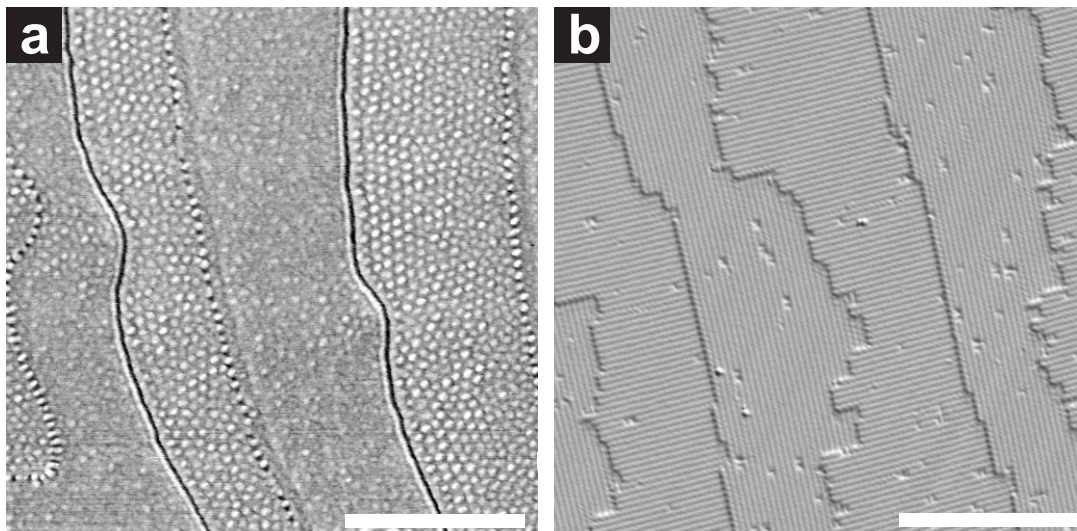


Figure 3: (a) TappingMode™ SFM phase image of a SBM¹⁶² film showing the two different kinds of terraces at the free surface. Scale bar: 1 μm . (b) Scanning tunneling microscopy image of a stepped Si(100) surface forming a (2x1) surface reconstruction (Courtesy of M.G. Lagally, University of Wisconsin, Madison). The different orientations of neighboring terraces are clearly visible. Scale bar: 5 nm.

PMMA [21] and to some shrinkage of the film during the preparation process. The layered structure of the films is also reflected in SFM topography images of regions, where the film thickness is laterally varying. Here, the annealing process leads to the formations of areas of well-defined thickness (terraces), separated by steps of well-defined height H_{step} (Fig. 2b). The terraced structure of the film surface is also found on spincoated samples after solvent vapor annealing. So far the results closely resemble the behavior of diblock copolymer thin films. SFM measurements of the step heights H_{step} , however, yield values of only about half the lamellar period $L_{0, film}$ found in the bulk of the film ($L_{0, film} \approx 30$ nm). The absolute values are found to vary somewhat between different experiments. The relative values $H_{step} / L_{0, film}$, however, always follow the same trend, i.e., $H_{step} \approx \frac{1}{2} L_{0, film}$. We note, though, that the determination of the lamellar spacing in the bulk of the film $L_{0, film}$ presents only a lower boundary to the actual value due to the beam damage on the PMMA blocks. In any case, we find that the step heights determined by SFM are always considerably smaller than the lamellar spacings determined from the cross sectional TEM images.

If the lamellar structure would proceed throughout the entire sample to the free surface of the film, a laterally homogenous surface layer rich in one of the end blocks would be expected. However, higher resolution SFM images show unexpected lateral patterns on the terraces (Figs. 2a, 3a). Two different types of lateral patterns are observed, which strictly alternate

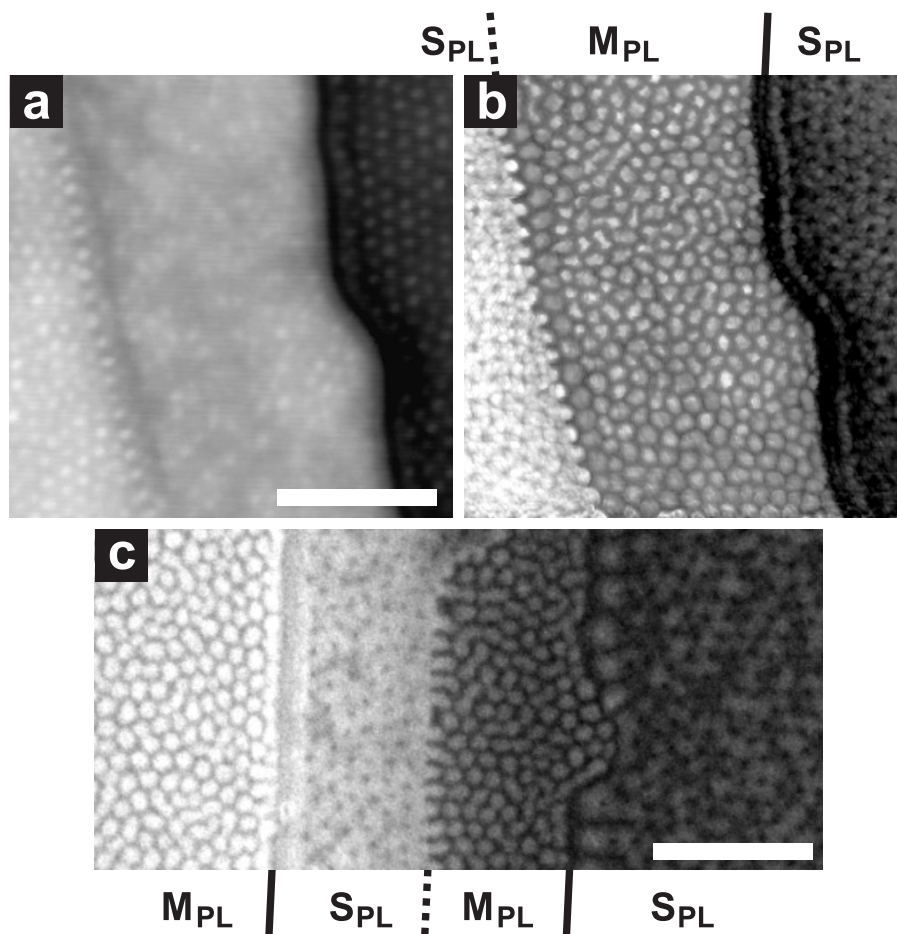


Figure 4: SFM height images of a SBM¹⁶² film before (a) and after (b) etching with RF plasma. (c) shows a SEM image of a RuO₄ stained SBM¹⁶² film. The dark regions correspond to PMMA rich areas. Scale bars: 1 μ m.

between successive terraces. For further reference and for reasons to become clear below, we refer to the two terrace structures as S_{PL} and M_{PL}, respectively. S_{PL} is characterized by isolated bright dots with a typical lateral repeat distance of some 60 ± 3 nm embedded in a continuous matrix. Terrace M_{PL} shows a similar pattern however with less contrast. Along with the terraces, the shape of the steps between them is found to alternate as well. As we move downward on the sample (from left to right in Fig. 3a), the step from M_{PL} down to S_{PL} is continuous and rather featureless, while the step from S_{PL} down to M_{PL} has a dotted appearance in the SFM phase image.

To gain further insight into the near surface microdomain structure and to distinguish between the different materials we made use of the different etching rates of the three blocks in an oxygen plasma. The samples were exposed to an RF plasma in air (Harrick Plasma Cleaner, 1 mbar, 60 W at 13.56 MHz, 45 sec). As determined from SFM measurements prior to and after the etch, this procedure removes about the topmost 14 nm of the polymeric material. Note that

the same spot was imaged with SFM before (Fig. 4a) and after etching (Fig. 4b). Before etching terrace S_{PL} exhibits an array of protrusions, while no significant roughness is detected on terrace M_{PL} . After the etch, the protrusions on terrace S_{PL} have turned into depressions while terrace M_{PL} now exhibits an array of protrusions. We have determined the etching rates for the three components in a separate experiment [22,23] and found that the B and M blocks are etched twice as fast as the S block. Therefore, we can assign the continuous phase remaining after the etch on terrace S_{PL} as PS. The same holds for the protrusions formed on M_{PL} during the etch. To further distinguish between PB and PMMA, we have treated the films with RuO_4 , which is known to selectively stain the PB and PS blocks. The samples were then investigated with a field emission SEM (Fig. 4c). Under the employed imaging conditions the stained regions appear bright in the SEM images. Therefore, the dark areas can be assigned to M. From Fig. 4c, we conclude that on terrace M_{PL} we have a continuous matrix of M, whereas on S_{PL} , isolated M domains are present.

Summarizing the results discussed so far, the following picture evolves. The bulk of the thin film exhibits a lamellar structure with the lamellae being aligned parallel to the film by virtue of interactions with the substrate (cross sectional TEM). The film develops “quantized” thicknesses, which are found to be integer multiples of half the lamellar spacing $L_{0, film}$ (SFM height images). Two different surface terminations of the lamellar structure are observed (M_{PL} and S_{PL}), which strictly alternate between neighboring terraces (SFM phase images). Terrace M_{PL} consists of isolated PS microdomains (SFM & etching) in a continuous matrix of PMMA (SEM & staining), while terrace S_{PL} is characterized by PMMA domains (SEM &

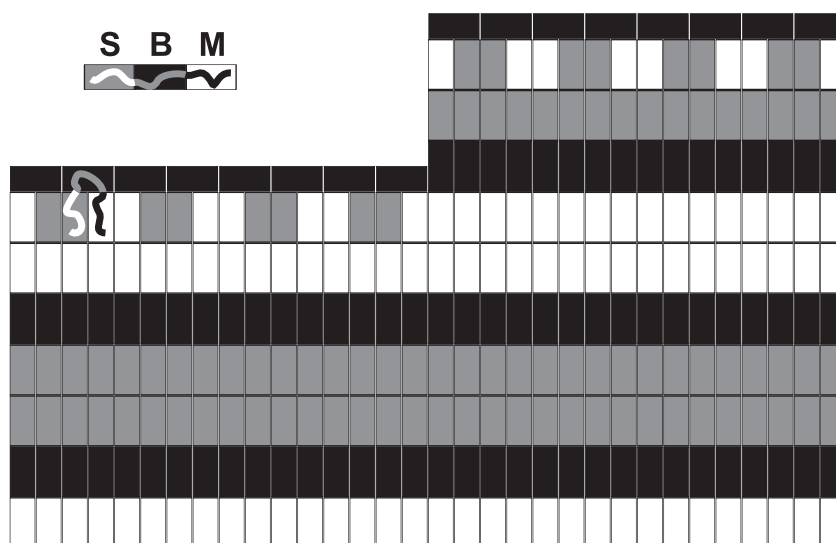


Figure 5: Schematic model of the near surface morphology of SBM¹⁶² (see text for explanation).

staining) in a continuous matrix of PS (SFM & etching). In other words, terrace M_{PL} can be looked at as a perforated PMMA lamella with PS inclusions and vice versa for terrace S_{PL} . This finding led us to the notations M_{PL} and S_{PL} , respectively.

To visualize the potential structure of our films, Fig. 5 shows a model comprising all the experimental results. In addition, the model allows for the fact that from the three components of our triblock copolymer, the PB middle block has the lowest surface energy. Therefore, we expect the surface to be covered homogeneously by a thin PB layer. In contrast to the ideal surface, which would be terminated with a PS block, the polymer rearranges,

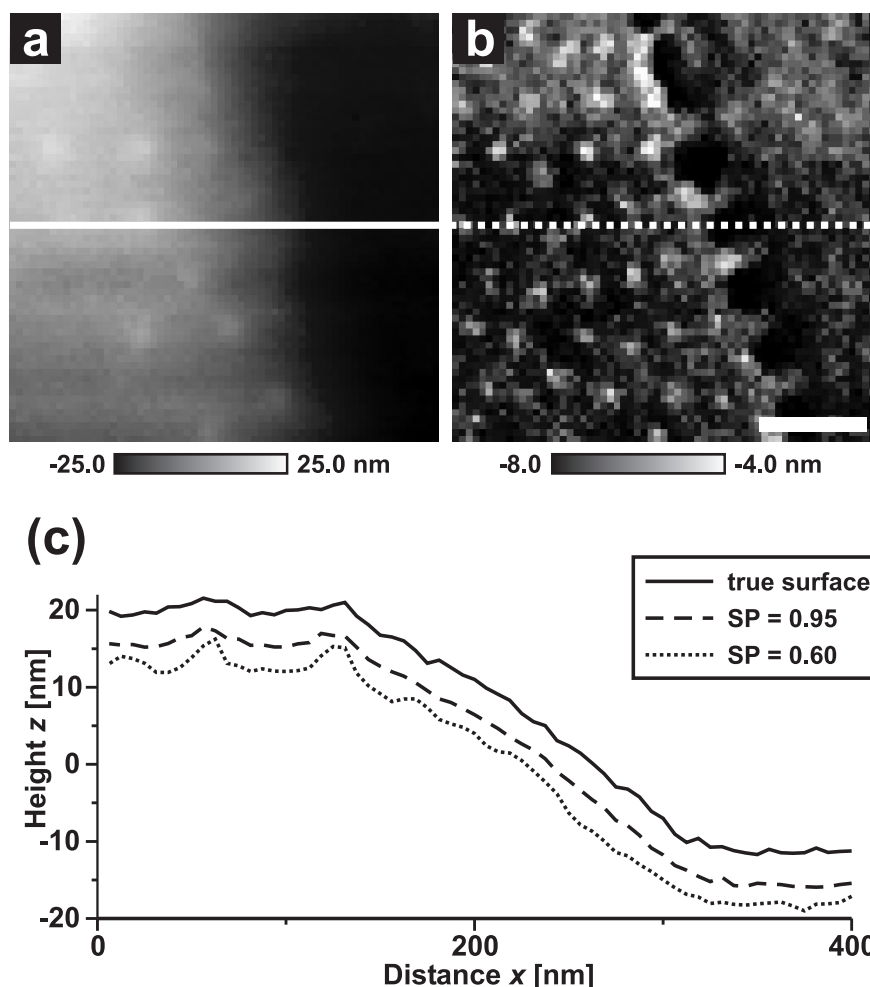


Figure 6: SFM images of a step from a S_{PL} terrace down to a M_{PL} terrace (from left to right). (a) Image of the true surface. (b) Image of the indentation with an amplitude setpoint of 0.6. It is the difference between the true surface image shown in (a) and the height image taken at a setpoint of 0.6; scale bar: 100 nm. (c) Profiles of the true surface shown in (a) and of height images determined from amplitude/phase vs. distance curves for setpoints of 0.95 and 0.6. Tapping with a setpoint of 0.95 is usually called ‘soft tapping’. Note that there is no height offset between the three curves.

folding back the S chains into the adjacent M domain and thereby giving way to PB to cover the surface. Below this thin PB layer the near surface structure is a continuous layer of PMMA perforated by isolated PS micro domains (M_{PL}). Accordingly, if a lamella would ideally terminate with PMMA, the respective process leads to a perforated layer of PS including isolated M micro domains. In both cases, a continuous layer of PB can cover the surface. The model explains both the existence of two different terminations which strictly alternate between neighboring terraces as well as the observation that the step heights H_{step} amount to only about half the lamellar spacing $L_{0, film}$ in the bulk of the film.

The existence of a homogeneous layer of polybutadiene on the surface of both S_{PL} and M_{PL} is - although expected in terms of surface energy - difficult to establish experimentally. We can get indirect evidence, however, by quantitative measurements of the indentation depths of the SFM tip during TappingMode imaging. As both PS and PMMA are glassy solids at room temperature, the SFM tip can indent only by small amounts under the typical imaging conditions. PB, on the other hand, is easily indented by several nanometers under typical imaging conditions, since it is a rubbery liquid at room temperature. SFM TappingMode height images of surfaces with a laterally varying stiffness do not necessarily represent the topography of the surface but are complex superpositions of both true surface topography and lateral variations in the indentation depth of the tip. Following a protocol devised by Knoll *et al.*²⁴, we therefore have determined both an image of the true sample surface (Fig. 6a) and of the absolute indentation depth at a setpoint of 0.6 (Fig. 6b). The images consist of 64 x 64 data points, each of which is calculated from an entire amplitude/phase vs. distance curve taken at the respective location. In Fig. 6c three line scans taken at different setpoints are shown. All heights are in absolute values. Indeed, the indentation of the tip is much higher than on a pure PS or PMMA surface. It is comparable to what was found on the surfaces of thin films of polystyrene-*block*-polybutadiene-*block*-polystyrene (SBS) exhibiting PS cylinders in a PB matrix [24]. Here, as well, the hard PS domains are covered with a continuous, soft PB layer. Our data therefore corroborate the presence of a continuous PB layer covering both surface terminations M_{PL} and S_{PL} found on the SBM surface.

In the thinnest regions of the film, yet another surface pattern is observed. This can be seen in the bottom of Fig. 2 (middle part). Figures 7a and 7b show higher magnification images of the boundary between this layer and the neighboring S_{PL} terrace. This pattern has the highest contrast in the SFM phase image. The most distinguished features are the stripe-like domains oriented perpendicular to the boundary with the neighboring terrace [25]. We note that we have used this particular boundary structure to unambiguously identify the “layer number”

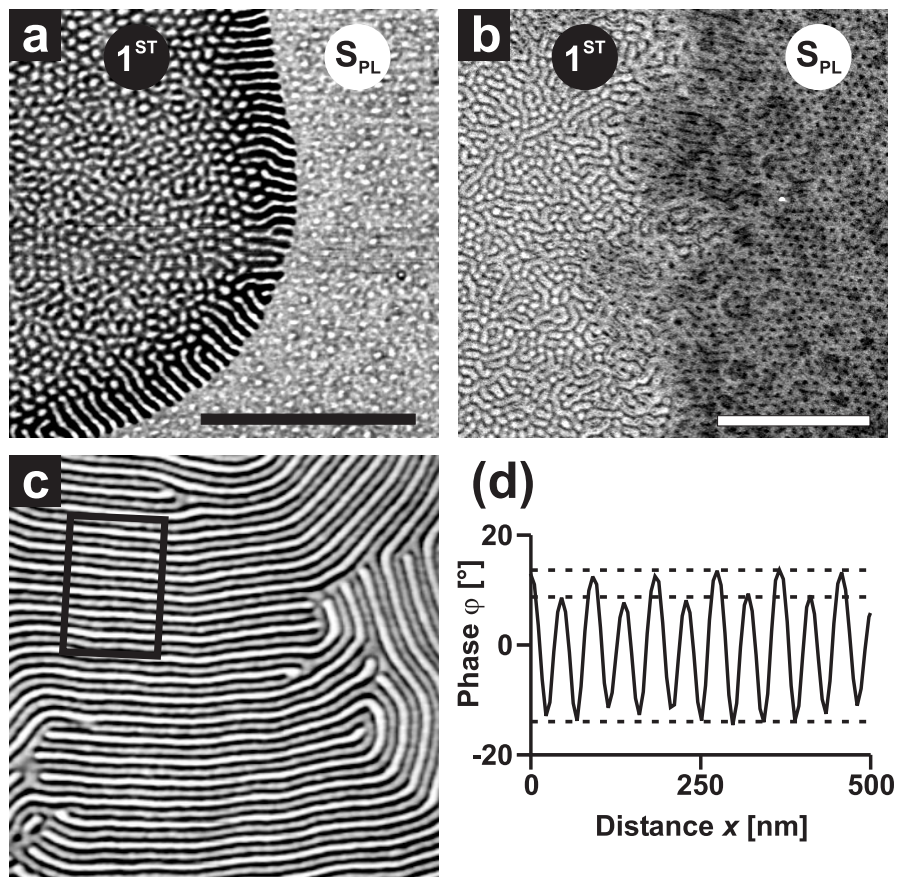


Figure 7: (a) TappingMode™ SFM phase image of an SBM¹⁶² film. It shows the step between the first terrace and the neighboring S_{PL} terrace. (b) SEM image (RuO₄ stained) of a step between the first terrace and the neighboring S_{PL} terrace. (c) TappingMode™ SFM phase image of the stripe pattern appearing in regions with a film thickness of t_{film} ≈ 18 nm. (d) Profile of the phase signal averaged along the short side of the boxed area in Fig. 4c. The dotted lines are a guide to the eye.

both in the SFM and in the SEM experiments referred to above in order to assign S_{PL} and M_{PL} in the images taken by the two different techniques. We also note that in some of our experiments, this particular boundary pattern was found to extend over rather larger lateral areas. This can be seen in Fig. 7c, which shows an SFM phase image of an area of thickness 18±2 nm. A cross section through the phase image (Fig. 7d) reveals that all three blocks are arranged in a stripe like fashion which may best be described as a perpendicular lamella. Although this particular structure may be of interest in the context of nanopatterning applications, we shall not discuss it in any further detail since this is not a surface reconstruction but an effect of confinement and shall be discussed elsewhere.

5.3.2 Effect of block copolymer molecular weight: SBM⁵⁴

So far our discussion concerned the SBM¹⁶² triblock copolymer only. We have performed similar experiments on thin films of the lower molecular weight SBM⁵⁴ triblock copolymer (Fig. 8). This material shows qualitatively the same behavior, while all characteristic lengths, L_0 , $L_{0, film}$, H_{step} , as well as the in-plane characteristic spacing are considerably smaller. The step heights are again significantly smaller than the lamellar period found in bulk samples. In the SFM phase images we observe a weaker contrast between the different blocks. This may be attributed in part to the smaller lateral domain size. In addition, PS and PMMA will be less incompatible at this rather small molecular weight. In consequence, the PS/PMMA interfaces are considerably wider and the two polymers exhibit weaker segregation. However, qualitatively the same features are observed: Two different surface terminations are found to alternate between neighboring terraces and two types of steps can be identified on top of an otherwise lamellar structure.

Aside from the differences in molecular weight, SBM⁵⁴ exhibits an almost perfectly symmetric composition ($\phi_{PS}=0.34$, $\phi_{PB}=0.37$, $\phi_{PMMA}=0.29$), while in SBM¹⁶² the PB block is significantly larger than the PMMA block ($\phi_{PS}=0.33$, $\phi_{PB}=0.47$, $\phi_{PMMA}=0.20$). The observation that SBM⁵⁴ shows qualitatively the same surface behavior therefore clearly indicates that the effects described above for the higher molecular weight material *are not due* to its asymmetric composition.

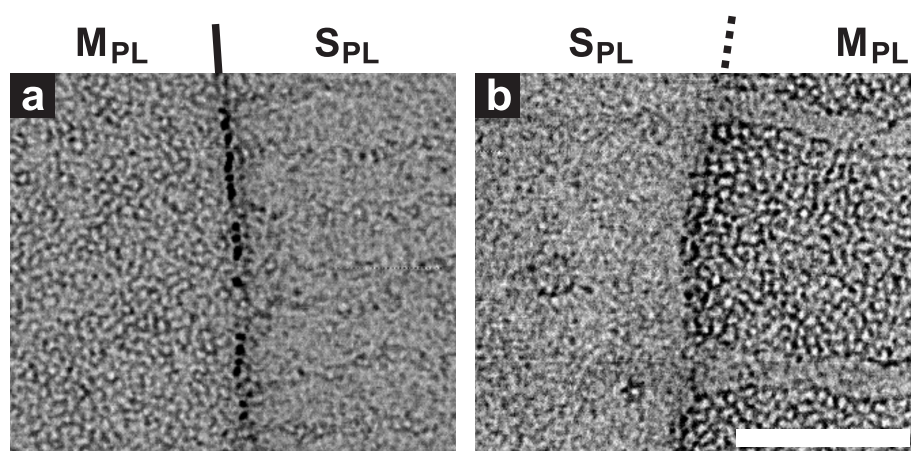


Figure 8: (a), (b) TappingModeTM SFM phase images of a SBM⁵⁴ film. They show, from left to right, a step from an M_{PL} terrace down to an S_{PL} terrace (a) and a step from an S_{PL} terrace down to an M_{PL} terrace (b). Scale bar: 500 nm

5.3.3 Role of molecular topology: BSM

In the above discussion, we have identified the lower surface energy of the PB middle block as the driving force for the rearrangement of the near-surface micro domain structure of SBM thin films. In order to test this hypothesis, we have extended our investigations to thin films of BSM triblock copolymers, where the low surface energy PB block has been moved from the middle to one of the ends of the block copolymer. In this case, the lamellar structure should extend throughout the entire film, and we expect a lateral homogeneous film surface. We start again with the cross sectional TEM image (Fig. 1b), which shows a lamellar microdomain morphology. Since we only stain the PB block by RuO_4 and PS and PMMA domains are no longer separated by PB, we can not distinguish all three blocks. However, the alignment of the lamellae parallel to the plane of the film is clearly visible. We also find a certain shrinkage of the films perpendicular to the lamellae, i.e. the lamellar period $L_{0, \text{film}}$ is again smaller than the bulk value L_0 [19]. SFM height images show regions of well defined thickness separated by steps of height H_{step} . To determine the absolute thickness of the different regions with SFM, we applied a scratch to the film, which reached down to the substrate surface (Fig. 9a). From the height profiles obtained this way (Fig. 9c), we find that $H_{\text{step}} \approx L_{0, \text{film}}$ for all but the first steps. The first step, i.e. the thickness of the thinnest regions of the film amount to about $\frac{1}{2} L_{0, \text{film}}$. Again the absolute values of film thickness H_{film} vary due to differences in preparation, but the relative values all follow the relation $H_{\text{film}} \approx (n + \frac{1}{2}) L_{0, \text{film}}$ with $n = 0, 1, 2, \dots$. Closer inspection of the surfaces by SFM imaging did not reveal any lateral structure on the terraces (Fig. 10a and 10b).

The results on BSM resemble the well-known behavior of lamella forming diblock copolymer thin films under asymmetric wetting conditions, i.e., when one of the blocks preferentially wets the substrate while the other preferentially wets the surface of the film [9]. This behavior is found, e.g., for PS-*block*-PMMA diblock copolymers on polar substrates: Having a lower surface energy, PS accumulates at the free surface while PMMA is attracted to the polar substrate. Consequently, the smallest “quantized” value of film thickness compatible with these boundary conditions is $\frac{1}{2} L_0$. Thicker films will tend to form $(n + \frac{1}{2})$ multiples of L_0 . In BSM, the B block has the lowest surface energy while the M block is attracted to the substrate. The S middle block can be considered “neutral” with respect to the boundary surfaces and therefore does not interfere with the lamellar structure in the thin film.

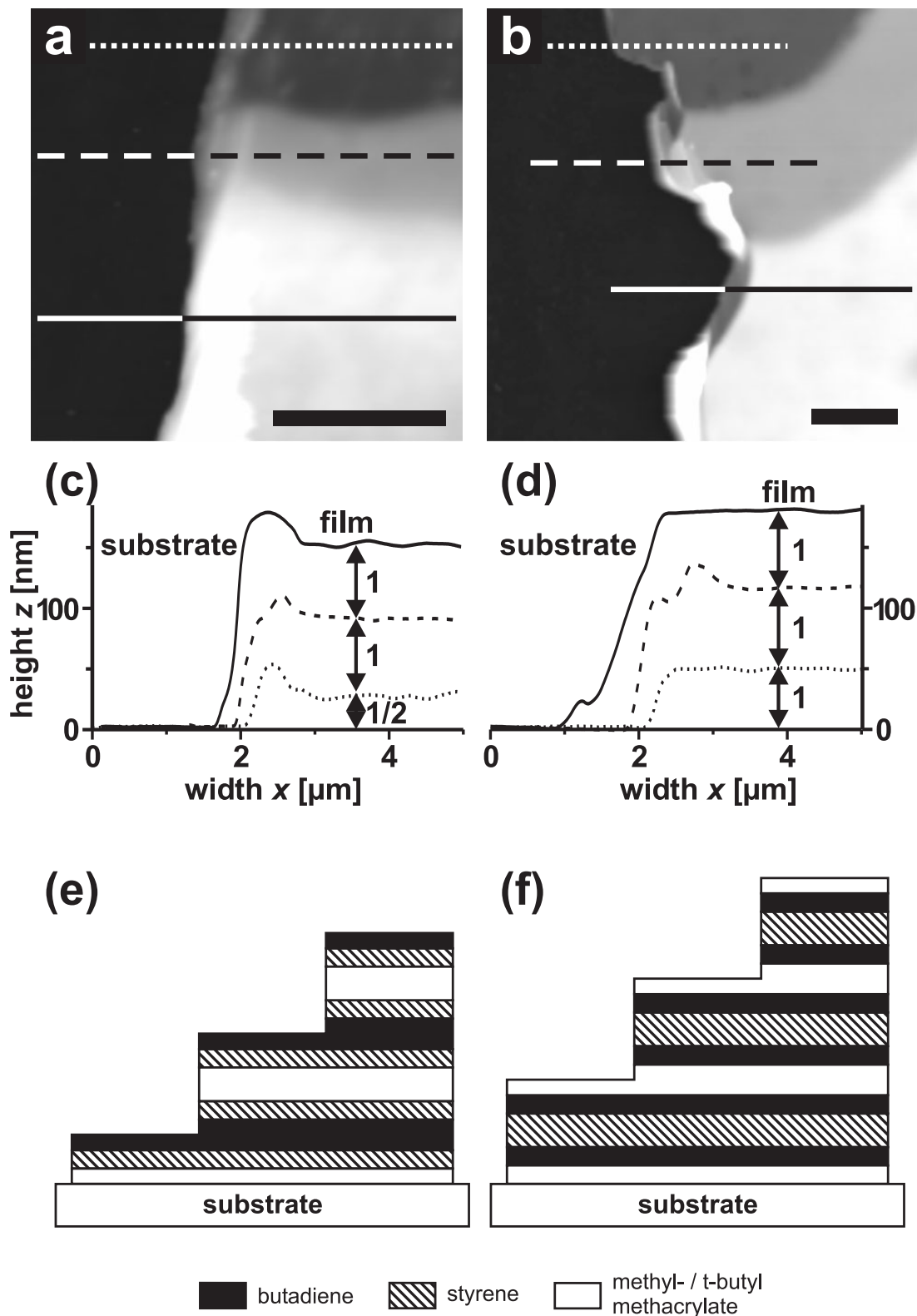


Figure 9: SFM height images of a scratch (at the left side of the images) in a BSM (a) and an SBT film (b). (c) and (d) show height profiles of the corresponding lines in (a) and (b), respectively. (e) and (f) are schematic models of BSM (e) and SBT (f) films. Scale bars: 2 μm .

5.3.4 Strength of the surface field: SBT

We turn back to the surface reconstruction observed in the SBM system, where we have identified the gain in surface energy as the driving force for the formation of a different near surface structure. One has to realize, though, that the proposed “backfolding” of the PS and PMMA blocks into the topmost PMMA and PS lamellae, respectively, will lead to an increase in free energy, both by unfavorable chain conformations (entropic contribution) and by the creation of additional PS/PMMA interfaces (enthalpic contribution). In case of SBM, this cost in free energy seems to be more than compensated for by the gain in surface free energy realized by the exposition of PB to the free surface.

This is not necessarily the case. To demonstrate the competition between the different contributions to the free energy, we have studied thin films of SBT as well. The incompatibility between the two end blocks PtBMA and PS is larger than in the case of PS and PMMA [19]. In addition, the surface energy difference between the middle block PB and the lower surface energy end block PtBMA is smaller than in the case of SBM [26]. In consequence, one may expect a different surface behavior. We again start our discussion with the cross sectional TEM results (Fig. 1c). A lamellar morphology is observed as in the two

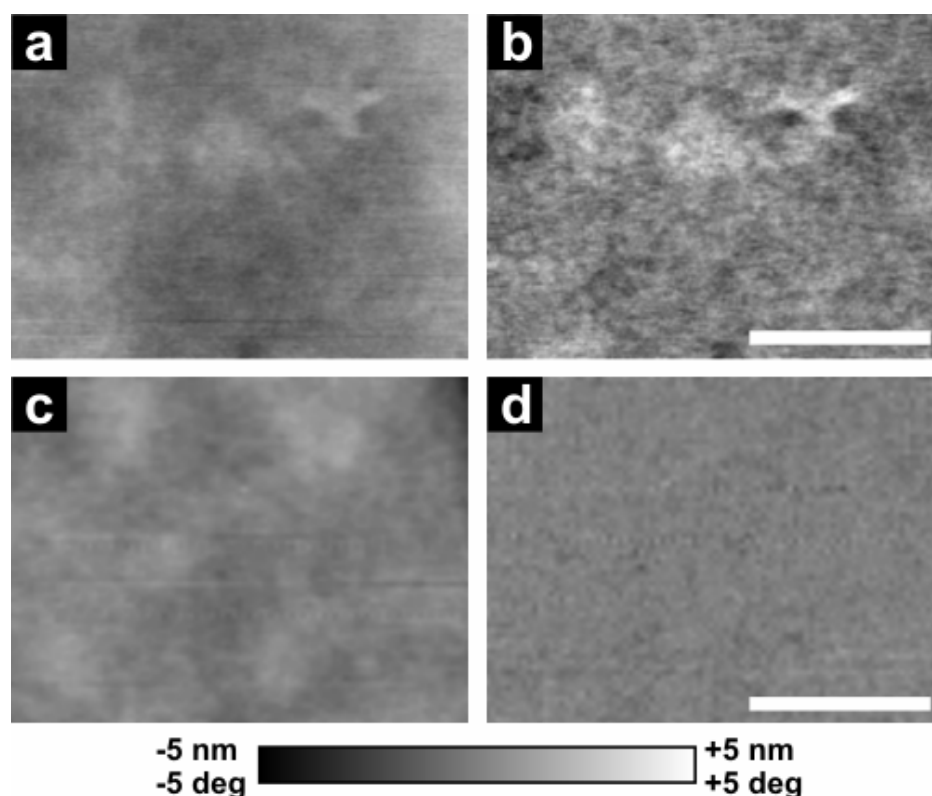


Figure 10: TappingMode™ SFM height (left) and phase images (right) of the free surface of BSM (a, b) and SBT (c, d), respectively. Scale bar: 400 nm.

preceding cases. The lamellae are aligned parallel to the plane of the film. Also a terraced film topography is formed. In contrast to both preceding cases, however, SFM investigation of the height profiles (Fig. 9b and 9d) show that the quantized values of film thickness are *integer* multiples of the lamellar spacing, i.e., $H_{film} \approx n L_{0,film}$ with $n = 1, 2, 3, \dots$. As detected by SFM topography (Fig. 10c) and phase imaging (Fig. 10d), the surfaces of the films do not exhibit any lateral features.

This result is comparable to what is known for lamella forming diblock copolymers under symmetric wetting conditions, i.e., when the same block preferentially wets both interfaces [20]. The increased interfacial tension between PS and PtBMA together with a decreased driving force (i.e., a smaller surface energy difference between PtBMA and PB) prohibits the formation of a lateral surface structure, which would allow the lower surface energy component B to be exposed at the free surface. A comparison of the behavior of SBM and SBT indicates that a subtle balance between the different contributions to the free energy of the system determines whether or not the termination of the bulk structure at the free surface is “ideal” or whether a reconstruction of the near-surface structure is energetically favorable.

5.4 Discussion

The experiments described above clearly show that the near-surface structure of a block copolymer sample can deviate from the bulk structure by formation of a surface reconstruction. By comparing the behavior of different ABC triblock copolymers, we have identified the gain in surface free energy as the driving force for this surface reconstruction. Moreover, we have given evidence that the gain in surface free energy must be large enough to balance other (positive) contributions to the free energy related to the deviation from the bulk structure in order for a surface reconstruction to be formed. In the following, we shall briefly recall the concept of surface reconstructions as introduced in classical surface science and identify some similarities and differences between the different classes of materials. We shall then propose a general nomenclature for block copolymer surface reconstructions. Finally, we shall discuss the experimental conditions required for a successful study of block copolymer surface structures.

5.4.1 Similarity to surface reconstructions of inorganic crystals

We start our discussion by considering a perfect single crystal, which is terminated along one of its crystal planes by a surface. If the crystal structure of the respective planes remains

unchanged all the way to the surface layer, one often refers to this termination as the *ideal surface* of the crystal. However, quite often the atomic layers near the surface do not exhibit the same structure as the respective bulk crystal planes. Due to the absence of neighboring atoms, the distribution of electron density and atomic nuclei experience a potential considerable different from the bulk. As a consequence, a different spatial distribution of electron density and nuclei may result, representing the lowest free energy state of the system. In the case of so-called *surface relaxations*, the in-plane structure of the surface layers remains unchanged and only the layer spacing is affected by the presence of the surface. Often however, the in-plane structure is changed as well. This situation is referred to as a *surface reconstruction*. While many metal surfaces exhibit surface relaxations only, covalently bound materials often exhibit complex surface reconstructions.

The Si(100)-(2x1) surface represents a well-known example for a surface reconstruction. In the case of the ideal Si(100) surface, two half-filled electronic orbitals (so called *dangling bonds*) would extend from each surface atom into free space (Fig. 11a). This state is characterized by a rather high surface energy. A lower free energy is reached by the formation of atomic dimers in the surface layer, which cuts the number of dangling bonds in half and thereby considerably reduces the surface energy. Different microscopic models have been proposed for the detailed structure of the Si(100)-(2x1) surface reconstruction and a discussion of them would be beyond the scope of the present article [27-29]. We only note

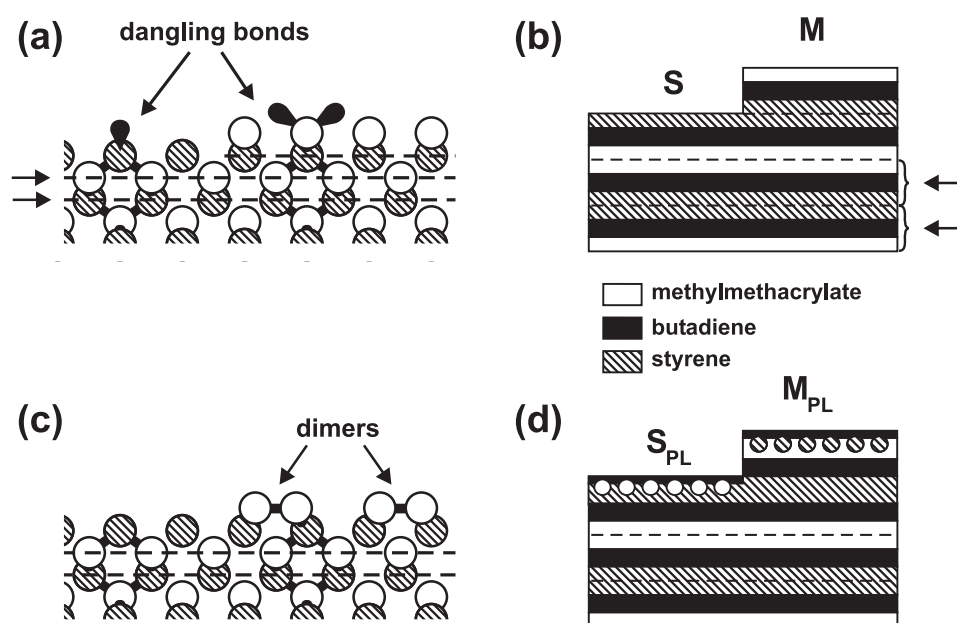


Figure 11: Schematic model of ideal (left) and reconstructed surfaces (right) of Si(100) (a, c) and SBM (b, d). The arrows in (a) and (b) indicate the non-equivalent layers.

that the formation of dimers breaks the four-fold symmetry of the (100) lattice plane of the cubic diamond lattice and leaves the surface with only two-fold symmetry. This is clearly revealed by scanning tunneling microscopy images [29] of the reconstructed surface as shown in Fig. 3b. The image has been taken on a stepped surface. Each of the terraces exhibits straight lines resulting from rows of Si dimers. Quite interestingly, the orientation of these dimer rows rotates by 90° between successive terraces. Therefore, the stepped surface is characterized by two non-equivalent terminations, which strictly alternate between successive terraces. Along with the orientation of the dimer rows, the shape of the monoatomic steps alternates as well between rather straight steps and meandering steps, the latter being rich in kinks.

The alternation between two different dimer row orientations results from the particular crystal structure of silicon. We may view the diamond lattice as a stack of (100) planes. As we move perpendicular to this stack, the orientation of the two bonds connecting between atoms in adjacent (100) layers rotates by 90° from layer to layer. Therefore, the orientation of the Si dimers at the surface rotates by 90° between adjacent terraces on a stepped surface as well. We may therefore envisage the diamond lattice as an alternating stack of two non-equivalent (100) layers, which have different surface properties, i.e. different orientations of the Si dimer rows. We note that the two layers are transformed into each other by reflection at a mirror plane along (100).

The observations on the SBM surfaces closely resemble the situation of the Si(100) surface: The near-surface region exhibits a structure different from the *ideal* case, which would be a laterally homogeneous termination by one of the end blocks of the block copolymer. Moreover, two different terminations are observed, which strictly alternate between adjacent terraces on a stepped block copolymer surface. Finally, the shape of the steps limiting the terraces alternates between two different possibilities as well. Similar to the case of the diamond lattice, the bulk structure of a lamellar ABC triblock copolymer can also be described as an alternating stack of two non-equivalent layers, i.e., ABC and CBA. Also the two layers are transformed into each other via reflection at a mirror plane along the layers. While equivalent in the bulk, these two layers will have different surface properties, as they lead to ideal surfaces terminated with one or the other end block.

The structure of a classical crystal is described by the periodic spatial arrangement of electron density and *point-like* nuclei. Therefore its symmetry belongs to the class of *point groups*. The microdomain structure of a block copolymer on the other hand is described by the density of

its components (S, B, and M in case of SBM) and a region with an increased density of one component is called a microdomain. Microdomains can form spheres, cylinders, lamellae or more complex shapes, which self-assemble into regular periodic structures resembling crystal like order. However, as cylinders and lamellae exhibit (partial) continuous translational symmetry, the corresponding bulk microdomain structures belong to the more general class of *space groups*. (Smectic and columnar phases of liquid crystals exhibit a similar symmetry.)

The lateral order within the layers of the bulk structure is different for the two materials: Si is a classical crystal with 2D lattice symmetry within its (100) plane, while the SBM bulk structure is lamellar with continuous 2-dimensional translational symmetry (Euclidian symmetry) within the lamellae. In both cases the symmetry of the reconstructed surface is lowered with respect to the ideal surface, however in very different ways. In case of the Si(100) surface the size of the unit cell of the 2D surface lattice doubles. In case of SBM, the Euclidian symmetry is broken. We emphasize the fact that in both cases a laterally homogeneous boundary imposed in the direction *perpendicular* to the layer breaks the *in-plane* symmetry of the ideal surfaces. This indicates that all three spatial coordinates are coupled on an underlying microscopic scale. This coupling is due to the 3-dimensional nature of the underlying elements (atoms in one case and polymer molecules in the other). The same phenomenon is found in other fields of physics (e.g., high energy physics), where the type of symmetry breaking can reveal properties of underlying (invisible) microscopic particles and processes.

5.4.2 Nomenclature

The notation used for crystal surfaces can also be applied to surfaces and surface reconstructions of block copolymers (Table 2). This further illustrates the analogy between both classes of materials. Usually first the material and its crystal structure is identified, for instance, α -Sn, 6H-SiC, or GaAs. For denoting the bulk microdomain structures of block copolymers we have followed the notation of Stadler *et al.* [18] (In order to focus on the microdomain structures, we have not denoted the stoichiometry and the total molecular weight of the block copolymers in Table 2.) For ABC triblock copolymers a two-letter prefix is used to indicate the shape of the two main structural elements. For instance, *ll* denotes the S and M lamellae in the SBM triblock copolymer that we have studied. In the case of the SBM triblock copolymer studied by Stocker *et al.* [14], the bulk structure is referred to as “lamellar-spherical” [18] which is denoted by the prefix *ls*. The next part of the notation identifies the surface and its orientation, for instance, (100) or (111). Miller indices can also be used to

Material (surface)	Surface reconstruction	Notation	Acronym	Experiment	Theory ^a
a) Inorganic crystals					
α -Sn	--	--	--	--	--
6H-SiC	--	--	--	--	--
GaAs(111)	Ideal A surface	GaAs(111) <i>A</i>	--	30	--
Si(100)	(2×1) buckling row	Si(100)-(2×1)	--	28, 29	--
Si(111)	(7×7)	Si(111)-(7×7)	--	7	--
b) Block copolymers					
<i>c</i> -SBS(C_{\perp})	Ideal surface	<i>c</i> -SBS(C_{\perp})	C_{\perp}	32, 39 ^b , 40 ^b	32, 41-45
<i>c</i> -SBS(C_{\parallel})	Ideal surface	<i>c</i> -SBS(C_{\parallel})	C_{\parallel}	24, 32, 39 ^b , 40 ^b , 46	32, 41-45
<i>c</i> -SBS(C_{\parallel})	Perforated lamella	<i>c</i> -SBS(C_{\parallel})-PL	PL	34 ^b , 32	32, 42, 43, 45
<i>c</i> -AB(C_{\parallel})	Lamella	<i>c</i> -AB(C_{\parallel})-L	L	34 ^b	32, 41-43
<i>c</i> -AB(C_{\parallel})	Wetting layer	<i>c</i> -AB(C_{\parallel})-W	W	33 ^b	32, 41-43, 45
<i>ll</i> -SBM(L_{\parallel})	Ideal M surface	<i>ll</i> -SBM(L_{\parallel})M	M	--	--
<i>ll</i> -SBM(L_{\parallel})	Perforated lamella M	<i>ll</i> -SBM(L_{\parallel})M-PL	M_{PL}	this work	--
<i>ll</i> -SBM(L_{\parallel})	Perforated S lamella	<i>ll</i> -SBM(L_{\parallel})S-PL	S_{PL}	this work	--
<i>ls</i> -SBM(L_{\perp})	Missing row	<i>ls</i> -SBM(L_{\perp})-(2×1)	--	14	--
c) Block copolymers (hybrid structures)					
<i>c</i> -SBS(C_{\parallel})	Cylinders with necks	<i>c</i> -SBS(C_{\parallel})-necks	--	45	47
<i>c</i> -SB	PL and spheres	--	--	48 ^b	47

^a Only in Ref. [32] cylinder forming triblock copolymers are studied; all other studies investigate diblock copolymers.

^b Work on cylinder forming diblock copolymers.

Table 2: Examples of ideal surfaces and surface reconstructions. See text for explanation.

denote planes (and surfaces) in block copolymer microdomain structures. However, as single crystals of block copolymers are rare, there is no general agreement on the assignment of unit cells for the various microdomain structures, in particular for the rather new ABC triblock copolymers. Another difficulty is that many microdomain structures, in particular cylinders and lamellae, have continuous symmetry. Although it is straightforward to define unit cells also for these systems, the definition is not unique. To avoid this problem we have used the "natural" block copolymer language to specify lattice planes and surfaces in cylinder and lamella forming systems. In a lamellar system, the lattice planes (and surfaces) parallel and perpendicular to the lamellae are well defined and we have denoted them as L_{\parallel} and L_{\perp} , respectively. In a polar system different surfaces with the same Miller indices are denoted with a suffix, for instance, GaAs(111)*A* [30]. Analogous to this notation we have denoted the two different ideal surfaces of lamella forming SBM with a suffix which indicates the component at the free surface. For instance, l -SBM(L_{\parallel})M denotes the ideal M-covered surface parallel to a lamella. In analogy to the notation used for inorganic crystals, the type of surface reconstruction is added to the "name" of the ideal surface. For example, the full name of the M_{PL} perforated lamella reconstruction of a surface parallel to a bulk lamella is l -SBM(L_{\parallel})M-PL. With this notation also other surface structures can be described (see Table 2). For instance, Stocker *et al.* [14] have reported at the surface of SBM a striped surface structure with twice the period of the lamellar bulk structure and have interpreted it as a missing row surface reconstruction. Analogous to crystal surfaces, the period doubling along (only) one lattice direction is denoted as a (2×1) reconstruction.

5.4.3 Experimental conditions for block copolymer surface studies

Similar to the situation for inorganic crystals, most impurities tend to be surface active and enrich in the near-surface region when the sample is driven towards thermal equilibrium. Therefore, the actual surface structure may easily be dominated by even smallest amounts of impurities present in the bulk of the material. Indeed, complex block copolymers often contain considerable amounts of residues of the synthesis process, such as homopolymers, other (lower generation) block copolymers, oligomers or other additives. While in the case of many classical crystals, the bulk material can be depleted from impurities by iterative cycles of thermal annealing and surface cleaning (e.g. by ion sputtering), no such cleaning procedures are established for block copolymer surfaces. Therefore, bulk pieces of block copolymer material are questionable candidates for surface studies. Indeed, transmission electron studies of the near-surface region of diblock copolymer samples have revealed

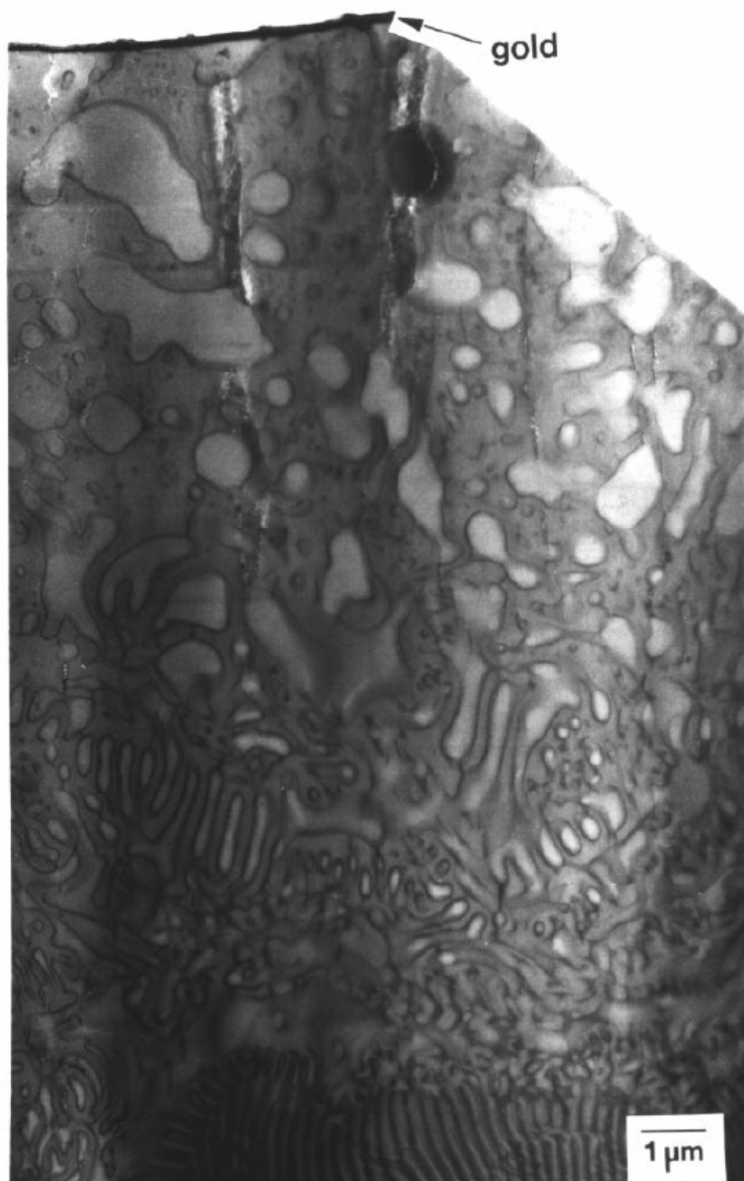


Figure 12: Cross-sectional TEM micrograph (OsO₄ stained) of the near-surface morphology of an SB 80/80 diblock copolymer sample showing the complex morphology with a contaminant thought to be a fully polymerized PS block with varying lengths of PB. The external surface has been marked with a layer of gold. The normal lamellar structure is ~10 μm below the surface. (Figure taken from Ref. [31]; Courtesy of E.L. Thomas, Massachusetts Institute of Technology, Cambridge.)

significant deviations from the bulk structure, which were attributed to accumulation of impurities (Fig. 12) [31].

In case of classical surface science, two alternative routes have been devised for cases in which clean surfaces can not be achieved by successive annealing and surface cleaning. At first, cleavage of bulk pieces of material can be used to create “clean” surfaces. Since a single

crystal typically cleaves along a preferred low-index crystallographic plane, a surface of well-defined crystallographic orientation is created. However, for a study of the equilibrium structure these surfaces will have to be annealed as well and a compromise has to be found concerning the annealing conditions, in order to avoid a significant amount of bulk impurities migrating to the newly created surface. Secondly, thin films of the material of interest can be prepared on suitable substrates again creating a clean surface. Here, the total amount of material (including impurities) is purposely kept small and the problem of impurities accumulation at the surface is less severe. However, the film thickness has to be chosen large enough in order to assure that the (bulk) crystal structure of interest is actually formed underneath the surface. Otherwise, confinement effects may dominate the entire structure of the film and the results will not reflect the surface properties of a bulk piece of the same material.

For block copolymers, the same two routes are in principle accessible. Instead of cleavage, a new surface may be created within the bulk of a sample by (cryo) microtoming and subsequent (short) annealing. As in the case of classical crystals, one has to assure that the annealing is sufficient to create the equilibrium surface structure, however, does not allow significant impurity migration. In contrast to the favorable situation of classical single crystals, the newly created surface will not be a low index crystallographic plane but will rather cut through a variety of grains at arbitrary orientation. Large scale alignment of the block copolymer microdomain structure in external fields prior to cutting may be a successful approach.

Alternatively, the surfaces of thin films may be investigated. Here, one has to assure that the “bulk” of the films is thick enough to form the structure expected for the bulk block copolymer material. As in the case of classical crystals, confinement effects may dominate the micro domain structure in very thin films [32]. In contrast, though, the characteristic film thickness above which bulk behavior is to be expected will be significantly larger in the case of block copolymers due to the inherent large molecular length scales. If the film thickness is kept small enough, though, the interactions with the supporting substrate can lead to micro domain alignment and a free surface of well-defined crystallographic orientation may be created. In any case, the “bulk morphology” of the thin film has to be experimentally established (see Fig. 1) before potential surface reconstructions can be identified.

5.4.4 Comparison to earlier experimental results

The concept of block copolymer surface reconstructions was first introduced in a paper by Stocker *et al.* [14], who investigated the surface structure of an SBM triblock copolymer bulk sample with a rather small volume fraction of the B middle block and about equal volume fractions of the S and M end blocks. In the bulk, the material formed lamellae of S and M with B spheres located at the S/M interfaces. At the surface, indications of a perpendicular orientation of the lamellae were observed and the B spheres were visualized by TappingModeTM SFM by virtue of their different mechanical properties. The SFM results indicated an in-plane periodicity different from the bulk periodicity determined by TEM. This difference was attributed to a surface reconstruction.

Other studies have reported thin film structures different from the respective bulk structures, which can also be attributed to surface reconstructions. Indeed, in cylinder forming block copolymer systems, a variety of thin film structures has been reported on, including a laterally homogeneous wetting layer [33], spherical microdomains [34] and a perforated lamella [34]. Systematic studies of the thin film phase behavior as a function of both surface interaction and film thickness have recently been performed both experimentally and by dynamic density functional calculations [32]. These studies have revealed that in thin films both surface reconstructions and confinement play a role and the resulting equilibrium structures are determined by the interplay of the two.

Other studies have reported on particular thin film structures such as the so-called hybrid structure in lamellar forming diblock copolymer thin films [35] and cylinders exhibiting necks towards the free surface in cylinder forming block copolymers [23]. In the former case, asymmetric wetting conditions were shown to lead to a parallel alignment of the lamellae at the substrate interface, while a perpendicular orientation of the lamellae was found at the free surface. This finding, however, may rather be attributed to the observation of two grains exhibiting the bulk structure, divided by a planar grain boundary stabilized by surface interactions. The observation of cylinders with necks may be described in similar terms.

Other, more complex thin film structures have recently been described for ABC triblock copolymer thin films [36,37]. Here, however, it remains unclear to what extent thermal equilibrium has been reached during film preparation. Further studies will be needed to unambiguously classify the respective structures in the framework provided here.

5.5 Conclusion

We have shown that differences in surface energy between the different constituent materials of a block copolymer can lead to deviations of the near surface structure from the bulk structure, so called *surface reconstructions*. Despite the fundamental differences between the materials, the type of order and symmetry, and the length scales, these surface reconstructions exhibit many similarities to the well-known surface behavior of classical crystals. This finding indicates that the concept of surface reconstruction is not limited to classical crystals but can appear in similar ways for other kinds of ordered materials as well. For the particular case of block copolymers, the concept of surface reconstructions and the clear distinction between surface reconstructions and confinement effects can lead to a deeper understanding of the underlying physics determining block copolymer thin film structures.

5.6 References

- [1] Bates, F. S.; Fredrickson, G. H. *Physics Today* **1999**, *52*, 32.
- [2] Witten, T. A. *Rev. Mod. Phys.* **1999**, *71*, S367.
- [3] Seul, M.; Andelman, D. *Science* **1995**, *267*, 476.
- [4] Tsori, Y.; Andelman, D. *J. Chem. Phys.* **2001**, *115*, 1970.
- [5] Hashimoto, T.; Bodycomb, J.; Funaki, Y.; Kimishima, K. *Macromolecules* **1999**, *32*.
- [6] Zangwill, A., *Physics at Surfaces*; Cambridge University Press, Cambridge, 1988.
- [7] Binnig, G.; Rohrer, H.; Gerber, C.; Weibel, E. *Phys. Rev. Lett.* **1983**, *50*, 120.
- [8] Ragosti, A. K.; Pierre, L. E. S. *J. Coll. Interf. Sci.* **1969**, *31*, 168.
- [9] Anastasiadis, S. H.; Russell, T. P.; Satija, S. K.; Majkrzak, C. F. *Phys. Rev. Lett.* **1989**, *62*, 1852.
- [10] Krausch, G. *Materials Science and Engineering Reports* **1995**, *14*, 1.
- [11] Fasolka, M. J.; Mayes, A. M. *Ann. Rev. Mat. Res.* **2001**, *31*, 323.
- [12] Pickett, G. T.; Balazs, A. C. *Macromol. Theory Simul.* **1998**, *7*, 249.
- [13] Chen, H.-Y.; Fredrickson, G. H. *Journal of Chemical Physics* **2002**, *116*, 1137.
- [14] Stocker, W.; Beckmann, J.; Stadler, R.; Rabe, J. P. *Macromolecules* **1996**, *29*, 7502.

- [15] Elbs, H.; Fukunaga, K.; Sauer, G.; Stadler, R.; Magerle, R.; Krausch, G. *Macromolecules* **1999**, *32*, 1204.
- [16] Fukunaga, K.; Elbs, H.; Krausch, G. *Langmuir* **2000**, *16*, 3474.
- [17] Rehse, N.; Knoll, A.; Konrad, M.; Magerle, R.; Krausch, G. *Phys. Rev. Lett.* **2001**, *87*, 035505.
- [18] Stadler, R.; Auschra, C.; Beckmann, J.; Krappe, U.; Voigt-Martin, I.; Leibler, L. *Macromolecules* **1995**, *28*, 3080.
- [19] Goldacker, T., Ph.D. Thesis, Universität Bayreuth, Bayreuth, 1999.
- [20] Anastasiadis, S. H.; Russell, T. P.; Satija, S. K.; Majkrzak, C. F. *J. Chem. Phys.* **1990**, *92*, 5677.
- [21] Brinkmann, S.; Stadler, R.; Thomas, E. L. *Macromolecules* **1998**, *31*, 6566.
- [22] Konrad, M., Diploma Thesis, Universität Bayreuth, Bayreuth, 1999
- [23] Konrad, M.; Knoll, A.; Krausch, G.; Magerle, R. *Macromolecules* **2000**, *33*, 5518.
- [24] Knoll, A.; Magerle, R.; Krausch, G. *Macromolecules* **2001**, *34*, 4159.
- [25] A similar pattern has been observed at terrace edges with diblock copolymer films. Carvalho, B. L.; Thomas, E. L. *Phys. Rev. Lett.* **1994**, *73*, 3321.
- [26] Mark, J. E. *Physical Properties of Polymers Handbook*; Woodbury: New York, 1996.
- [27] Tromp, R. M.; Hamers, R. J.; Demuth, J. E. *Phys. Rev. Lett.* **1985**, *55*, 1303.
- [28] Dijkamp, D.; Hoeven, A. J.; Loenen, E. J. v.; Lenssinck, J. M.; Dieleman, J. *Appl. Phys. Lett.* **1990**, *56*, 39.
- [29] Swartzentruber, B. S.; Kitamura, N.; Lagally, M. G.; Webb, M. B. *Phys. Rev. B* **1993**, *47*, 13432.
- [30] Ohtake, A.; Nakamura, J.; Komura, T.; Hanada, T.; Yao, T.; Kuramochi, H.; Ozeki, M. *Phys. Rev. B* **2001**, *64*, 045318.
- [31] Schwark, D. W., Ph.D. Thesis, Massachusetts Institute of Technology, Cambridge, MA, 1992.
- [32] Knoll, A.; Horvat, A.; Lyakhova, K. S.; Krausch, G.; Sevink, G. J. A.; Zvelindovsky, A. V.; Magerle, R. *Phys. Rev. Lett.* **2002**, *89*, 035501.

- [33] Karim, A.; Singh, N.; Sikka, M.; Bates, F. S.; Dozier, W. D.; Felcher, G. P. *J. Chem. Phys.* **1994**, *100*, 1620.
- [34] Radzilowski, L. H.; Carvalho, B. L.; Thomas, E. L. *J. Poly. Sci. B Poly. Phys.* **1996**, *34*, 3081.
- [35] Fasolka, M. J.; Banerjee, P.; Mayes, A. M.; Pickett, G.; Balasz, A. *Macromolecules* **2000**, *33*, 5702.
- [36] Elbs, H.; Drummer, C.; Abetz, V.; Hadziioannou, G.; Krausch, G. *Macromolecules* **2001**, *34*, 7917.
- [37] Elbs, H.; Drummer, C.; Abetz, V.; Krausch, G. *Macromolecules* **2002**, *35*, 5570.
- [38] Breiner, U., Ph.D. Thesis, Universität Mainz, Mainz, 1996.
- [39] Kim, G.; Libera, M. *Macromolecules* **1998**, *31*, 2569.
- [40] Kim, G.; Libera, M. *Macromolecules* **1998**, *31*, 2670.
- [41] Turner, M. S.; Rubinstein, M.; Marques, C. M. *Macromolecules* **1994**, *27*, 4986.
- [42] Huinink, H. P.; Brokken-Zijp, J. C. M.; van Dijk, M. A.; Sevink, G. J. A. *J. Chem. Phys.* **2000**, *112*, 2452.
- [43] Huinink, H. P.; van Dijk, M. A.; Brokken-Zijp, J. C. M.; Sevink, G. J. A. *Macromolecules* **2001**, *34*, 5325.
- [44] Pereira, G. G. *Phys. Rev. E* **2001**, *63*, 061809.
- [45] Wang, Q.; Nealy, P. F.; Pablo, J. J. d. *Macromolecules* **2001**, *34*, 3458.
- [46] van Dijk, M. A.; van den Berg, R. *Macromolecules* **1995**, *28*, 6773.
- [47] Lyakhova, K. S.; Sevink, G. J. A.; Zvelindovsky, A. V.; Horvat, A.; Magerle, R. *to be published*.
- [48] Harrison, C.; Park, M.; Chaikin, P. M.; Register, R. A.; Adamson, D. H.; Yao, N. *Macromolecules* **1998**, *31*, 2185.

6 Summary / Zusammenfassung

6.1 Summary

In the first part of this thesis an improved process is presented to prepare laterally structured substrates via hierarchical self organization. A miscut silicon surface annealed at 1400 K under ultra high vacuum conditions is used. The resulting facets are stable against oxidation and form a topographic pattern which can be further modified to a chemical pattern via evaporation of gold on every other facet. By controlling the time of annealing, we create structures with a reproducible mean width ranging from 40 to 400 nm. Despite the rather complex ultra high vacuum treatment and an additional evaporation step, we are able to produce substrates in a relatively short time (36 h). These substrates show a nanometer sized structure over an area of 0.5 cm². The automation of the cleaning process and a controlled heating during the annealing increases the yield of high-quality, stepped substrates.

These structures allowed us to study the behavior of ultra-thin polystyrene films on topographically structured substrates. The film thickness of some nanometers is comparable to the radius of gyration of the polymers. The substrate corrugation causes a regular variation of the film thickness. We start with a homogeneous film, which is annealed above the glass transition temperature. During annealing the films are stable or form long polymer nanochannels, which lie in the grooves of the substrate structure. The balance of the radius of gyration and the film thickness controls the stability of the polymer film, while the corrugation only triggers the dewetting. The same behavior is found for films on flat substrates. Here small contaminations nucleate the formation of holes.

Evaporation of gold stripes and their modification with self assembled monolayers leads to chemical patterned substrates. This expands the possibilities to manipulate the substrate wettability on the nanometer scale.

The second part of the thesis describes the formation of ordered structures in block copolymer films. ABC triblock copolymers show a large variety of morphologies in thin films. We have shown that surface reconstructions play an important role in the structure formation process of these structures. In very thin films, where the film thickness is smaller than the long period of the polymer's micro domains, confinement effects overlap with the surface effects. The component with the lowest surface energy is accumulated at the free surface. It needs a subtle

balance between the different surface energies (external fields) and the interaction of the three polymer blocks (internal fields) to create a surface reconstruction. This was shown by variation of the chemistry of the end block and by changing the sequence of blocks in the experiment. To analyze the surface reconstruction we used selective staining along with scanning electron microscopy, selective etching in oxygen plasma in combination with scanning probe microscopy, as well as quantitative TappingMode atomic force microscopy. Surface reconstructions of block copolymers show remarkable similarities with reconstructions of single crystal surfaces. In both cases the driving force for a rearrangement is the decrease in surface free energy of the ideal surface. A second analogy between the lamella forming SBM triblock copolymer and Si(100) is the fact that two non-equivalent layers of matter aligned parallel to the free surface lead to two different terminations at the surface. This shows that the phenomenon of surface reconstructions is not limited to classic crystals.

The results of this thesis give new insights in the behavior of polymers at surfaces and in thin films. This gives the opportunity to create or manipulate nanometer sized structures accurately via self assembly, external stimuli, or a combination of both.

6.2 Zusammenfassung

Im ersten Teil dieser Arbeit wurde ein verbesserter Prozess zur Herstellung von lateral strukturierten Substraten durch hierarchische Selbstorganisation vorgestellt. Dazu wird eine fehlgeschnittene Siliziumoberfläche im Ultrahochvakuum bei 1400 K getempert. Die entstandenen Facetten bleiben auch nach der Oxidation als topographische Struktur erhalten und lassen sich durch Aufdampfen einer Goldschicht auf jede zweite Facette mit einer chemische Struktur versehen. Durch gezielte Wahl der Temperdauer im Ultrahochvakuum lässt sich der mittlere Abstand der Strukturen reproduzierbar zwischen 40 und 400 nm einstellen. Trotz der scheinbar aufwendigen Ultrahochvakuum-Behandlung und einem weiteren Präparationsschritt im Vakuum lassen sich in verhältnismäßig kurzer Zeit (36 h) Substrate herstellen, die auf 0,5 cm² ganzflächig eine Nanostrukturierung besitzen. Die automatische Reinigung und die geregelte Temperatursteuerung während der Temperbehandlung erhöhen die Ausbeute an qualitativ hochwertigen, gestuften Substraten.

Im Folgenden wurde das Verhalten von sehr dünnen Polystyrolfilmen auf solchen rein topografischen strukturierten Substraten untersucht. Die Filmdicke von wenigen Nanometern lag im Bereich des Gyrationradius der untersuchten Polymere. Die Topografie des Substrates

führt zu einer regelmäßigen Variation der Filmdicke. Unmittelbar nach der Präparation beobachten wir einen homogenen Film, der je nach Dicke beim Tempern oberhalb der Glasatemperatur stabil bleibt oder in lang gezogene Polymerkanäle aufbricht, die in den Gräben der Substratstruktur liegen. Das Wechselspiel von Gyrationradius und Filmdicke bestimmt dabei die Stabilität des Polymerfilms, wobei die Korrugation das Aufbrechen lediglich nukleiert. Dasselbe Verhalten wird auch bei Filmen auf glatten Substraten beobachtet. Dort nukleieren Verunreinigungen das Aufbrechen des Films.

Durch Aufdampfen von Goldstreifen und die Modifikation mit selbst organisierenden Monolagen kann das Substrat chemisch strukturiert werden. Damit erweitern sich die Möglichkeiten, die Benetzbarkeit des Substrates auf der Nanometerskala zu manipulieren.

Der zweite Teil der Arbeit befasst sich mit der Entstehung geordneter Strukturen in Blockcopolymerfilmen. ABC Dreiblockcopolymere zeigen eine große Vielfalt von Morphologien in dünnen Filmen. Es wurde gezeigt, dass Oberflächenrekonstruktionen bei der Strukturbildung eine wichtige Rolle spielen. In sehr dünnen Filmen, deren Dicke kleiner ist als die Langperiode der Mikrodomänenstruktur, treten zusätzliche Effekte durch die eingeschränkte Geometrie auf. Bei Blockcopolymeren reichert sich die Komponente mit der niedrigsten Oberflächenenergie an der freien Oberfläche an. Durch die Variation der Chemie des Endblocks sowie der Reihenfolge der Blocksequenz eines symmetrischen ABC Dreiblockcopolymeres konnten wir zeigen, dass es eines feinen Wechselspiels aus unterschiedlichen Oberflächenenergien (externe Felder) und den Wechselwirkungen der Blöcke untereinander (interne Felder) bedarf, um eine Oberflächenrekonstruktion zu bilden. Die Oberflächenrekonstruktion wurde unter Zuhilfenahme von Elektronenmikroskopie gezielt kontrastierter Proben, quantitativer TappingMode Rasterkraftmikroskopie, sowie unterschiedlicher Ätzzraten der Polymere im Sauerstoffplasma aufgeklärt. Die Oberflächenrekonstruktionen von Blockcopolymeren sind vergleichbar mit Rekonstruktionen von Einkristalloberflächen. In beiden Fällen ist die treibende Kraft die Energieminimierung der idealen Oberfläche durch Umordnung der Struktur. Die zweite Analogie zwischen lamellenbildendem SBM Dreiblockcopolymer und Si(113) besteht in dem Entstehen zweier unterschiedlicher Oberflächenstrukturen, wenn in der Volumenstruktur eine Abfolge zweier nicht-äquivalenter Schichten senkrecht zur Oberfläche zu finden ist. Dies zeigt, dass das Phänomen der Oberflächenrekonstruktion nicht auf Einkristalle beschränkt ist.

Die in dieser Arbeit gewonnen Erkenntnisse liefern einen wichtigen Beitrag zum Verständnis von Polymeren an Oberflächen und in dünnen Filmen. Sie eröffnen damit Möglichkeiten,

nanometergroße Strukturen durch Selbstorganisationprozesse, externe Einflüsse oder der Kombination beider Methoden gezielt herzustellen oder zu manipulieren.

7 Acknowledgement / Danksagung

Georg Krausch danke ich für die Möglichkeit an diesem großartigen Lehrstuhl arbeiten zu können, für seine Unterstützung in vielen, auch nicht-wissenschaftlichen Dingen und seine Geduld.

Ein großer Dank geht auch an **Robert Magerle** für viele ergiebige Diskussionen und Einfälle, für aufmunternde Worte und den finalen Kick.

Bei meinem jahrelangen Büronachbarn **Armin Knoll** bedanke ich mich für seine ständige Diskussions- und Hilfsbereitschaft, seine physikalische Sicht der Dinge, die manches in anderem Licht erscheinen ließ und die vielen Stunden mit Schredd.

Ohne die tatkräftige Unterstützung von **Markus Hund** bei der Herstellung der strukturierten Substrate und ohne seine geduldige Wartung der AFMs wären viele Teile dieser Arbeit so nicht realisierbar gewesen.

Tracy C. Wang gilt mein Dank für die tolle Zusammenarbeit auf dem Gebiet der Entnetzung von dünnen Polymerfilmen und für einige kulinarische Entdeckungen.

Mark Geoghegan hat mir geduldig bei den Grundlagen zum Thema Entnetzung geholfen. Sein englischer Humor und die unnachahmlichen Hinweise zur originalgetreuen Aussprache werden noch immer schmerzlich vermisst.

Die Polymere von **Thorsten Goldacker** und später von **Volker Abetz** aus der Makromolekularen Chemie ließen diese Arbeit in weiten Teilen erst möglich werden.

Bei **Sabine Ludwigs** bedanke ich mich für ihre Messungen an BSM und SBT Dreiblockcopolymeren während ihres Praktikums, für ihre stete Diskussionsbereitschaft, sowie für viele lustige Momente bei Postern.

Für die netten und fruchtbaren Stunden am REM und das Auge für oft entscheidende Details geht mein Dank an **Clarissa Abetz** vom BIMF.

Vielen Dank auch an **Carmen Kunert** für die – oft frustrierende – Präparation der TEM Proben und die Hilfe bei den TEM Messungen und beim alljährlichen Säcke stopfen.

Weiterhin gilt mein Dank **Andriana Horvat**, die mir bei meinen ersten Schritten mit der Mesodyn Software geholfen hat.

Für das Korrekturlesen und die seelische Unterstützung auf den letzten Metern danke ich **Sabine Scherdel**.

Bei **Frau Zimmermann** und **Wolfgang Häfner** möchte ich mich für die Unterstützung in allen Fragen des Beschaffungs-, Verwaltungs- und Anmeldekampfes bedanken.

Die **Lutscher und Bonbons** sorgten für die entspannenden Stunden nach dem Laboralltag beim wöchentlichen CTF-Zocken.

Für alles und vieles mehr, was sich nicht auf dieser Seite ausdrücken lässt einen riesengroßen Dank an die **Mitarbeiter, die Ehemaligen und Freunde des Lehrstuhls PC II**. Es war eine verdammt schöne Zeit mit Euch.